

**FACTORS INFLUENCING THE TRANSPORT AND DEPOSITION OF  
*SALMONELLA* AND COLLOIDS FROM EVAPORATING SESSILE  
DROPLETS ON POLYDIMETHYLSILOXANE SURFACES OF  
FRESH PRODUCE AND SIMPLE MICROPATTERNS**

by

Anna K. Jurusik

A thesis submitted to the Faculty of the University of Delaware in partial fulfillment of the requirements for the degree of Master of Science in Plant and Soil Sciences

Winter 2019

© 2019 Anna K. Jurusik  
All Rights Reserved

**FACTORS INFLUENCING THE TRANSPORT AND DEPOSITION OF  
*SALMONELLA* AND COLLOIDS FROM EVAPORATING SESSILE  
DROPLETS ON POLYDIMETHYLSILOXANE SURFACES OF  
FRESH PRODUCE AND SIMPLE MICROPATTERNS**

by

Anna K. Jurusik

Approved: \_\_\_\_\_  
Yan Jin, Ph.D.  
Professor in charge of thesis on behalf of the Advisory Committee

Approved: \_\_\_\_\_  
Erik Ervin, Ph.D.  
Chair of the Department of Plant and Soil Sciences

Approved: \_\_\_\_\_  
Mark Rieger, Ph.D.  
Dean of the College of Agriculture and Natural Resources

Approved: \_\_\_\_\_  
Douglas J. Doren, Ph.D.  
Interim Vice Provost for Graduate and Professional Education

## ACKNOWLEDGMENTS

First and foremost, I would like to thank my advisor, Dr. Yan Jin, for the incredible opportunity to study under her thoughtful, patient, and skillful guidance, and I am forever grateful to have learned so much from a mentor who exemplifies such integrity. I also thank my committee members, Dr. Kristi Kiick, Dr. Jeffry Fuhrmann, Dr. Dallas Hoover, and Dr. Gang Wang for their invaluable support, insights, and critique on this work. My gratitude extends further to Dr. Kristi Kiick, who ignited my interests in research science and supported me throughout my research endeavors as an exemplary mentor, and to Dr. Jeffry Fuhrmann, who not only facilitated my graduate teaching experiences but also offered compassionate mentoring throughout my graduate degree.

Thank you to the University of Delaware Nanofabrication Staff for facilitating my research with funding, and a special thank you to Dr. Kevin Lister, who was with me from Day 1 of my “Adventures in the Nanofab,” and who helped develop the work in this thesis. Special thank you to Sarah Geiger and Tao Wang who also helped train me in my nanofabrication work. Support by the Bioimaging Center and staff that helped facilitate this work is greatly appreciated. Thank you to all of the members of the Plant and Soil Sciences department, and to all of the professors at the University of Delaware who facilitated my learning and growth as a scientist in today’s world. I also extend sincere gratitude to all of the staff members who facilitate the University in ways that we often don’t acknowledge.

Thank you so much to my labmates past and present. Your hard work and dedication were inspiring, and I have no doubts of the great successes that await you in your futures. Each and every person I met during my graduate experience helped shape my interpersonal and professional growth. Thank you to all of the friends I've made along the way.

Thank you to the very special people in my life who remind me of what's most important. Your unconditional love is everything.

Finally, I dedicate this work to my awesome brother-in-law, Dan Pannullo. We will forever carry you in our hearts.

## TABLE OF CONTENTS

LIST OF TABLES .....	viii
LIST OF FIGURES.....	ix
ABSTRACT.....	xii
Chapter	
1 LITERATURE REVIEW .....	1
1.1 Introduction.....	1
1.2 The Dilemma with Fresh Produce.....	1
1.3 The Need for Improved Decontamination Strategies.....	3
1.4 The Physicochemical Characteristics of Plant Surfaces and Their Role in Human Bacteria-Plant Interactions .....	5
1.4.1 Hydrophobicity .....	6
1.4.2 Topography and Roughness.....	8
1.5 Particle Transport and Deposition on Surfaces from Evaporating Sessile Droplets.....	12
1.5.1 Sessile Droplet Evaporation.....	13
1.5.2 Capillary Forces and Film Thickness in Particle Transport and Deposition .....	18
1.5.2.1 Capillary Forces .....	18
1.5.2.2 Film Thickness.....	19
1.6 Research Motivation and Approach.....	22
1.7 Research Objectives.....	23
2 FACTORS INFLUENCING THE TRANSPORT AND DEPOSITION OF <i>SALMONELLA ENTERICA</i> AND COLLOIDS IN EVAPORATING SESSILE DROPLETS ON POLYDIMETHYLSILOXANE SPINACH AND LETTUCE.....	24
2.1 Introduction.....	24
2.2 Materials and Methods.....	25
2.2.1 Fabrication of Polydimethylsiloxane Spinach and Lettuce Surfaces .....	25
2.2.2 Surface Hydrophobicity .....	27
2.2.3 Surface Roughness .....	27
2.2.4 Sessile Droplet Evaporation.....	28
2.2.5 Droplet Evaporation via Confocal Microscopy .....	29

2.2.5.1	Deposition Patterns .....	29
2.2.5.2	Droplet Evaporation Characteristics .....	30
2.2.6	Image and Statistical Analyses.....	31
2.3	Results.....	32
2.3.1	Surface Properties .....	32
2.3.1.1	Surface Roughness .....	32
2.3.1.2	Surface Hydrophobicity .....	33
2.3.2	Qualitative Analysis of Deposition Patterns .....	35
2.3.2.1	Deposition Patterns from Water Droplets.....	35
2.3.2.2	Deposition Patterns from 0.01% Tween 80 Droplets...	38
2.3.3	Droplet Evaporation Characteristics .....	42
2.3.3.1	Evaporation Time and Contact Area.....	42
2.3.3.2	Droplet Contact Line Behavior .....	44
2.4	Summary .....	48
3	<b>FACTORS INFLUENCING THE TRANSPORT AND DEPOSITION OF SALMONELLA ENTERICA AND COLLOIDS IN EVAPORATING SESSILE DROPLETS ON POLYDIMETHYLSILOXANE MICROPATTERNED SURFACES.....</b>	<b>49</b>
3.1	Introduction .....	49
3.2	Materials and Methods.....	50
3.2.1	Micropattern Fabrication via Standard Lithography .....	50
3.2.2	Polydimethylsiloxane (PDMS) Soft Lithography .....	52
3.2.3	Surface Hydrophobicity .....	53
3.2.4	Surface Roughness .....	53
3.2.5	Sessile Droplet Suspension .....	54
3.2.6	Droplet Evaporation via Confocal Microscopy .....	55
3.2.6.1	Deposition Patterns from Evaporated Droplets.....	55
3.2.6.2	Droplet Evaporation Characteristics .....	56
3.2.7	Image and Statistical Analyses.....	57
3.3	Results and Discussion.....	57

3.3.1	Micropatterned Surface Properties.....	57
3.3.1.1	Surface Roughness of Micropatterns .....	57
3.3.1.2	Surface Hydrophobicity of Micropatterns .....	58
3.3.2	Qualitative Analysis of Deposition Patterns .....	60
3.3.2.1	Deposition Patterns from Water Droplets .....	60
3.3.2.2	Deposition Patterns from 0.01% Tween 80 Droplets...	64
3.3.3	Droplet Evaporation Dynamics.....	67
3.3.3.1	Droplet Evaporation Time.....	67
3.3.3.2	Droplet Contact Line Behavior .....	69
3.4	Summary .....	73
4	DISCUSSION, CONCLUSIONS, AND FUTURE WORK .....	75
4.1	Discussion .....	75
4.1.1	Mechanisms Leading to <i>Salmonella</i> and Colloid Transport and Deposition in Evaporating Sessile Droplets.....	75
4.1.1.1	Surface Roughness .....	75
4.1.1.2	Surface Hydrophobicity .....	77
4.1.1.3	Hydrodynamics, Capillary Forces, and Film Thickness.....	79
4.1.1.4	Particle Characteristics.....	84
4.2	Conclusions .....	85
4.3	Future Work .....	87
	REFERENCES.....	88
	Appendix	
A	PARTICLE CHARACTERISTICS .....	97

## LIST OF TABLES

Table 1.1:	Characterized surface properties of selected fruits and vegetables.....	8
Table 2.1:	Surface roughness (n=5) and hydrophobicity (n=3) of Glass, PDMS Flat, PDMS Spinach, and PDMS Lettuce in DI Water or 0.01% Tween 80 droplets.....	32
Table 3.1:	Surface roughness (n=5) and hydrophobicity (n=3) of Glass, PDMS Flat, PDMS Pillars, PDMS Depressions, and PDMS Grooves in DI Water or 0.01% Tween 80 droplets .....	58
Table A.1:	Particle characteristics.....	90

## LIST OF FIGURES

Figure 2.1:	Confocal images of PDMS Lettuce (A) and PDMS Spinach (B)..	26
Figure 2.2:	Schematic of droplet transect measurement over time for an evaporating droplet. The transect length, similar to a diameter, is measured between two points at the droplet's edges over time during evaporation and depicted in a figure of length vs. time..	31
Figure 2.3:	Equilibrium contact angle measurements for DI water (purple) and 0.01% Tween 80 (teal) droplets. ....	34
Figure 2.4:	Representative confocal images (780 LSM) of the deposition patterns of colloids (red) and <i>Salmonella</i> (green) in Water droplets. A) Glass; B) PDMS Flat; C) PDMS Lettuce; and D) PDMS Spinach. The transmission channel was removed to improve visibility. Scale bar is 200 $\mu\text{m}$ . ....	36
Figure 2.5:	Representative confocal images (780 LSM) of the close-up regions of deposition patterns from Water droplets containing colloids (red) and <i>Salmonella</i> (green). A) Glass; B) PDMS Flat; C) PDMS Lettuce; and D) PDMS Spinach. Scale bar is 20 $\mu\text{m}$ .....	37
Figure 2.6:	Representative confocal images (780 LSM) of the deposition patterns of colloids (red) and <i>Salmonella</i> (green) in 0.01% Tween 80 droplets. A) Glass; B) PDMS Flat; C) PDMS Lettuce; and D) PDMS Spinach. The transmission channel was removed to improve visibility. Scale bar is set to 200 $\mu\text{m}$ but varies by length due to the different scales in the images. ....	40
Figure 2.7:	Representative confocal images (780 LSM) of the close-up regions of deposition patterns from 0.01% Tween 80 droplets containing colloids and <i>Salmonella</i> . A) Glass; B) PDMS Flat; C) PDMS Lettuce; and D) PDMS Spinach. Scale bar is 20 $\mu\text{m}$ . Arrows point to surfactant globules/micelles.....	41
Figure 2.8:	Droplet evaporation for Water (purple) and 0.01% Tween 80 (teal) droplets on the different surfaces (n=3) with standard error bars. ....	42
Figure 2.9:	Droplet contact area for Water (purple) and 0.01% Tween 80 (teal) droplets on the different surfaces (n=3) with standard error bars. ....	43

Figure 2.10: Plot of the contact line behavior for a representative Water (purple) and 0.01% Tween 80 (teal) droplet on A) Glass; B) PDMS Flat; C) PDMS Lettuce and D) PDMS Spinach. The y-axis refers to a transect through two edge points over the droplet contact area, similar to a diameter. Due to the heterogeneity of the surface features, a true diameter is not apparent. Arrows point to example changes in contact line behavior, and brackets indicate example contact line pinning stages.....	45
Figure 2.11: Confocal microscopy images (780 LSM) of <i>Salmonella</i> (green) and colloids (red) at contact lines during evaporation for Water (uppercase letters) and Tween (lowercase letters) droplets. A,a) Glass; B,b) PDMS Flat; C,c) PDMS Lettuce and D,d) PDMS Spinach. Scale bar is 20 $\mu\text{m}$ . White arrows indicate pinned regions. Yellow arrows indicate direction of contact line movement from the air-water interface. Green arrows indicate direction of particle movement.....	47
Figure 3.1: Confocal images of the PDMS micropatterns. A) PDMS Pillars; B) PDMS Grooves; C) PDMS Depressions. Scale bar is 100 $\mu\text{m}$ . .....	52
Figure 3.2: Equilibrium contact angles 5.0 $\mu\text{L}$ DI water droplets on Glass, PDMS Flat, PDMS Pillars, PDMS Depressions, and PDMS Grooves.....	59
Figure 3.3: Representative confocal images (780 LSM) of the deposition patterns of colloids and <i>Salmonella</i> in water droplets. A) Glass; B) PDMS flat; C) PDMS Pillars; D) PDMS Depressions; and E) PDMS Grooves. The transmission channel was removed to improve visibility. Scale bar is 200 $\mu\text{m}$ . .....	62
Figure 3.4: Representative confocal images (780 LSM) of the deposition patterns of colloids and <i>Salmonella</i> in DI water droplets at close-up regions. A) Glass; B) PDMS flat; C) PDMS Pillars; D) PDMS Depressions; and E) PDMS Grooves. Arrows point to localization at surface features from pinning. Scale bar is 20 $\mu\text{m}$ . .....	63
Figure 3.5: Representative confocal images (780 LSM) of the deposition patterns of colloids (red) and <i>Salmonella</i> (green) in 0.01% Tween 80 droplets. A) Glass; B) PDMS flat; C) PDMS Pillars; D) PDMS Depressions; and E) PDMS Grooves. The transmission channel was removed to improve visibility. Scale bar is set to 200 $\mu\text{m}$ but varies by length due to the different scales in the images. ....	65

Figure 3.6: Representative confocal images (780 LSM) of the deposition patterns of colloids (red) and <i>Salmonella</i> (green) in 0.01% Tween 80 droplets at close-up regions. A) Glass; B) PDMS flat; C) PDMS Pillars; D) PMS Depressions; and E) PDMS Grooves. Arrows point to regions with deposition in features or in surfactant micelles. Scale bar is 20 $\mu\text{m}$ . .....	67
Figure 3.7: Droplet evaporation for Water (purple) and 0.01% Tween 80 (teal) droplets on the different surfaces, with standard error bars. ....	68
Figure 3.8: Plot of the contact line evolution for representative Water (purple) or 0.01% Tween 80 (teal) droplets on A) Glass; B) PDMS Flat; C) PDMS Pillars, D) PDMS Depressions, and E) PDMS Grooves. The y-axis refers to a transect through two edge points over the droplet contact area, similar to a diameter. Due to the heterogeneity of the surface features, a true diameter is not apparent. Arrows point to changes in contact line behavior.. ....	70

## ABSTRACT

The transport and deposition of colloids and biocolloids (e.g., bacteria) are important processes that occur in environmental (e.g., the vadose zone) and engineered (e.g., wastewater treatment) systems. Although the major mechanisms surrounding colloid transport and retention are known, less is known about these mechanisms in the context of unsaturated systems (e.g., porous media and on biological surfaces) compared to saturated systems, particularly for biocolloids such as bacteria. Importantly, bacteria that are pathogenic to humans, such as *E. coli* O157:H7 and *Salmonella* spp., are found in agricultural systems throughout the farm-to-fork continuum, including soil and manure, irrigation water, and on crop surfaces. Human pathogenic bacteria attach to and survive on the surfaces of ready-to-eat fresh produce, which can lead to large-scale outbreaks of foodborne illness and even death. The most recent outbreak involving *E. coli* O157:H7 on Romaine lettuce in 2018 underscores the value of fresh produce safety research: there is a dire need to understand how fresh produce contamination with human bacterial pathogens occurs and to develop effective mitigation strategies. Currently, the most widely-used approach, chlorine sanitation, achieves just 1-2 log reduction of colony-forming units (CFU) per gram of produce and is even less effective at removing bacteria attached in biofilms. Researchers have developed alternative methods to remove contaminants, but these methods do not achieve significantly higher sanitation rates. To date, how human pathogens are deposited and retained on plant surfaces as well as how these pathogens survive throughout processing are research areas not fully elucidated.

The focus of this research was to improve the understanding of how (bio)colloids interact on produce surfaces. To do this, polydimethylsiloxane (PDMS)

surfaces of spinach and lettuce were used in addition to micropatterned surfaces of simple geometries fabricated via standard lithography procedures. A major effort of this work was to visualize the transport and deposition of (bio)colloids from contact lines of evaporating droplets on different surfaces using confocal microscopy, and to correlate the qualitative data to the mechanisms involved in colloid transport theory considering the influence of surface, solution, and (bio)colloid properties. PDMS is an optically-clear and inert material that faithfully replicates surface features to nanometer scales. Using PDMS mimics of the surfaces also reduced the confounding variations found on natural plant surfaces and is a suitable material for imaging purposes.

Evaporating droplets in either water or surfactant Tween 80 were used as the system to deposit *Salmonella enterica* sv. Enteritidis, an important foodborne pathogen, and polystyrene latex microspheres (diameter = 2  $\mu\text{m}$ ), used as an ideal particle for comparison to the bacteria, on the different surfaces. Tween 80, a nonionic surfactant, allowed for the manipulation of surface tension of the droplet suspension to consider the effect of capillary forces on particle transport and deposition. Tween 80 is also approved by the FDA for use in washing fruits and vegetable surfaces and has been researched as an alternative method to chlorine but with limited success.

In Chapter 2 of this work, transport and deposition of bio(colloids) is considered in the context of fresh produce safety by using PDMS Lettuce and PDMS Spinach surfaces compared to smooth, flat PDMS and Glass surfaces. In Chapter 3, PDMS micropatterns of raised pillars, depressed dots, and grooved features were compared to smooth, flat PDMS and Glass surfaces to further explore the role of surface topography/roughness in addition to the other factors influencing particle

transport and deposition. In addition to the visualization of evaporation and resulting patterns, the physicochemical characteristics, surface roughness and hydrophobicity, along with the evaporation characteristics, evaporation time, contact line behavior, and droplet contact areas, were quantified. Taken together, it was demonstrated in this work that:

1) The surface properties (roughness and hydrophobicity) strongly influenced the spatiotemporal deposition of colloids and *Salmonella enterica* sv. Enteritidis. Deposition pattern morphology of the bacteria and colloids were clearly different based on surface architecture and roughness. Surface roughness features caused contact lines of the evaporating droplets to pin at the features, where transport to these regions and ultimately deposition was observed. Additionally, surface hydrophobicity, which is influenced by surface roughness, influenced the thickness of water films on the surfaces, which in turn altered transport behavior and resulting deposition patterns.

2) The transport behavior between colloids and *Salmonella* observed in this study demonstrated that bacteria better mobilize with the contact line and form distinct rings around the final contact line area, where the bacteria were rapidly transported during the last stages of droplet evaporation. Although a detailed quantitative comparison was not explored in this work, (bio)colloid size and shape likely play a role. When choosing a colloid as surrogate bacteria, researchers should use particles that have similar properties such as size and shape;

3) The addition of surfactant Tween 80 altered the transport and deposition behavior of *Salmonella* and colloids due to a reduction in capillary forces by decreasing the surface tension and film thickness, which changed the way the air-water-interface interacted on the particles and solid surfaces. In effect, the contact line

could not mobilize the particles and thus lead to deposition of particles over a larger area on the surfaces used.

4) Finally, no single parameter was solely responsible for the transport and deposition of particles in these studies. The combination of surface, solution, and particle properties all influenced the hydrodynamic flow, film thickness, and capillary forces in the evaporating droplets that dictated how particles were transported and deposited on the surfaces.

Visualizing the transport and deposition of (bio)colloids at contact lines, here by using evaporating droplets, improved the understanding of the factors influencing (bio)colloid interactions on surfaces. The food industry can devise improved strategies for decontamination of produce surfaces with the fundamental knowledge explored in this work. Future research can expand upon the work developed here with modeling and more detailed experiments to further develop these contributing factors in (bio)colloid transport and deposition, including ways to manipulate these surface-particle interactions.

# Chapter 1

## LITERATURE REVIEW

### 1.1 Introduction

A review of the literature surrounding produce contamination by human bacterial pathogens is summarized below with the relevant theoretical considerations for the factors influencing bacteria and colloid transport to and deposition on surfaces as a function of system properties, including surface topography, roughness, and hydrophobicity, and the conditions of the bulk fluid.

### 1.2 The Dilemma with Fresh Produce

A diet of fresh fruits and vegetables each day can prevent nutrient deficiencies and chronic conditions such as heart disease, cancer, diabetes, and obesity (WHO/FAO, 2015). In their latest communication, the World Health Organization (WHO) and Food and Agriculture Organization (FAO) reported that *insufficient* consumption of fresh produce accounted for “14% of gastrointestinal cancer deaths, [...] 11% of ischemic heart disease deaths, and about 9% of stroke deaths globally” (WHO/FAO, 2015). Fresh produce consumption has increased over the last few decades (Jung, Jang, and Matthews, 2014), and as agricultural production is scaled up to meet global needs, so, too, must efforts to minimize food safety risks.

Unfortunately, fresh fruits and vegetables cause the highest number of illnesses and the largest outbreaks out of all food commodities, including meat products (Center for Science in the Public Interest 2015 Outbreak Alert Report,

[www.cspinet.org/resource/outbreak-alert-2015](http://www.cspinet.org/resource/outbreak-alert-2015); Doyle and Erikson, 2008). The pathogens most commonly implicated in outbreaks involving fresh produce include *Salmonella* spp., *E.coli* O157: H7, and *Listeria monocytogenes* (Callejon et al., 2015; Sapers, Matthews, and Gerba, 2014). These pathogens can survive and persist in the environment, utilizing unique strategies such as biofilm formation that enable their survival throughout processing (Brandl, 2006; Critzer and Doyle, 2010; Kumar et al., 2015, 2017, 2018). Moreover, these pathogens may be introduced to fresh produce anywhere along the farm-to-fork continuum, which makes surveillance and mitigation efforts challenging (Heaton and Jones, 2008; Berger et al., 2010; FAO/WHO, 2008). These modes of introduction include irrigation water, run-off from nearby animal husbandry, soil and sediment, food handlers, storage, shipping containers, washing solutions, packaging conditions, and other post-harvest handling procedures (Kumar et al., 2017a, 2017b; Berger et al., 2010; Heaton and Jones, 2008; Sapers, Matthews, and Gerba, 2014; James, 2016). Of all produce-associated outbreaks, leafy greens have the highest rate and account for 26% of all foodborne illnesses (Painter et al., 2013).

These outbreaks have a severe economic impact: in the United States alone, product recalls, reduced economic growth, hospitalizations and other medical costs, surveillance efforts, and a reduction in sales for the causal product costs billions annually (CDC.gov). Fresh produce poses particular obstacles for food safety: minimal processing of raw fruits and vegetables and ineffective washing methods make complete decontamination of foodborne hazards difficult, and the risk of infection is greatest for the very young children, the immunocompromised, and the elderly (CDC.gov). As Barbara Mahon, MD, MPH Deputy Chief, Enteric Diseases

Epidemiology Branch at the Center for Disease Control, said: "...[F]or the most vulnerable people, food safety can literally be a matter of life and death."

### **1.3 The Need for Improved Decontamination Strategies**

Because vegetables and fruits are often consumed raw, the onus is on growers, shippers, processors, and retailers to safeguard the product and support consumer confidence in the industry (James, 2016). Scientists, government, and industry have devoted significant efforts to advise proper guidance and good agricultural practices (FDA/CFSAN, 2001a) and yet multiple outbreaks continue to occur each year.

Currently, the produce industry sanitizes with chlorine-based products added to wash water in dump or flume tanks at concentrations ranging from 50-200 ppm (Sapers, Matthews, and Gerba, 2014; James, 2016). Before bagging, fruits and vegetables brought in from harvest are dumped onto a hopper and conveyed into water flumes containing chlorinated water that undergoes a triple-wash process: 1) removal of large debris via washing with mild agitation in weakly-chlorinated water, 2) decontamination via washing with a higher concentration of chlorinated-water, and 3) rinsing via chlorine-free water (Sapers, Matthews, and Gerba, 2014; James, 2016).

Despite being a low-cost method, chlorination typically reduces only 1-2 log of bacterial colony-forming units (CFUs) per gram of fresh produce surfaces (Sapers, Matthews, and Gerba, 2014; James, 2016). Wash water may also cause cross-contamination (Jung, Jang, and Matthews, 2014). Notably, cut produce such as bagged lettuce is particularly at risk for contamination due to the increase in nutrient-rich attachment sites (Sapers, Matthews, and Gerba, 2014; Brandl, 2008). There's some promise in alternative methods to chlorine that include electrolyzed oxidizing water (e.g., Guentzel et al., 2008), ozone and ultraviolet light (e.g., Kumar et al., 2015),

ozone and plant antimicrobials (e.g., Gündüz et al., 2010; Kumar et al., 2018), and fatty acids (e.g., Kumar et al., 2017). However, most alternative methods to chlorine have comparable sanitation rates and similar inability to remove bacteria attached to produce surfaces (Kumar et al., 2017; Gibson et al., 1999; Beuchat et al., 2004; Wang et al., 2012; Sapers, Matthews, and Gerba, 2014; Meireles et al., 2016). For example, Sagong et al. (2011) exposed Iceberg lettuce contaminated with *Bacillus cereus* spores to combinations of ultrasound and Tween surfactants. Their most successful combination, 0.1% Tween 20 with ultrasound, only achieved 1 log greater reduction in CFU/g than 200 ppm chlorine (2.49 log CFU/g compared to ~0.7 log CFU/g, respectively). Huang et al., (2018) evaluated the effectiveness of ultrasound with and without surfactant Tween 20 on the removal of *E.coli* O157:H7 and other bacteria on lettuce and found that the combination treatment did not improve pathogen removal compared to water and only achieved a 0.5 log CFU/cm<sup>2</sup> reduction.

Similar methods can result in different efficacies for different produce surfaces, which may be due to the differences in the physicochemical properties of each produce surface (Lima et al., 2013; Wang et al., 2012; Fernandes et al., 2014). For example, Wang et al. (2009) characterized the surface roughness and hydrophobicity of apple, avocado, orange, and cantaloupe. They inoculated the various fruit surfaces with *E. coli* O157:H7 and exposed the surfaces to water, acidic electrolyzed water (AEW), and peroxyacetic acid (POAA). They found a variation in the residual bacteria population within a given treatment based on the type of fruit surface. In AEW, apples had a residual bacteria population of  $2.60 \pm 1.22$  log CFU/cm<sup>2</sup> compared to cantaloupe, which had  $5.98 \pm 0.03$  log CFU/cm<sup>2</sup>. For water,

apple had a residual bacteria population of  $2.61 \pm 0.20$  log CFU/cm<sup>2</sup> while cantaloupe had  $6.03 \pm 0.29$  log CFU/cm<sup>2</sup>, which are comparable to the AEW treatment.

Plant surface features, such as the crevices and grooves, may offer protective sites for attached bacteria against sanitation treatments (Flemming et al., 2016; Srey et al., 2013; Heaton and Jones, 2008; Yaron and Romling, 2014). Human pathogens are further protected from chemical treatments if they form biofilms on plant surfaces (Kumar et al., 2017; Yaron and Romling, 2014), which can further obfuscate removal (Shi and Zhu, 2009; Sapers, Matthews, and Gerba, 2014). To date, there are only a few studies on the influence of physicochemical factors on bacteria adhesion to fruits and vegetables (e.g., Lima et al., 2013; Wang et al., 2009, 2012; Zhang et al., 2014; Lazouskaya et al., 2016).

#### **1.4 The Physicochemical Characteristics of Plant Surfaces and Their Role in Human Bacteria-Plant Interactions**

Water droplets on plant surfaces may contain nutrients, soil particles, and microbes (Koch et al., 2008; Wang et al., 2009, 2012; Lazouskaya et al., 2016; Zhang et al., 2014; Beuchat et al., 2002; Doan and Leveau, 2015). The characteristics of plant surfaces, including topography, roughness, and hydrophobicity, dictate where water, and thus nutrients and bacteria, localize and form strong attachment sites (Crawford et al., 2012; Koch et al., 2008; Whitehead and Verran, 2006), which may have a stronger contribution to bacterial adhesion compared to active bacterial mechanisms (Crawford et al., 2012; Solomon and Matthews, 2006; Wang et al., 2009). The Lotus plant (*Nelumbo nucifera*) has a very high contact angle of  $\sim 145^\circ$  and is the most famous example of how the architecture of the surface features, the presence of surface

roughness and cuticular wax structure, allows for water droplets “roll off” the surface, carrying soil and other particulates with it (Koch et al., 2008; Zhang, 2013).

Plant surface features can be characterized by standard physicochemical principles of surface topography, roughness, and hydrophobicity (Koch et al., 2008). Below follows a discussion regarding how plant surfaces are quantitatively characterized and how these parameters influence human pathogen associations on the surfaces of fresh produce.

#### 1.4.1 Hydrophobicity

Plant surface hydrophobicity can be determined empirically by the equilibrium contact angle, which forms at the solid-liquid-vapor triple-point of a liquid droplet on a surface due to a force balance of the interfacial tensions between solid-vapor (SV), solid-liquid (SL), and liquid-vapor (LV). The equilibrium contact angle is given by the classic Young’s equation in **Equation 1.1**:

$$\cos \theta = \frac{\gamma_{SV} - \gamma_{SL}}{\gamma_{LV}} \quad (1.1)$$

where  $\theta$  is Young’s contact angle and  $\gamma$  is the interfacial tension between two phases. Knowing the contact angle allows researchers to classify surfaces as hydrophobic or hydrophilic: surfaces are hydrophilic if  $\theta < 90^\circ$  and hydrophobic if  $\theta > 90^\circ$ . Most aerial plants surfaces are covered in a waxy, extracellular membrane called the cuticle (Koch et al., 2008). The structure and composition of the cuticle make most, but not all, plant surfaces hydrophobic to varying degrees (Koch et al., 2008).

To date, there are only few studies on the influence of plant surface hydrophobicity on attachment and retention of human bacterial pathogens. Wang et al. (2009) characterized the surface hydrophobicity of different fruits and found that apples, avocados, oranges, and cantaloupes had contact angles  $\theta$  of  $77.27 \pm 4.57$ ,

78.23 ± 8.37, 56.33 ± 5.16, and 47.20 ± 18.52, respectively, meaning all of their surfaces were hydrophilic. They correlated the hydrophobicity values, along with surface roughness  $R_a$  values, to *E. coli* O157:H7 adhesion and found that since apples and avocados had similar contact angle values but different  $R_a$  values, surface roughness may be a stronger contributing factor to *E. coli* O157:H7 adhesion. In Lazouskaya et al. (2016), all of the surfaces tested were hydrophobic with contact angles  $\theta \sim 90 - 110^\circ$ , including orange, apple, tomato, and spinach, except for lettuce, which had a contact angle  $\theta \sim 50^\circ$ . They concluded that there was a strong connection between colloid retention and water retention and distribution on all the surfaces (except for apple), which was dictated by hydrophobicity *and* surface roughness (discussed further in 1.4.2). A summary of selected characterizations of surface hydrophobicity for a selected number of fruits and vegetables is summarized in **Table 1.1**.

The breakdown of epicuticular wax may be partially responsible for increased susceptibility of plants to bacterial adhesion. A study by Brandl et al. (2008) determined that middle-aged lettuce leaves were 27x more contaminated with *E. coli* O157:H7 than younger leaves due to the breakdown of epicuticular wax located on the leaf surface. As plant leaves age and cuticular wax breaks down, and the plant surface becomes more wettable, which may increase plant susceptibility to bacterial colonization (Lindow, 2004; Koch et al., 2008; Brandl, 2008).

Studies determining the influence of bacteria cell surface hydrophobicity indicate a connection between hydrophobic bacteria and attachment to hydrophobic surfaces (Solomon and Sharma, 2009). However, because bacteria cell surface hydrophobicity strongly depends on the strain, serotype, growth media, and growth

conditions (Boyer et al., 2007; Goulter et al., 2009; Rijnaarts et al., 1993; Hassan and Frank, 2004), connections between cell surface hydrophobicity and attachment are not straightforward (Wang et al., 2012) and are not considered further in this discussion.

**Table 1.1** Characterized surface properties of selected fruits and vegetables

Surface	Roughness, $\mu\text{m}$	Hydrophobicity, $\theta_e$	Reference
Apple	$1.43 \pm 0.13 (R_a)$ < 2 ( $S_a$ )	$77.27 \pm 4.57$ ~ 100	<i>Wang et al., 2009</i> <i>Lazouskaya et al., 2016</i>
Avocado	$9.58 \pm 0.27 (R_a)$	$78.23 \pm 8.37$	<i>Wang et al., 2009</i>
Cantaloupe	$14.18 \pm 0.25 (R_a)$ > 3 ( $S_a$ )	$47.20 \pm 18.52$ ~ 90 – 110	<i>Wang et al., 2009</i> <i>Lazouskaya et al., 2016</i>
Lettuce	~ 4 ( $S_a$ )	~ 50	<i>Lazouskaya et al., 2016</i>
Orange	$10.94 \pm 0.07 (R_a)$ < 2 ( $S_a$ )	$56.33 \pm 5.16$ ~100	<i>Wang et al., 2009</i> <i>Lazouskaya et al., 2016</i>
Spinach	~ 4 – 6 ( $S_a$ ) 6.88 ( <i>RMS</i> )	~90 – 100 ~ 60 – 65	<i>Lazouskaya et al., 2016</i> <i>Zhang et al., 2014</i>
Tomato	< 2 ( $S_a$ )	> 100	<i>Lazouskaya et al., 2016</i>

$R_a$  is the arithmetic average of the absolute values of the profile height deviations from the mean line (<http://www.harrisonep.com/electropolishing-ra.html>)

$S_a$  is the surface area analog of  $R_a$

*RMS* is the root mean square average of the profile height deviations from the mean line (<http://www.harrisonep.com/electropolishing-ra.html>)

#### 1.4.2 Topography and Roughness

Beneath the cuticle are the plant epidermal cells. These cells vary in size, shape, height, and width and give rise to surface topography and roughness (Koch et al., 2008). As summarized by Wang et al., (2009):

The topography at a stereo- microscopic scale is dictated by huge undulations on the surface that involve tens or hundreds of cells, almost

like huge cavernous valleys. At a more local scale, topography is represented by the shape and curvature of the anticlinal walls of individual epidermal cells. Both scales may impact the ability of a water drop and hence bacteria (assuming in aqueous state) to arrive on any particular region of the surface. At an even smaller scale [...] topography is determined by roughness on the surface of individual epidermal cells. At this scale, the surface roughness and surface hydrophobicity strongly influence the movement of the water/bacterial suspension, and thus the distribution of bacteria.

A non-destructive method for analyzing surface roughness of plants is confocal microscopy (Wang et al., 2009; Lazouskaya et al., 2016). Confocal microscopy, unlike contact-mode profilometers used in nanofabrication, can take 3-D optical slices of the plant surface and record the height variations with depth in the images without damaging the plant tissues. Software programs such as Zen2010d (Zeiss, Jena, Germany) have built-in topography functions that automatically analyze surface roughness based on the obtained confocal images. One of the most common surface roughness parameters is the mean height roughness,  $S_a$ , (Crawford et al., 2012; Whitehead and Verran, 2006), defined as the absolute difference in height of each point compared to the arithmetical mean of the surface and is the surface-area analog to  $R_a$  (Keyence, <https://www.keyence.com/ss/products/microscope/roughness/surface/parameters.jsp>), given by **Equation 1.2**:

$$S_a = \frac{1}{N_x N_y} \sum_{i=1}^{N_x} \sum_{j=1}^{N_y} [z(x_i, y_j)] \quad (1.2)$$

where  $N_x, N_y$  are the numbers of points in x- or y-direction, and  $z(x_i, y_j)$  is the height difference between each point and the reference surface (Lazkouskaya et al., 2016; Wang et al., 2009). Researchers have successfully applied microscopic methods for evaluating surface roughness to a variety of natural and fabricated plant surfaces, including spinach (Lazouskaya et al., 2016; Zhang et al., 2014), lettuce (Lazouskaya et

al., 2016), oranges (Wang et al., 2009; Lazouskaya et al., 2016), tomato (Lazouskaya et al., 2016; Wang et al., 2009), and more. The roughness values obtained for different fruits and vegetable surfaces are summarized in **Table 1.1**.

Research indicates a strong, positive correlation between colloids/bacteria attachment and surface roughness of fresh produce (Wang et al., 2009, 2012; Lazouskaya et al., 2016; Zhang et al., 2014) and other surfaces (Katsikogianni and Missirlis, 2004). In Wang et al. (2009), the authors determined a positive, linear correlation ( $r=0.96$ ) of roughness  $R_a$  and *E. coli* O157:H7 adhesion to fruit surfaces. They characterized the surface roughness,  $R_a$ , for apple, avocado, orange, and cantaloupe and found that  $R_a$  was positively correlated to bacterial adhesion rate. For example, the  $R_a$  for apples was  $1.43 \pm 0.13$  and  $14.18 \pm 0.25$  cantaloupe, and the subsequent adhesion rates in water were  $490 \pm 6$  and  $920 \pm 6$ , respectively. Adhesion rate was defined as the ratio  $1000 \times (\text{residual bacteria counts} / \text{initial bacteria counts})$  (Wang et al., 2009). Lazouskaya et al. (2016) characterized the surface roughness  $S_a$  and hydrophobicity of tomato, orange, apple, lettuce, spinach, and cantaloupe and correlated the values to the retention of spherical polystyrene colloids used as bacterial surrogates. They divided their surfaces into two roughness scales:  $S_a < 2 \mu\text{m}$ , which included tomato, orange, and apple, and  $S_a > 3 \mu\text{m}$ , which included lettuce, spinach, cantaloupe. They concluded that there was a strong connection between colloid retention and water retention and distribution on all the surfaces (except for apple), which was dictated by surface roughness and hydrophobicity.

Most often reported is that bacterial adhesion occurs between the valleys and grooves of protruding features rather than at the top of features (Hou et al., 2011; Lu et al., 2016; Perni and Prokopovich, 2013), indicating a potential relationship between

cell surface topography, as in the shape curvature of cells, and bacterial adhesion. Research on bacterial adhesion and retention on simpler surfaces have also identified similar connections between surface roughness and hydrophobicity. Hou et al. (2011) evaluated *E. coli* RP437/pRSH103 adhesion onto polydimethylsiloxane surfaces with microtopographic patterns of varying dimensions and spacing. They found that cells preferentially attached and formed biofilms in the valleys between protruding features regardless of the dimensions of the features and spacing. However, they noted that attachment on protruding features occurred for patterns larger than 20 x 20  $\mu\text{m}$ , indicating the influence of pattern dimensions on cell attachment. Hsu et al. (2013) found that *E. coli*, *L. innocua*, and *P. fluorescens* attachment on micropatterned circular wells (diameter of 500 nm and interwell spacing of 200 nm), rectangular wells (dimensions of 1 x 1.5  $\mu\text{m}$  and interwell spacing of 2  $\mu\text{m}$ ), wide wells (1 x 2  $\mu\text{m}$  and interwell spacing of 500 nm), and smooth silica substrates demonstrated different cell morphologies and attachment as a function of topography and suggested that bacteria may utilize different mechanisms of attachment in response to surface. Bacteria also appear in aggregates at the base of major topographical structures, such as these epidermal cell wall junctions, trichomes, and stomata (Beatie and Lindlow, 1999; Lindlow, 2004). This type of attachment may offer protection from washing treatments: Crawford et al. (2012) noted that grooved and pitted surfaces can shelter bacteria from external forces. In Solomon and Matthews (2006), live and dead *E. coli* O157:H7 attachment on lettuce found that the surface properties of lettuce entrapped the bacteria within grooved features, which protected the cells from washing treatments and lead to retention. Wang et al. (2009) demonstrated that *E. coli* O157:H7 attached to and became entrap within the grooves and cavities of various

fruits due to the increased surface area, which also offered protection from shear forces.

### **1.5 Particle Transport and Deposition on Surfaces from Evaporating Sessile Droplets**

Colloids are defined as particles with effective diameters ranging between 10 nm and 10  $\mu\text{m}$ . Bio-colloids, such as *Salmonella* spp. and other bacteria, fall into this broad classification. Research into the mechanisms influencing (bio)colloid transport and retention indicate the important contributions of surface properties in addition to the hydrodynamics and bulk fluid properties of the system (Bradford and Torkzaban, 2008). Studies often use column experiments for understanding transport and retention in unsaturated systems (e.g., porous media) but less is known for transport on plant surfaces and other bio-interfaces, for which column experiments are not suitable. Currently, models disregard how confined waterscapes can influence bacterial and particle deposition, attachment, and subsequent removal in the context of fresh produce (Doan and Leveau, 2015). One that can be used to study particle transport and deposition is to use evaporating droplets, which is a dynamic process that can be applied to a variety of different surfaces. Rijnaarts et al. (1993) noted how the transport of microbes from bulk to surfaces is more efficient in dynamic systems (convection and diffusion) than static batch systems (diffusion-only) and is affected by the physicochemical interactions of the bacteria and the surface. A detailed discussion regarding the use of droplets to model (bio)colloid transport and deposition follows.

### **1.5.1 Sessile Droplet Evaporation**

A sessile droplet is a liquid droplet on a solid surface and is characterized by its contact angle, radius/diameter, and height. Droplets on surfaces will eventually evaporate caused by a variety of factors such as the ambient conditions, physicochemical properties of the substrate, and properties of the fluid (Parsa et al., 2018). Multi-component water droplets, such as those containing particles like bacteria and colloids, can also influence the evaporation dynamics (Thiele, 2014).

Two main flow regimes occur in evaporating droplets: capillary flow and Marangoni flow (Parsa et al., 2018). Factors that can influence the flow within evaporating droplets include the properties of the substratum, solutions with multiple phases, and temperature (Parsa et al., 2018). In the capillary flow regime, a convective flux directs liquid to the edges of the droplet, where the contact line is pinned on the surface. The evaporation rate is higher at the edges of the droplet compared to the center, which causes an outward flow from the center of the droplet to this region to replenish the evaporated fluid. In Marangoni flow, there is a convective current that redirects the fluid at the edges back to the top of the droplet. Marangoni flow occurs when there are gradients in surface tension that can be induced by temperature gradients or the addition of a surfactant (Still et al., 2012; Hu and Larson, 2006; Yildirim Erbil, 2015). Demonstrated by Hu and Larson (2006), the temperature gradients in a droplet depend on the droplet contact angle, indicating the combined role of surface and solution properties.

Researchers (e.g., He et al., 2017; Hwang et al., 2017) have characterized the stages of droplet evaporation in four broad categories, 1) constant contact radius/line (CCR/CCL); 2) constant contact angle (CCA); 3) mix-mode; and 4) stick-slip (Parsa et al., 2018). These evaporation modes, described below, are based on the underlying

hydrodynamics of the evaporation process and can help to understand the influence of surface and particle properties in transport and deposition.

1) Constant contact radius/line (CCR/CCL) mode: the contact line is pinned (immobilized) and the contact radius is constant, causing a convective flow to the edges and a decrease in the droplet height with time;

2) Constant contact angle (CCA) mode: the droplet height and radius decrease with time as the droplet evaporates and maintains a constant contact angle;

3) Mix-mode: a combination of the two previous modes, where both the radius and contact angle simultaneously change, or the evaporation proceeds from one mode to another, typically from CCR  $\rightarrow$  CCA;

4) Stick-slip: the droplet is in CCR mode where the contact line is pinned (stick phase) but then de-pins (slip phase) at a threshold contact angle to a new position, thereby decreasing the contact radius. The contact line may pin and de-pin again, and this cycle can continue throughout the evaporation event. The majority of the droplet evaporation event exists in the stick/pinned phase.

Although the exact mechanisms are complex and not fully elucidated, droplet pattern formation resulting from evaporating droplets can provide a lot of information regarding particle transport and mobilization processes (Parsa et al., 2018; Thiele, 2014). Similar factors influencing evaporation dynamics also affect the resulting deposition pattern after a droplet evaporation event. The work of Deegan et al. (2000) demonstrated the mechanisms behind the coffee ring pattern, the most ubiquitous deposition pattern (Parsa et al., 2018). They described how particles are carried to the pinned contact line by capillary flow, accumulate, deposit, and result in a concentric ring at the edges. This often occurs on hydrophilic surfaces and is characterized by the

“CCR” evaporation mode (Parsa et al., 2018). Evaporating droplets on hydrophobic surfaces tend to form “dot” or uniform patterns (Parsa et al., 2018). Due to the lack of wettability (i.e., smaller contact area), there is less convective flow to the edges and a faster evaporation rate at the apex of the droplet (Zhao and Yong, 2017). Evaporation tends to follow the constant contact angle (CCA) mode, where the wetted contact area shrinks without a change in the contact angle (Parsa et al., 2018). Since the edges are not pinned, there is no particle flux to this region of the droplet. Particles may aggregate in the bulk of the droplet due to the lack of flow to the edges and an increase in particle-particle interactions (Michen et al., 2014; Parsa et al., 2018) and may inhibit their ability to be transported to the contact line. Marangoni flow may also be present and redirect fluid to the center of the droplet (e.g., Still et al., 2012). When the droplet height decreases to a critical contact angle and film thickness, capillary flow to the edges can occur if the droplet edges pin (Parsa et al., 2018).

Surface roughness can cause pinning of contact lines that lead to the deposition of particles (Paxson and Varanasi, 2013) and is demonstrated to influence attachment and detachment of colloids (e.g., Shen et al., 2012, 2013). Surface irregularities, such as depressions, can temporarily pin/immobilize the contact line and cause an evaporative flux at this local region. This can drive particles to surface features and lead to deposition. At a critical contact angle, the contact line will de-pin (slip) to a new equilibrium position. As evaporation progresses, the contact line can pin again (stick) and similarly de-pin, and the process can repeat throughout the evaporation event. The stick-slip modal can lead to deposition as the contact line “jumps” to a new position. The resulting deposition pattern can resemble multiple coffee rings or periodical deposits based on the roughness of the surface. It should be noted that

contact lines can also temporarily self-pin on surfaces without roughness as discussed previously (e.g., Deegan, 2000). This phenomenon would also depend on the thickness of liquid films on the surface, which is influenced in part by the surface properties.

Particle characteristics (e.g., concentration, shape, size) can also influence the resulting deposition patterns and similarly reflect the dynamics in flow/transport, and deposition from the bulk fluid to the substrate. Particle concentration can change the number of particles at pinned contact lines (Thiele, 2014). Sefiane et al. (2010) demonstrated that the thickness of the ring in coffee ring patterns increased with increasing  $\text{Al}_2\text{O}_3$  concentration. Particle-particle interactions (e.g., aggregation) would also dictate if the hydrodynamics can transport particles with the fluid fluxes to the air-water-solid interface (Parsa et al., 2018). For example, Yunker et al. (2011) observed a decrease in coffee ring formation in evaporation of droplets containing both ellipsoidal and spherical particles. They observed particle-particle interactions between ellipsoidal particles that lead to aggregation in the bulk fluid and prevented transport to the edge of the contact line, unlike the spherical colloids. Work by researchers (e.g. Liu et al., 2010; Aramrak et al., 2013) have demonstrated the influence of particle shape in mobilization in porous media: if the minor axis of an ellipsoid is smaller than the diameter of a spherical colloid, ellipsoid particles can align with flow regimes and demonstrate different transport behavior compared to spherical colloids. Particles may also pin the contact line and temporarily immobilize it, which may further drive transport of particles to this region (Thiele, 2014). Further, colloids are commonly used as surrogate bacteria (e.g., Lazouskaya et al., 2016), but the validity of colloids as substitute particles in transport, deposition, and retention is not well vetted. Bacteria may be on the size order of colloidal particles but are non-

ideal; they are deformable and biologically active with varying cell surface features (e.g., pili, extracellular slime production, fimbriae) and surface charge that are strongly dependent on the surrounding environmental conditions. Biocolloids differ from the classic Derjaguin–Landau–Verwey–Overbeek (DLVO) theory, which assumes the particle is a smooth and spherical, rigid abiotic colloid (Verwey and Overbeek, 1948). Similar to Yunker et al (2011) who used spherical and ellipsoidal particles in the same system, comparing colloids and bacteria in the same system is a way to better understand the differences in the transport, adhesion, and retention and determined the important criteria for colloids as surrogates for bacteria in studies.

Currently, there are a few reports on bacterial transport and deposition in evaporating droplets. Thokchom et al., 2014 determined the effect of chemotaxis on flow and pattern formation in evaporating droplets containing live and dead *E. coli*. Without a chemoattractant, flow regimes and resulting deposition patterns for live and dead *E. coli* were similar, but in the presence of a chemoattractant, there was a concentration of bacteria towards the nutrient source, which resulted in a unique deposition pattern compared to that of the dead *E. coli*. In Sempels et al. (2013), droplets containing *Pseudomonas aeruginosa* lead to a homogeneous deposition of the bacteria upon drying due to the presence of biosurfactants, which induced oscillatory flows within the droplet. Interestingly, Hennes et al. (2017) visualized active de-pinning of *Bacillus subtilis*-containing droplets at the contact line, suggesting the ability of motile bacteria to potentially compete with hydrodynamics and capillary forces. The motility of bacteria, in addition to other biological factors, precludes the applicability of the classic DLVO theory (Engström et al., 2015). In Wang and Or (2010), capillary forces confined bacteria mobility, and suggested that free swimming

microbes are not probable in most unsaturated systems (Engström et al., 2015). More reports correlating the qualitative and quantitative visualization of bacteria transport and deposition will improve the ability to model bacteria from current transport, adhesion, and retention theories that incorporate the inherent biology of living particles.

## **1.5.2 Capillary Forces and Film Thickness in Particle Transport and Deposition**

Particles suspended in droplets on plant surfaces experience a range of interfacial forces that dictate if they will move with the droplet contact line or deposit on the surface. They may be pinned by the forces of the air-water interface or be immobilized by interfacial interactions of the solid and particle. The forces involved in these dynamic interactions include adhesion force ( $F_A$ ), the physicochemical interaction force between the colloid and the substrate; hydrodynamic drag force ( $F_D$ ), the force exerted on an attached spherical particle in an imposed shear flow; and the surface tension force (i.e., capillary force;  $F_\sigma$ ) which acts along the contact line between the colloid and air-water-solid interface, or AWSI (Lazouskaya et al., 2013). Here, the role of capillary forces and film thickness are considered.

### **1.5.2.1 Capillary forces**

Capillary forces are influenced by the surface tension of the bulk fluid, the size and shape of colloids, and the contact angles formed by the air-water-solid interface and colloid (Lazouskaya et al., 2013). Capillary force, also called surface tension force, is expressed in **Equation 1.3** as,

$$F_\sigma = 2\pi r \sigma \sin\phi \sin(\theta - \phi) \quad (1.3)$$

where  $\sigma$  is the liquid surface tension,  $\theta$  is the dynamic contact angle on the colloid surface, and  $\phi$  is the angle determining the AWI position on the colloid surface. Thus, the magnitude and direction of the surface tension force depends on the colloid radius, surface tension, and colloid and substrate dynamic contact angles. Also, a balance between capillary force, drag force, and the interfacial interactions of the particle-solid-liquid at the evaporating contact line are critical parameters for the deposition or mobilization with the contact line. For example, as evaporation progresses and the contact line moves, a capillary force is exerted on the colloids in contact at the AWSI. If this force is stronger than the particle-surface interactions, then the colloids can mobilize with the contact line. If the capillary forces are weak and/or the adhesion forces strong, the colloids will deposit or remain on the surface. From **Equation 1.3**, decreasing the liquid surface tension,  $\sigma$ , by adding a surfactant (e.g., Tween 80) can reduce the surface tension forces that interact with a colloid at the AWSI. This would influence if the particle can be mobilized with the contact line or deposit on the surface, in addition to the contributions from the surface properties. Additionally, altering the bulk fluid properties and properties of the surface can change the contact angles of the surface and position of the AWI and subsequently influence the interfacial forces experienced by a particle that impacts transport and deposition.

#### **1.5.2.2 Film thickness**

The thickness of water films, influenced by both the surface and solution properties, plays an additional role in colloid transport, deposition, and retention. Although the mechanisms are complex and yet to be realized for surfaces with heterogeneities, some application of the current state-of-art can be made in the context

of particle transport to and deposition on surfaces from evaporating droplets. In the simplest case, transport of particles to contact lines occurring for droplets evaporating on smooth, hydrophilic surfaces are a result of hydrodynamic forces (dominated by capillary flow). Particles at the contact line accumulate at this region as the droplet evaporates and the contact line mobilizes. Here at the edges, colloids experience a thin film compared to the rest of the droplet. At this stage, the contact line is pinned, and colloids experience the interfacial interactions between the AWI and the surface. Colloid retention at this region is enhanced by these interactions between the colloids and surface due to this close interfacial contact and can also be influenced by the particle-particle interactions that lead to aggregation. For example, as particle concentration at local region increases, the receding contact line can become thinner and thinner. If the film is thick enough, and the surface tension force is greater than the hydrodynamic drag and adhesion forces, particles will mobilize with the contact line. If the surface tension force is weaker, particles will deposit and retain at surface features. Other factors such as surface roughness, hydrophobicity, and particle shape alter this transport to and deposition from the contact line by changing the thickness of water films, which in turn influences the hydrodynamics that affect particle transport to and from the contact line.

Film straining also affects transport and retention processes due to an imposition of thin water films at the air-water-solid interfaces (Lazouskaya, Jin, and Or, 2006). Although the mechanisms are not fully elucidated, research has shown that the combination of hydrodynamics, solution chemistry, particles properties (e.g. type and size), and particle concentration all factor into (bio)colloid retention at air-water-

solid interfaces due to film straining (Bradford and Torkzavan, 2008; Lazouskaya, Jin, and Or, 2006). As stated in Wang and Or (2010),

As film thickness becomes similar to bacterial size, strong capillary forces emerge and result in pinning resistance hindering bacterial motility.

Lazouskaya and Jin (2008) demonstrated that hydrophilic colloids retained in thin water films at the edge of the air-water-solid interface instead of the air-water interface, which highlights the importance of the contributions from the surface component (also demonstrated in Xu et al., 2016). Also, Lazouskaya et al. (unpublished) noted that the droplet deposition patterns between carboxylate-modified and sulfate-modified colloids, which had the same diameter of 1  $\mu\text{m}$ , on glass slides were overall similar, and indicated that the colloid contact angle (i.e., hydrophobicity) of the colloids was not essential to affect the colloid behavior and deposition at the contact line. Thus, other particle characteristics such as size and shape may have more impact on the factors, such as capillary forces and film thickness/straining, influencing colloid transport, deposition, and retention at air-water-solid interfaces.

In summary, the contact line behavior at solid-liquid-particle and air-solid-particle interfaces is critical for the transport and deposition of particles and is influenced by the physicochemical properties of the surface and particles, the solution conditions and hydrodynamics, and the forces interacting at these interfaces. These factors in particle transport and flow have not been explicitly characterized in the context of plant surfaces and other bio-interfaces. Understanding these processes from this physicochemical perspective is an opportunity to apply these principles to understanding the fundamental processes behinds particle flow, transport, and retention in a variety of applications.

## 1.6 Research Motivation and Approach

This research aims to address the underlying mechanisms contributing to particle transport and deposition as influenced by the properties of the surface, solution, and particle. In **Chapter 2**, a perspective of fresh produce safety is considered while in **Chapter 3**, a more fundamental approach is considered due to the applicability of this work to broader research areas.

Here, microscopic visualization was employed to observe evaporating droplets of either DI water or surfactant Tween 80 (100 ppm, or 0.01%) containing colloids and *Salmonella enterica* sv. Enteritidis, an important foodborne pathogen, on polydimethylsiloxane (PDMS) molds of natural produce surfaces, spinach (*S. oleracea*) and lettuce (*L. sativa*) and simple micropatterns, raised pillars, circular depressions, and grooves, compared to flat PDMS and glass surfaces. PDMS faithfully replicates surface topography and roughness and is inert and optically transparent, making it suitable for microscopy. The simple micropatterns were developed using standard nanofabrication techniques and aided in the understanding of the contributions of simple topography and roughness to the observations made in the experiments (**Chapter 3**). Finally, this work compares the theoretical parameters for colloid mobilization with the microscopic observations to understand the factors leading to bacteria and colloid transport and deposition. The solution conditions varied by the addition of surfactant Tween 80 allowed for the evaluation of the impact of altered surface tension forces in particle-surface-solution interactions leading to transport and deposition. In the context of fresh produce, this information will be helpful to guide the produce industry in improving methods that are based on a mechanistic understanding of the appropriate forces required to remove particles like bacteria from fresh produce surfaces. Only a few reports detail the influence of

physicochemical factors on bacteria adhesion to and removal from fruits and vegetables (Lima et al., 2013; Wang et al., 2009, 2012; Zhang et al., 2014; Lazouskaya et al., 2016). The heterogeneity of plant surfaces may explain why the same methods applied to different produce surfaces have very different results in removal efficiencies (Lima et al., 2013; Wang et al., 2012; Fernandes et al., 2014), and why chemical agents such as surfactants applied at various concentrations don't always work. Currently, the industry lacks this type of in-depth knowledge that can be directly translated into practical application in ways that maximize removal forces. In a broader context, the use of simple micropatterned surfaces (**Chapter 3**) allows to even further interpret and model the underlying dynamics behind particle flow, transport, deposition, and retention. Such information is useful to a wide variety of industries, including biomedicine, inkjet printing, wastewater management, and more (Parsa et al., 2018).

## 1.7 Research Objectives

The objectives of this work were to:

- (I) Characterize the surface roughness and hydrophobicity of the experimental surfaces
- (II) Determine the influence of surface, solution, and particle properties on the translocation/deposition patterns of bacteria (*Salmonella enterica* sv. Enteritidis, an important foodborne pathogen) and colloids, an ideal particle
- (III) Provide mechanisms and a theoretical framework for the influence of surface, solution, and particle characteristics on bacteria and colloid transport/deposition.

## Chapter 2

### FACTORS INFLUENCING THE TRANSPORT AND DEPOSITION OF *SALMONELLA ENTERICA* AND COLLOIDS IN EVAPORATING SESSILE DROPLETS ON POLYDIMETHYLSILOXANE SPINACH AND LETTUCE SURFACES

#### 2.1 Introduction

Human bacterial pathogens like *Salmonella* spp. can survive on fresh produce surfaces throughout the farm-to-fork continuum. These interactions are not fully elucidated but there is growing evidence of the influence of plant surface architecture on bacterial transport, attachment, and biofilm formation. Surface features of plants may also shield pathogens from removal and sanitation efforts, which has devastating consequences of wide-spread foodborne illness. Understanding the mechanisms behind the bacterial transport and deposition to plant surfaces is of critical importance in food safety for implementing effective decontamination strategies.

In this study, the deposition patterns of evaporated Water of 0.01% Tween 80 droplets containing *Salmonella enterica* sv. Enteritidis and fluorescent polystyrene latex microspheres on polydimethylsiloxane (PDMS) produce surfaces, PDMS Spinach and PDMS Lettuce, were analyzed. To determine the influence of plant surface properties on *Salmonella* and colloid localization, the deposition patterns from the PDMS produce surfaces were compared to two experimental control surfaces, Glass (flat, hydrophilic) and PDMS (flat, hydrophobic). PDMS is an inert, optically transparent, and chemically homogeneous material that faithfully replicates the natural plant surface topography and roughness (Lazouskaya et al., 2016; Zhang et al., 2014) with reduced confounding variables of real plant surfaces.

Discussed in detail in **Chapter 4**, the results of the study conclude that i) Surface properties, roughness and hydrophobicity, changed the morphology of the

deposition patterns of *Salmonella* and colloids. Droplets on the PDMS produce surfaces exhibited contact line pinning at surface features, which lead to particle deposition; ii) Lowering the surface tension of the solution with surfactant Tween 80 influenced the capillary forces and thickness of water films, which influenced particle mobilization and deposition. Tween droplets resulted in an increase in the deposition area and more uniform deposition of particles; iii) Although the deposition patterns between colloids and bacteria were similar, *Salmonella* appeared to better mobilize with the contact line compared to colloids in the water droplets, which may be due to the particle shape and size, among other factors. These findings suggest that colloids used as bacteria surrogates should be modeled after the size and shape characteristics of the study bacterium in attachment and detachment studies.

## **2.2 Materials and Methods**

### **2.2.1 Fabrication of Polydimethylsiloxane Spinach and Lettuce Surfaces**

The surfaces used in this study were standard glass slides and polydimethylsiloxane (PDMS) surfaces: PDMS Flat, PDMS Spinach, and PDMS Lettuce. PDMS molds can replicate the micron and sub-micron features of natural plants surfaces (Zhang et al., 2014; Sun et al., *in review*). The following procedure is a modified adaptation from Sun et al. (*in review*). All procedures were performed in a chemical or biosafety hood where appropriate. Organic baby spinach (triple-washed, *S. oleracea*) and organic iceberg lettuce (*L. sativa*) were purchased at a local grocery store and maintained at 4°C for up to 2 days before use. For lettuce, the outer leaves were removed and discarded. In a biosafety hood, plant samples were sized to ~2 cm x 2 cm and carefully adhered to the bottom of a sterile petri dish with double-sided tape.

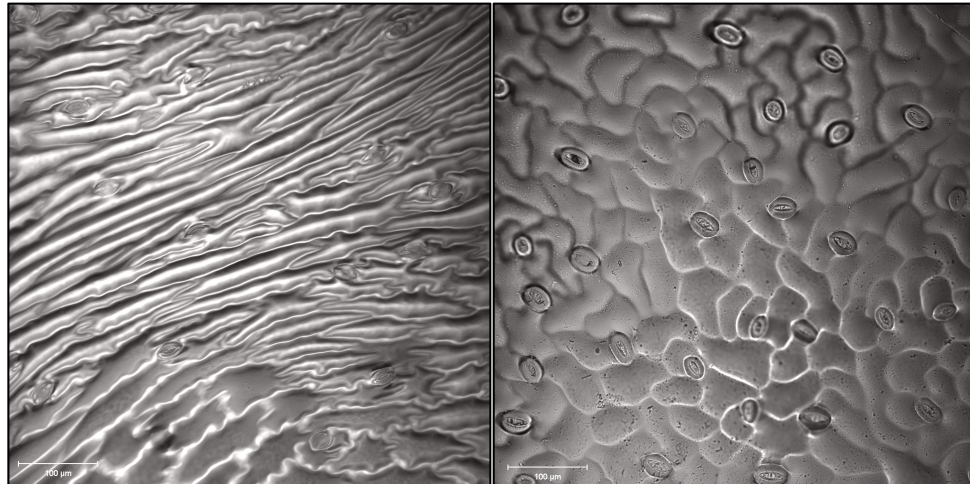


**Figure 2.1** Confocal images of PDMS Lettuce (A) and PDMS Spinach (B)

Briefly, the PDMS mixture of elastomer base and curing agent (SLYGUARD184 Silicone Elastomer Kit, Dow Corning Corporation) at 10:1 mass ratio was vigorously mixed for 5 min. The mixture was centrifuged at 2000 rpm (514 xg) for 2 min followed by degassing under vacuum for 10 min. Afterward, the PDMS mixture (~10 mL) was cast onto the fresh plant sample (spinach or lettuce), covered, and incubated at 40°C for 12 h. Once cooled to room temperature, the plant material was separated from the PDMS mold (negative) and discarded. The PDMS negative mold was rinsed with sterile, ultrapure DI water followed by ethanol (70% in DI water) and finally DI water again, and air dried with N<sub>2</sub> gas. To create the positive mold, the PDMS surfaces were treated with methyltrichlorosilane via vapor deposition for 10 min followed by degassing under vacuum for 10 min. Then, the PDMS mixture was applied to the PDMS negative mold and cured at 40°C for 12 h. After curing, the sample was cooled to room temperature, and the negative PDMS mold was separated from the positive replica, rinsed with DI water and 70% ethanol, dried with N<sub>2</sub> gas,

and stored until use. PDMS Flat surfaces were made by casting the PDMS mixture into an empty, sterile petri dish, covered, and prepared via the procedures described above. Glass slides were first cleaned with soap followed by DI water-70% ethanol-DI water rinse and dried with N<sub>2</sub> gas.

### 2.2.2 Surface Hydrophobicity

The equilibrium contact angle was used to determine surface hydrophobicity. A 5- $\mu$ L droplet of either DI water or 0.01% Tween 80 was applied onto each surface in triplicate and photographed with a high-resolution camera (Canon EOS T6i camera with Canon EF 100mm f/2.8 Macro Lens) immediately after deposition. Images were quantified with ImageJ DropSnake function (Schneider, Rasband, and Eliceiri, 2012), which calculates the contact angle via **Equation 1.1**. Surfaces are classified as hydrophobic if they have contact angles  $> 90^\circ$  and hydrophilic if they have contact angles  $< 90^\circ$ .

### 2.2.3 Surface Roughness

Surface roughness was evaluated by the parameter  $S_a$ , the surface area analog of line roughness,  $R_a$ , given by **Equation 1.2**. Five (5) random locations per sample were imaged using a confocal microscope (Zeiss 780 LSM, Carl Zeiss, Inc., Jena, Germany) equipped with a 20x air lens objective (EC Epiplan Apochromat HDIC 20x, 0.6 NA). Z-stack images were also collected for each sample location, and the thickness of the z-stacks varied by the sample. The imaging parameters were: 1024 x 1024-pixel frame size; 12-bit; 1:1 zoom. Individual measurements (n=5) were performed on the same day for a given sample. Only the transmission channel off of a 488 nm laser line was analyzed in the software using the built-topography function

(Zen2010d; Carl Zeiss, Inc., Jena, Germany). The images were fit to a plane to remove surface tilt, and a high-pass Gaussian filter with a long-wavelength cutoff  $\gamma$  at  $80 \mu\text{m}$  was applied to remove large-scale topography (Lazouskaya et al., 2016). As noted by Lazouskaya et al. (2016), a high-pass filter only affects the low-frequency features of surfaces that are above  $80 \mu\text{m}$  and therefore does not affect the roughness features of the sample surfaces and at the scales that are relevant to bacteria/colloids. Roughness was analyzed at the center of the image without any thresholding. Results were averaged and reported with  $\pm$  standard deviation values in **Table 2.1**.

#### **2.2.4 Sessile Droplet Suspension**

A suspension of pGFPuv-*Salmonella enterica* sv. Enteritidis (strain ME18, purchased from UGA Center for Food Safety, Griffin, GA) and sulfate-modified, red-fluorescent polystyrene latex colloids (Molecular Probes/Invitrogen, Eugene, OR) were prepared in either sterile ultra-pure DI water or 0.01% Tween 80. The bacteria were prepared via standard procedures: a pure colony of *Salmonella* from a Tryptic Soy Agar (TSA; Becton Dickinson, Franklin Lakes, NJ) plate supplemented with 0.01% (w/v) ampicillin (Sigma-Aldrich, St. Louis, MO; maintained at  $4^{\circ}\text{C}$ ) was transferred to a flask containing Tryptic Soy Broth (TSB, Becton Dickinson, Franklin Lakes, NJ) supplemented with 0.01% (w/v) ampicillin and incubated at  $30^{\circ}\text{C}$  with shaking (120 rpm) until stationary phase ( $\sim 16 - 18$  h, confirmed by OD 600 nm). The culture was centrifuged at  $4^{\circ}\text{C} / 5000$  rpm (3412 xg) / 25 min, washed 1x with sterile 1x PBS, and re-suspended in sterile DI water or 0.01% Tween 80 (100 ppm) to a concentration of  $\approx 10^6$  CFU/mL (via 1:1000 dilution; cell concentration was confirmed by a standard plate count method and OD 600 nm). For the colloid suspension, sulfate-modified polystyrene latex spheres were vortex-mixed for 2 min and suspended to a

final concentration of 2 ppm (colloid concentration  $\approx 10^6$  particles/mL) in the bacterial suspension in either Water or 0.01% Tween 80. Suspensions were carefully mixed by tube inversion.

*Salmonella* by this preparation were rod-shaped  $\sim 2.1 \pm 0.04$   $\mu\text{m}$  length x  $1.1 \pm 0.01$   $\mu\text{m}$  width, and the colloids were spherical with a diameter of 2  $\mu\text{m}$  (information provided by the manufacturer) (**Table A.1, Appendix A** for a summary of particle characteristics). Similar values for bacteria cell size are reported in the literature, e.g., Soni et al. (2008) determined  $2.2 \pm 0.3$  length for *Salmonella* spp. in TSB.

## **2.2.5 Droplet Evaporation via Confocal Microscopy**

### **2.2.5.1 Deposition Patterns**

The deposition patterns of Water and 0.01% Tween 80 droplets containing *Salmonella* and colloids were imaged using an upright 780 Zeiss confocal laser scanning microscope with either a 10x (EC-Plan Neofluar) or 20x (EC-Epiplan Apochromat, HD DIC, 0.6 NA) objective lens. The GFP-bacteria were imaged using a 488nm laser line (green channel), and the colloids using a 561nm laser line (red channel). The surfaces were imaged using a transmission channel (gray channel).

Briefly, a 0.5  $\mu\text{L}$  aliquot of the bacteria-colloid suspension was added to a surface (Glass, PDMS Flat, PDMS Lettuce, PDMS Spinach) and imaged within 1 min of deposition using a time-lapse function (968.14 mili-seconds acquisition speed) and 10x objective lens (to accommodate for the entire margin of the droplet) with a frame size of 512 x 512 pixels. After the droplet evaporation event, the entire droplet, as well as close-up regions were imaged using the 10x or 20x lens and a tile-scan function (from 2 x 2 to 3 x 3 tiles) if necessary (depending upon the size of the deposition

pattern), with a frame size of 1024 x 1024 pixels. Z-stack images were collected with image sizes of 1024 x 1024 pixels and varied in thickness depending upon the sample that was imaged. The experiments were carried out under ambient conditions (20-25°C and 48-55% relative humidity).

### **2.2.5.2 Droplet Evaporation Characteristics**

We quantified the droplet evaporation time, droplet contact area, and contact line evolution of colloid-only suspensions (2 ppm; used as a tracer) using a confocal microscope (LSM Zeiss 880, Carl Zeiss, Inc., Jena, Germany with a 10x (10x EC-Plan Neofluar) objective lens, which images from the bottom. A 0.5- $\mu$ L droplet of the colloid suspension (either DI water or 0.01% Tween 80) was deposited on a given surface and imaged within 1 min of deposition using a time-lapse function ( $\sim$ 968.14 msec acquisition time) with a frame size of 1024 x 1024 pixels. A 561 nm laser line captured the fluorescence of the particles (red channel), and a transmission channel captures the surfaces (gray channel). After the droplet evaporation event, the videos were analyzed using built-in software (Zen2010d) to determine the droplet evaporation time and to characterize the behavior of the contact line over the evaporation event. The total droplet evaporation time was quantified as the time between the start of the time-lapse imaging event (within 1 min of droplet deposition) and when the film breaks at the end of the evaporation event (n=3). The droplet contact area was determined by tracing the droplet perimeter and quantifying the area in ImageJ from the evaporation videos (n=3) using standard functions. The droplet contact line behavior was determined by measuring a transect from two points on the droplet edges throughout evaporation using Zen2010 software from a representative evaporation video for each surface, shown in **Figure 2.2**.

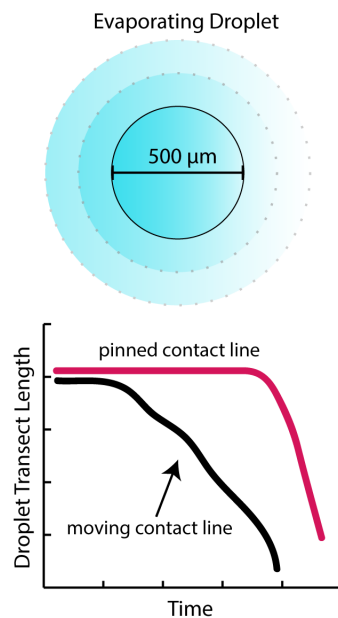


**Figure 2.2** Schematic of droplet transect measurement over time for an evaporating droplet. The transect length, similar to a diameter, is measured between two points at the droplet’s edge over time during evaporation and depicted in a figure of length vs. time.

The transect length was measured every 5 frames after the initial frame (frame 1,  $N_{time}=0$ ) for a normalized time, given by  $N_t/N_f$ , where  $N_t$  is the time,  $t$ , at a given frame and  $N_f$  is the time at the final frame,  $f$ . The experiments were carried out under ambient conditions (20-25°C and 48-55% relative humidity).

### 2.2.6 Image and Statistical Analyses

All microscopic data was analyzed using Zen2010D and ImageJ software (noted in text where appropriate). JMP® (SAS; Cary, NC, USA) statistical analysis program was used to determine the statistical significance at  $p<0.05$  via One-way or Two-way ANOVA (with replication) and Tukey-Kramer post-hoc analysis.

## 2.3 Results

### 2.3.1 Surface Properties

The equilibrium contact angle and surface roughness values are summarized in **Table 2.1** and **Figure 2.2**.

**Table 2.1** Surface roughness (n=5) and hydrophobicity (n=3) of Glass, PDMS Flat, PDMS Spinach, and PDMS Lettuce in DI Water or 0.01% Tween 80 droplets.

Surface	Roughness, $S_a$ $\mu\text{m}$ (n=5)	Equilibrium Contact Angle, $\theta_{\text{water}}$ , degrees (n=3)	Equilibrium Contact Angle, $\theta_{\text{Tween80}}$ , degrees (n=3)
Glass	$0.008 \pm 0.0004$	$34 \pm 5^\circ$ (hydrophilic)	$34 \pm 1^\circ$ (wetting)
PDMS Flat	$0.008 \pm 0.0004$	$106 \pm 4^\circ$ (hydrophobic)	$87 \pm 3^\circ$ (wetting/non-wetting)
PDMS Spinach	$3.420 \pm 1.20$	$122 \pm 9^\circ$ (hydrophobic)	$97 \pm 4^\circ$ (non-wetting)
PDMS Lettuce	$4.735 \pm 2.60$	$95 \pm 1^\circ$ (hydrophobic)	$88 \pm 10^\circ$ (wetting/non-wetting)

Averages reported with  $\pm$  standard deviation.

Ultra-pure deionized water,  $18.2 \text{ m}\Omega/\text{cm}^2$ ; ambient conditions.

#### 2.3.1.1 Surface Roughness

Surface roughness  $S_a$  values obtained from confocal microscopy (780 LSM) are shown with standard deviation (n=5) in **Table 2.1**. Both Glass and PDMS Flat surfaces had practically identical  $S_a$  values of  $\approx 0.008 \pm 0.0004 \mu\text{m}$ , while the average  $S_a$  for PDMS Spinach and PDMS Lettuce were  $3.420 \pm 1.20 \mu\text{m}$  and  $4.735 \pm 2.60 \mu\text{m}$ , respectively; PDMS replicas of the plant surfaces are spatially varied, which caused large deviations in the roughness values obtained. One-way ANOVA with Tukey-Kramer analysis revealed some significant differences in the  $S_a$  values: in general,

there was a significant difference between the  $S_a$  for a given PDMS rough surface (PDMS Lettuce or PDMS Spinach) and that of a smooth, flat surface (Glass or PDMS Flat), resulting in a p-value = 0.0005. There was no significant difference between the two “smooth” surfaces and between the glass and PDMS Flat surfaces (p-value = 1.000). Finally, there was no significant difference in the  $S_a$  values between the PDMS produce surfaces, PDMS Lettuce and PDMS spinach (p-value = 0.4920).

Given that the  $S_a$  values for Glass and PDMS Spinach are several orders of magnitude lower than the rougher PDMS Spinach and PDMS Lettuce surfaces, the Glass and PDMS Flat surfaces are considered as the smooth hydrophilic or hydrophobic surface, respectively, experimental controls, and PDMS Lettuce and Spinach as the “rough” surfaces.

### **2.3.1.2 Surface Hydrophobicity**

The equilibrium contact angles for 5- $\mu$ L DI Water or 0.01% Tween 80 droplets are reported in **Table 2.1** with standard deviation (n=3) and in **Figure 2.3** with standard error (n=3). By convention, surface hydrophobicity was determined as the equilibrium contact angle of water droplets on the different surfaces, while the classification for 0.01% Tween 80 droplets was determined as “wetting” for contact angles  $< 90^\circ$  and “non-wetting” for contact angles  $> 90^\circ$ . The results for Water in **Table 2.1** show that Glass was the only hydrophilic surface ( $\theta = 34 \pm 5^\circ$ ) while all of the PDMS surfaces were hydrophobic ( $\theta > 95^\circ$ ). The equilibrium contact angle of Water on Glass was the lowest compared to the PDMS surfaces and was statistically different ( $p < 0.0001$ , all comparisons). PDMS Spinach had the highest contact angle value and was more hydrophobic compared to PDMS Flat ( $p < 0.0001$ ) and PDMS Lettuce ( $p < 0.0016$ ), showing the influence of surface roughness on hydrophobicity.

Interestingly, PDMS Lettuce had a lower contact angle value than PDMS Flat, although this difference was not statistically significant ( $p = 0.1759$ ).

The equilibrium contact angle of 0.01% Tween 80 droplets on Glass were significantly different ( $p < 0.0001$ ) compared to the PDMS surfaces (all comparisons). Tween droplets on Glass were classified as “wetting” and “non-wetting” on the PDMS Spinach surface. PDMS Flat and PDMS Lettuce were classified as “wetting/non-wetting” due to the deviations in measured values. There were no significant differences between the Tween contact angles of PDMS Spinach x PDMS Flat ( $p = 0.2292$ ), PDMS Spinach x PDMS Lettuce ( $p = 0.4017$ ), and PDMS Lettuce x PDMS Flat ( $p = 0.9680$ ).

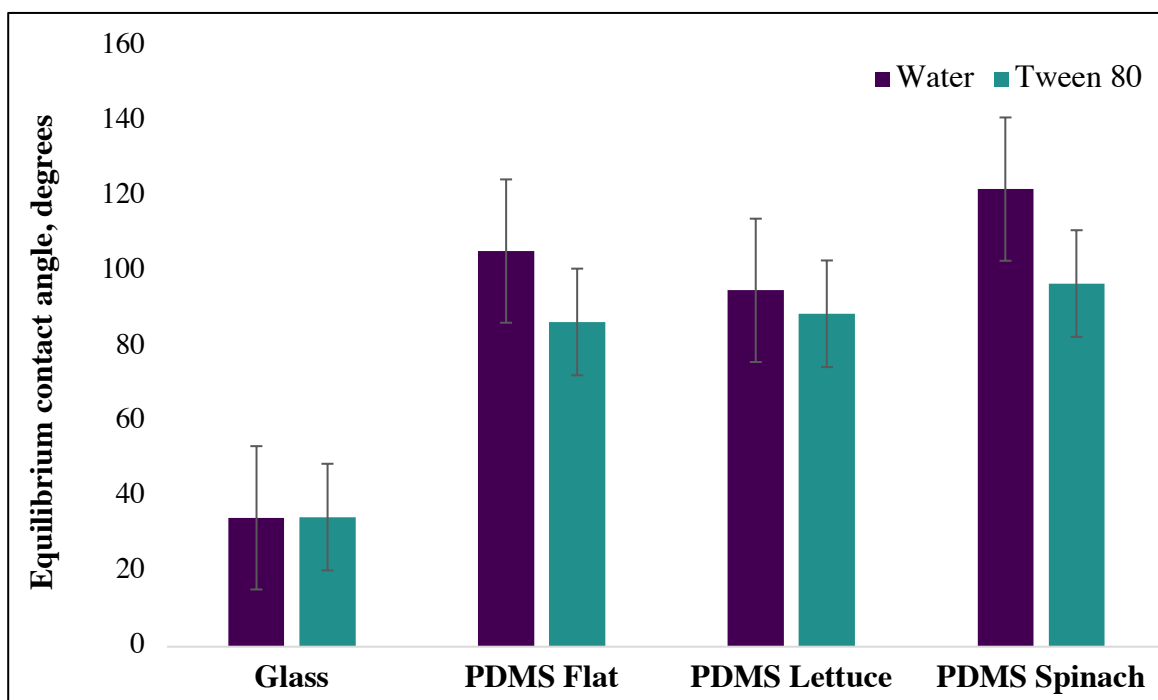


**Figure 2.3** Equilibrium contact angle measurements for DI water (purple) and 0.01% Tween 80 (teal) droplets.

**Figure 2.3** shows the comparison of the equilibrium contact angles obtained for Water and 0.01% Tween 80 droplets. Tween droplets resulted in lower contact angles compared to Water droplets on the different surfaces. The results of the Two-way ANOVA (with replication) and Tukey-Kramer analysis include a significant interaction term between the solution and surface type ( $df=3$ ;  $F=6.054$ ;  $p=0.0059$ ). In general, the equilibrium contact angle observed on a specific surface would depend on whether the solution was DI water or 0.01% Tween 80, which is expected based on the differences in surface tension of the solutions.

### **2.3.2 Qualitative Analysis of Deposition Patterns**

**Figures 2.4-2.5** and **Figures 2.6-2.7** show the deposition patterns of Water and 0.01% Tween 80 droplets, respectively, containing colloids and bacteria for each of the surfaces with a qualitative analysis of the patterns.

#### **2.3.2.1 Deposition Patterns from Water Droplets**

**Figure 2.4** shows the representative deposition patterns from evaporated Water droplets containing *Salmonella* and colloids on Glass (A), PDMS Flat (B), PDMS Lettuce (C), and PDMS Spinach (D). Representative close-up images of deposition patterns are shown in **Figure 2.5**. The morphology of the deposition patterns is clearly different for each of the surfaces, shown in **Figure 2.4**. As Water droplets evaporated on Glass, colloids and bacteria were deposited along the contact line that would temporarily pin, which led to a larger deposition area compared to the other surfaces.

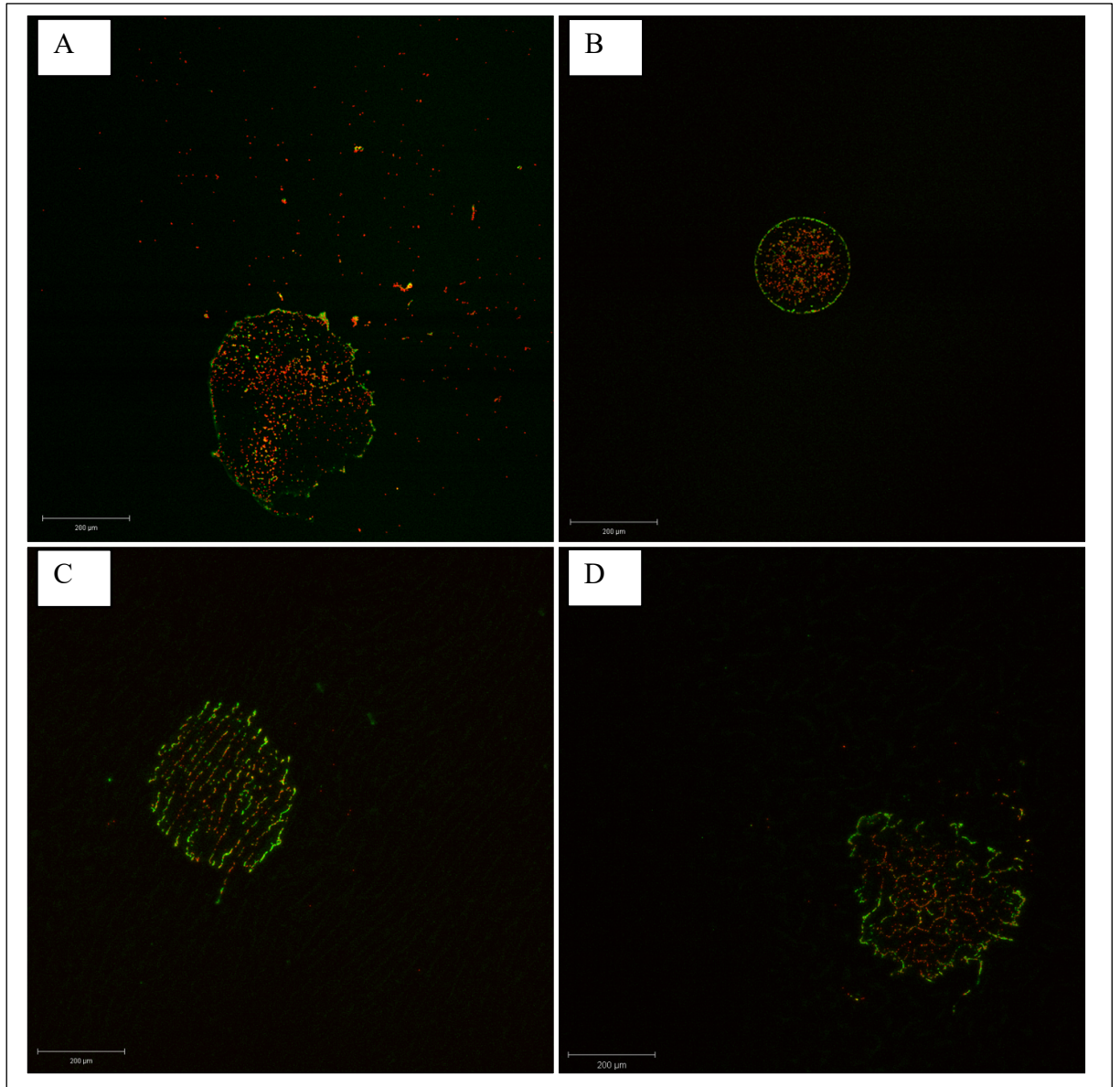


**Figure 2.4** Representative confocal images (780 LSM) of the deposition patterns of colloids (red) and *Salmonella* (green) in Water droplets. A) Glass; B) PDMS Flat; C) PDMS Lettuce; and D) PDMS Spinach. The transmission channel was removed to improve visibility. Scale bar is 200  $\mu\text{m}$ .

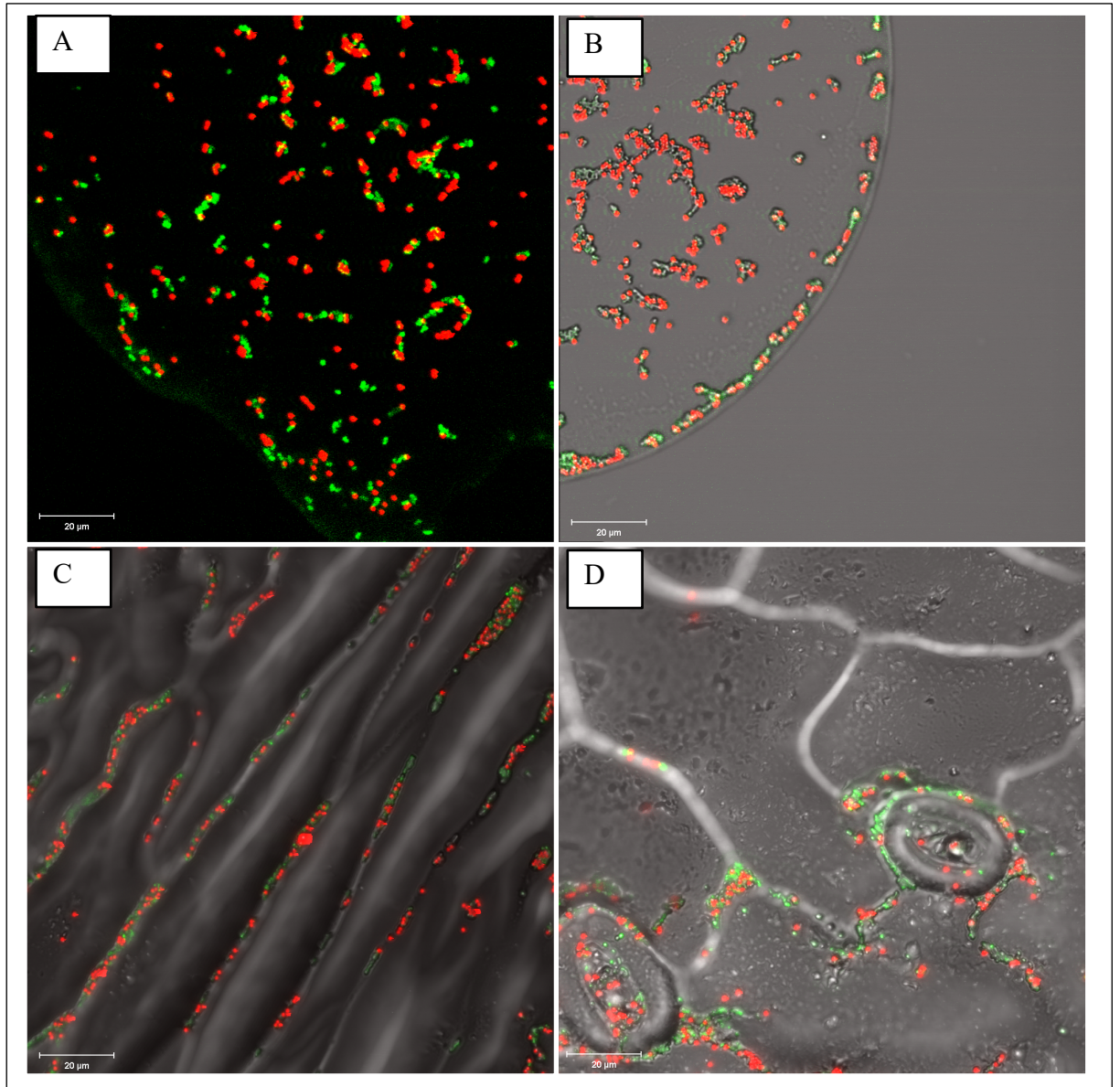


**Figure 2.5** Representative confocal images (780 LSM) of the close-up regions of deposition patterns from Water droplets containing colloids (red) and *Salmonella* (green). A) Glass; B) PDMS Flat; C) PDMS Lettuce; and D) PDMS Spinach. Scale bar is 20  $\mu\text{m}$

On PDMS Flat, *Salmonella* and colloids followed the contact line and did not deposit until the last stage of evaporation when the film ruptured, leaving a small

residue that outlined the final droplet contact area. The deposition patterns of the PDMS Lettuce and PDMS Spinach Surfaces clearly outline the surface topographical features. Some colloids and *Salmonella* deposited along the evaporating contact line, which occurred when the contact line pinned at surface features, although the majority were maintained within the droplet and deposited at the last stages of evaporation, similar to the PDMS Flat surface.

As shown in **Figure 2.5**, the localization of bacteria and colloids within grooved and pitted features (e.g., in between veins and in stomata) is apparent. On all surfaces, bacteria and colloids deposit in clusters when the film ruptures at the last stages of evaporation. Bacteria deposited mostly within the grooves of features rather than the tops of features compared to colloids, which deposited in both regions. Although the deposition patterns of colloids versus bacteria were similar, more bacteria than colloids appear to better mobilize with the contact line and localize at the edges of the final droplet contact area for all surfaces, seen as a distinct ring of green, similar to the famous coffee ring pattern.

#### **2.3.2.2 Deposition Patterns from 0.01% Tween 80 Droplets**

**Figure 2.6** shows the representative deposition patterns from evaporated 0.01% Tween 80 droplets containing *Salmonella* and colloids on Glass (A), PDMS Flat (B), PDMS Lettuce (C), and PDMS Spinach (D). Due to the variation in resulting deposition pattern area, the scale bars in **Figure 2.6** vary in length but are all set to 200  $\mu\text{m}$  for comparison. Similar to the Water deposition patterns, the morphology of the deposition patterns of Tween droplets is different for a given surface, highlighting the influence of surface properties. For Glass, PDMS Lettuce, and PDMS Spinach, there was minimal recession of the contact line due to the presence of a thin liquid film and

a pinned contact line, causing particles within the evaporating droplet to deposit in-place and giving rise to the larger deposition area. On Glass, two distinct rings of particle deposition similar to a coffee ring occurred: the first at the original contact line of the droplet and a second within this ring, which was the final droplet area. Due to the lack of surface features and the hydrophobicity of PDMS Flat, the particles within the droplets did not deposit until the latest stages of evaporation. Notably, PDMS lettuce and PDMS Flat have almost identical contact angles values in 0.01% Tween 80 ( $88 \pm 10^\circ$  and  $87 \pm 3$ , respectively) yet very different deposition patterns, which indicates the role of surface properties in transport and deposition.

Tween 80 droplets contain a non-ionic surfactant that remains after water evaporates from the droplet, leaving behind a residue, shown in **Figure 2.6**. This residue also causes auto-fluorescence in the green channel, seen in the close-up deposition patterns shown in **Figure 2.7**, which unfortunately obfuscates the bacteria signal. These globules of residual surfactant contain bacteria and colloids, deposited mostly within grooved/pitted features rather than the tops of surfaces. Bacteria and particles also appeared within smaller globules, likely surfactant micelles (e.g., **Figure 2.7-B**).

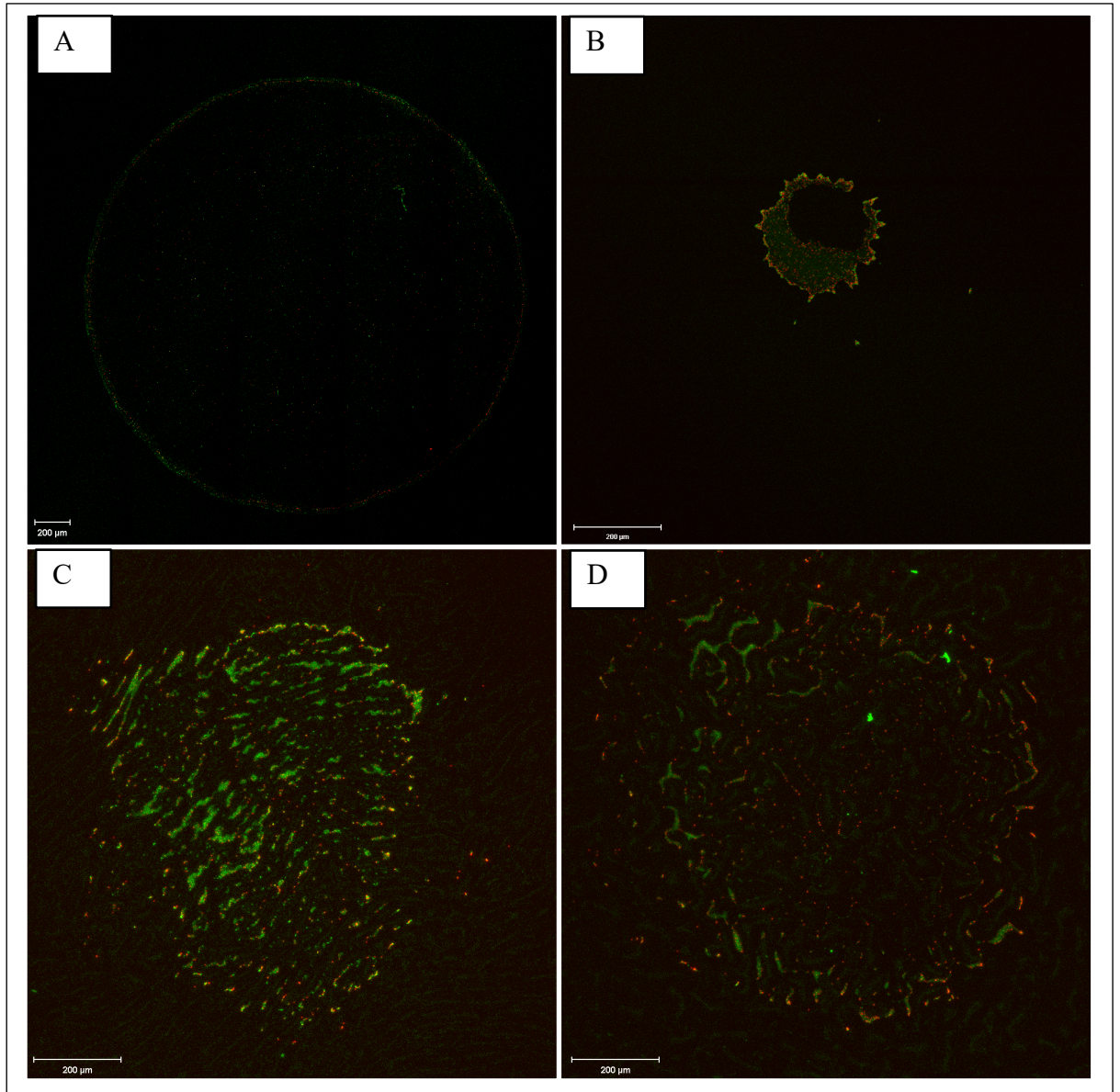


**Figure 2.6** Representative confocal images (780 LSM) of the deposition patterns of colloids (red) and *Salmonella* (green) in 0.01% Tween 80 droplets. A) Glass; B) PDMS Flat; C) PDMS Lettuce; and D) PDMS Spinach. The transmission channel was removed to improve visibility. Scale bar is set to 200  $\mu\text{m}$  but varies by length due to the different scales in the images.

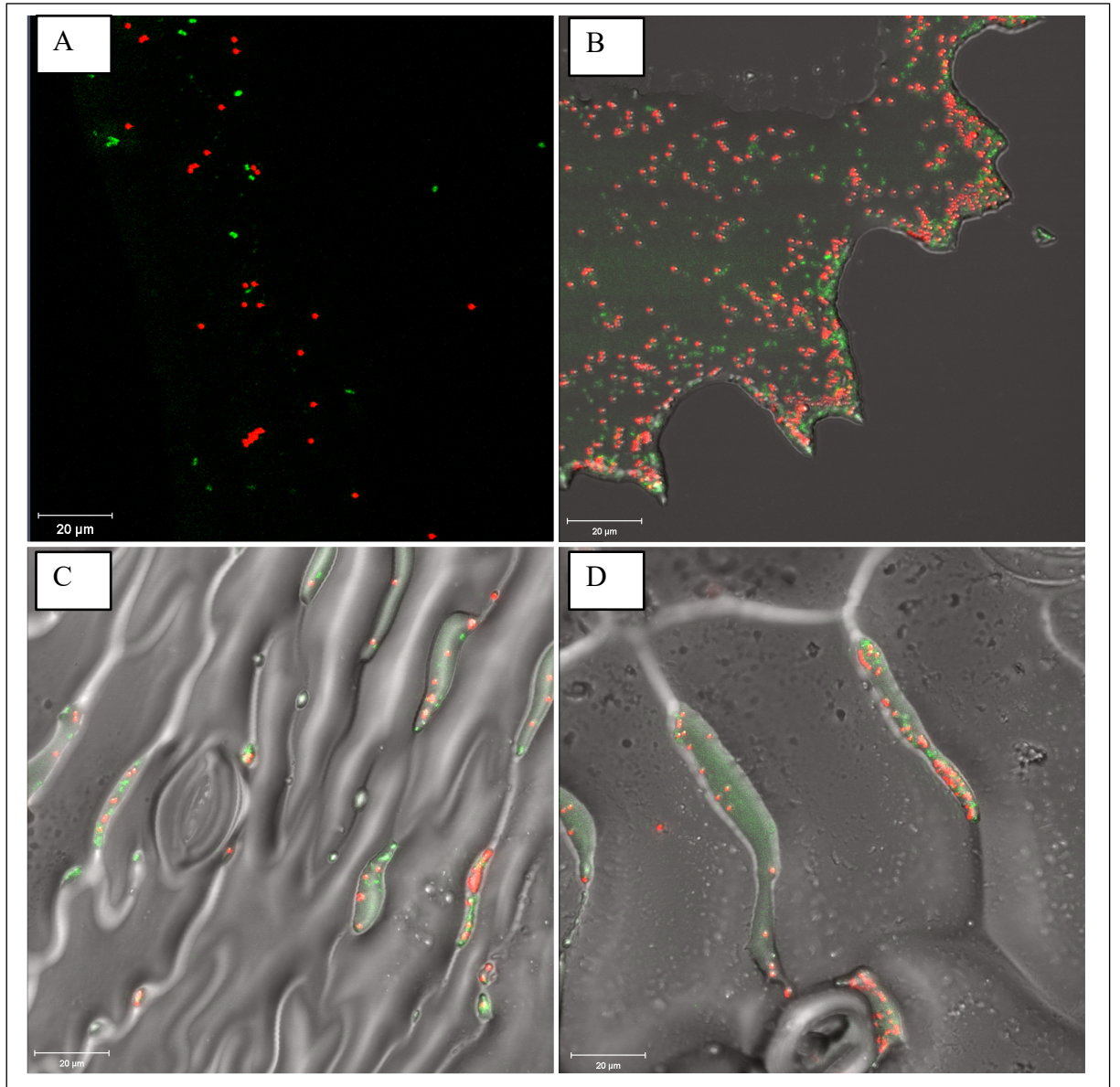


**Figure 2.7** Representative confocal images (780 LSM) of the close-up regions of deposition patterns from 0.01% Tween 80 droplets containing colloids (red) and *Salmonella* (green). A) Glass; B) PDMS Flat; C) PDMS Lettuce; and D) PDMS Spinach. Scale bar is 20  $\mu\text{m}$ . Arrows point to surfactant globules/micelles.

### 2.3.3 Droplet Evaporation Characteristics

Droplet evaporation time is summarized in **Figure 2.8**, droplet contact area in **Figure 2.9**, and contact line behavior in **Figure 2.10**.

#### 2.3.3.1 Evaporation Time and Contact Area

**Figure 2.8** and **Figure 2.9** show the droplet evaporation time and droplet contact area, respectively, for the Water and 0.01% Tween 80 droplets on the different surfaces recorded by video microscopy (880 LSM).

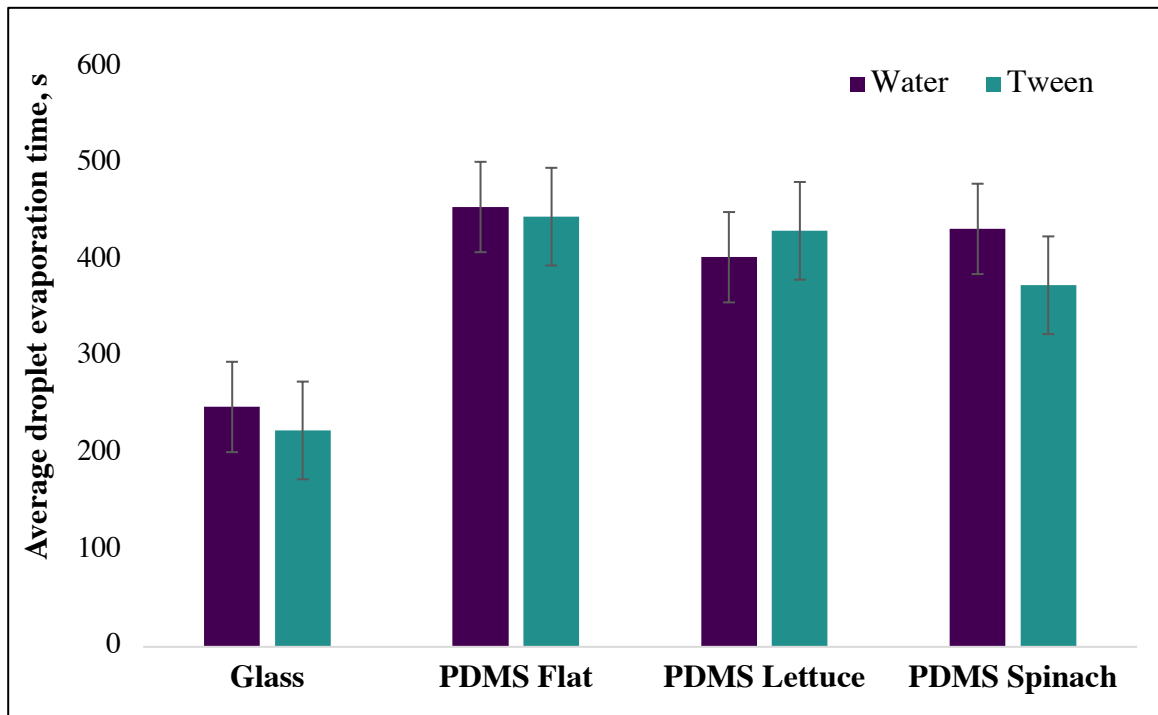


**Figure 2.8** Droplet evaporation for Water (purple) and 0.01% Tween 80 (teal) droplets on the different surfaces (n=3) with standard error bars.

As shown in **Figure 2.8**, the evaporation time for Glass is less for both water and Tween droplets compared to the PDMS Surfaces. Analysis via Two-Way

ANOVA resulted in insignificance for the interaction term ( $df=3$ ;  $F=1.1421$ ;  $p=0.3622$ ) but significance for the surface effect term ( $p<0.0001$ ). Results of the One-way ANOVA show that for both Water and Tween droplets, Glass surfaces were significantly different. For water droplets on Glass, this resulted in the following p-values for the comparisons: Glass x PDMS Flat,  $p < 0.0021$ ; Glass x PDMS Lettuce, 0.0002; and Glass x PDMS Spinach,  $p=0.0007$ . For Tween droplets on Glass, this resulted in the following p-values for the comparisons: Glass x PDMS Flat,  $p=0.0027$ ; Glass x PDMS Lettuce, 0.0042; and Glass x PDMS Spinach,  $p=0.0253$ .

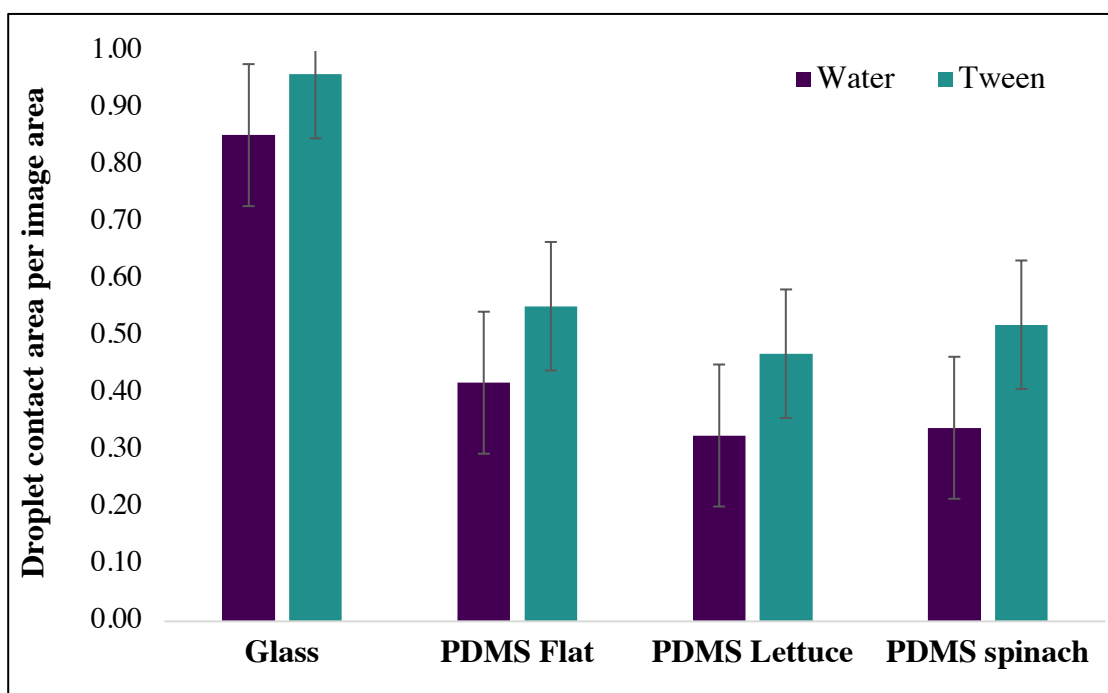


**Figure 2.9** Droplet contact area for Water (purple) and 0.01% Tween 80 (teal) droplets on the different surfaces, with standard error bars.

The Water and 0.01% Tween 80 droplet contact area per image area ( $n=3$ ) for the surfaces is shown in **Figure 2.9**. From the figure, Tween droplets have larger

contact areas than Water droplets for all surfaces analyzed. Also, the droplet contact area on Glass surfaces were on average larger than on the PDMS surfaces. Although it was expected that there would be significance in these observations, the results of the Two-Way ANOVA with Tukey-Kramer test did not find a significant interaction term ( $df=3$ ;  $F=0.04433$ ;  $p=0.7253$ ), but significance in the surface effect ( $p<0.0001$ ). Via One-Way ANOVA analysis, there was significance ( $p<0.0001$ ) in the droplet contact area for the Glass surface compared to the PDMS surfaces for Water and Tween droplets. This corresponds to the hydrophilic nature of Glass, which lends to better wetting than the PDMS surfaces, hence the larger contact area. This is supported by the deposition pattern images in **Figure 2.4-A** and **Figure 2.6-A**.

#### **2.3.3.2 Droplet Contact Line Behavior**

The contact line behavior was characterized by measuring the droplet transect length over the evaporation period for the different surfaces using Zen2010d software (**Figure 2.2**) and reported in **Figure 2.10**.

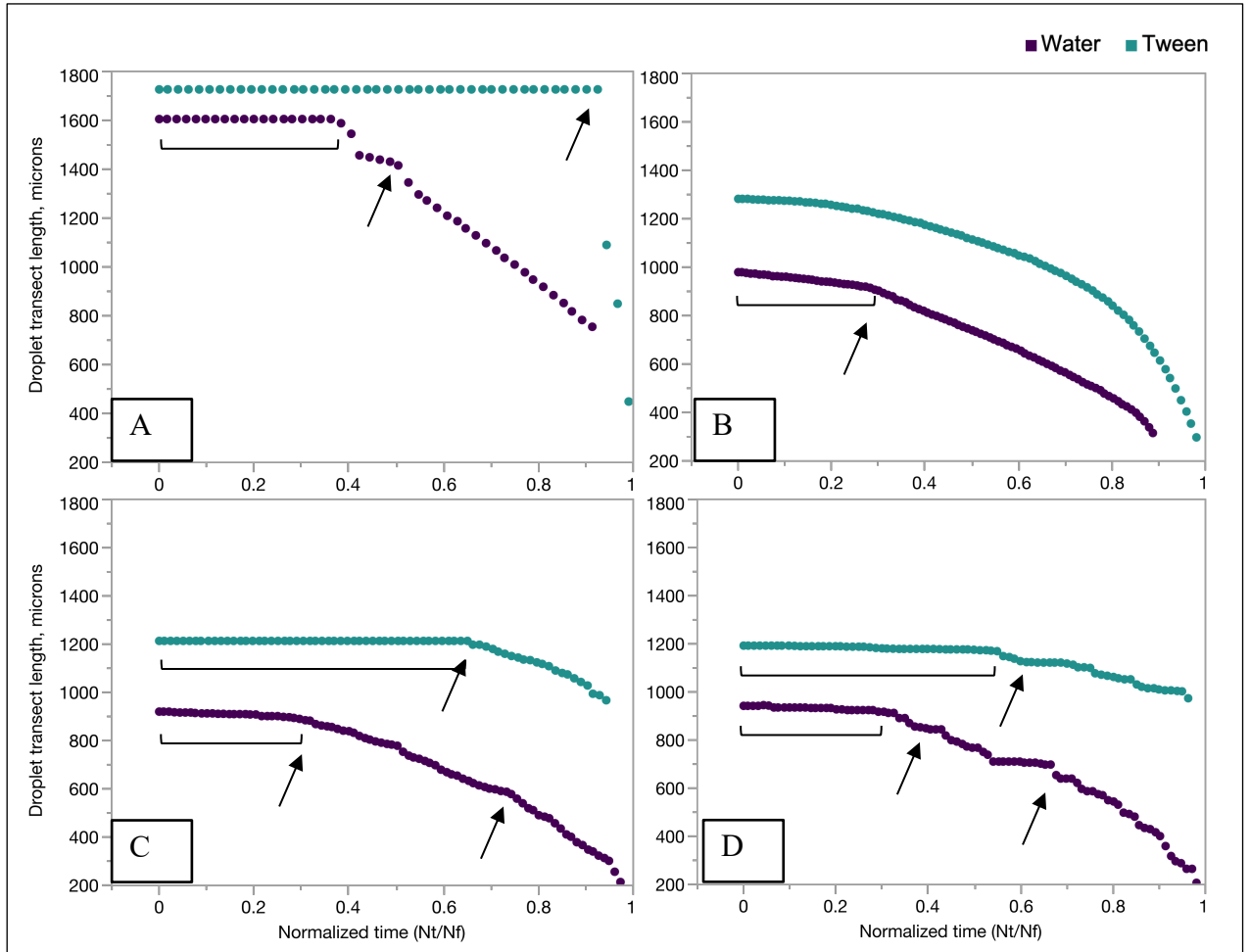


**Figure 2.10** Plot of the contact line behavior for a representative Water (purple) and 0.01% Tween 80 (teal) droplet on A) Glass; B) PDMS Flat; C) PDMS Lettuce and D) PDMS Spinach. The y-axis refers to a transect through two edge points over the droplet contact area, similar to a diameter. Due to the heterogeneity of the surface features, a true diameter is not apparent. Arrows point to example changes in contact line behavior, and brackets indicate example contact line pinning stages.

In these experiments, it is important to note that the variations in surface topography and roughness for the PDMS Spinach and PDMS Lettuce surfaces result in asymmetric droplet morphology at the edges. Typically, droplet contact radius or

diameter is reported (e.g., Yu, Wang, and Huang, 2017). The length of a transect from the x-plane between two edges of the droplet was measured. Measuring between two different points on the surface would yield a different but equally telling story of the contact line behavior.

Contact line behavior is influenced by the surface features and solution matrix. These factors are mapped in **Figure 2.10** by the changes in transect length with time. Regions of particular interest are annotated with arrows, which indicate example contact line changes. Droplets maintained their initial transect length in the initial stages of evaporation, evidenced by a relatively straight line but varies based on the surface. Contact line pinning was more pronounced for Tween droplets compared to Water droplets. Tween droplets maintained initial droplet length for > 50% droplet evaporation time, which indicates a CCL mode (constant contact line) that transitioned to a mix-mode. For Tween droplets on Glass, transect length was maintained for the majority of the evaporation event (~90%) followed by a rapid decrease in length with time. By comparison, Water droplet transect length decreased after ~30% evaporation time. PDMS Flat demonstrated a more gradual decrease in transect length continuously with time, similar to a CCA mode/mix-mode (**Figure 2.10**).

Water droplets on the different surfaces demonstrated repeated contact line pinning, either by surface feature or by particles, similar to stick-slip mode of evaporation. Notably, Water on Glass shows two distinct pinning regions where the contact line length was immobilized 1) the beginning of evaporation and 2) after ~50% evaporation time. The influence of surface roughness on contact line behavior is also apparent in **Figure 2.10**. For both Water and Tween droplets, a step-wise decrease in length occurs on PDMS Spinach and PDMS Lettuces surfaces. The PDMS

produce surfaces caused temporary contact line pinning more often in the evaporation time scale compared to the flat (PDMS Flat and Glass) surfaces. This step-wise fashion is more pronounced in Water droplets but is also evident in Tween droplets. The microscopy videos (880 LSM) showed a variation in the regions that pinned and de-pinned on the rough produce surfaces, i.e., when one region is pinned, a different region de-pins. Subsequently, the de-pinned region can become pinned while the pinned region then simultaneously de-pins. **Figure 2.11** demonstrates contact line pinning, particle transport, and deposition for the different surfaces.

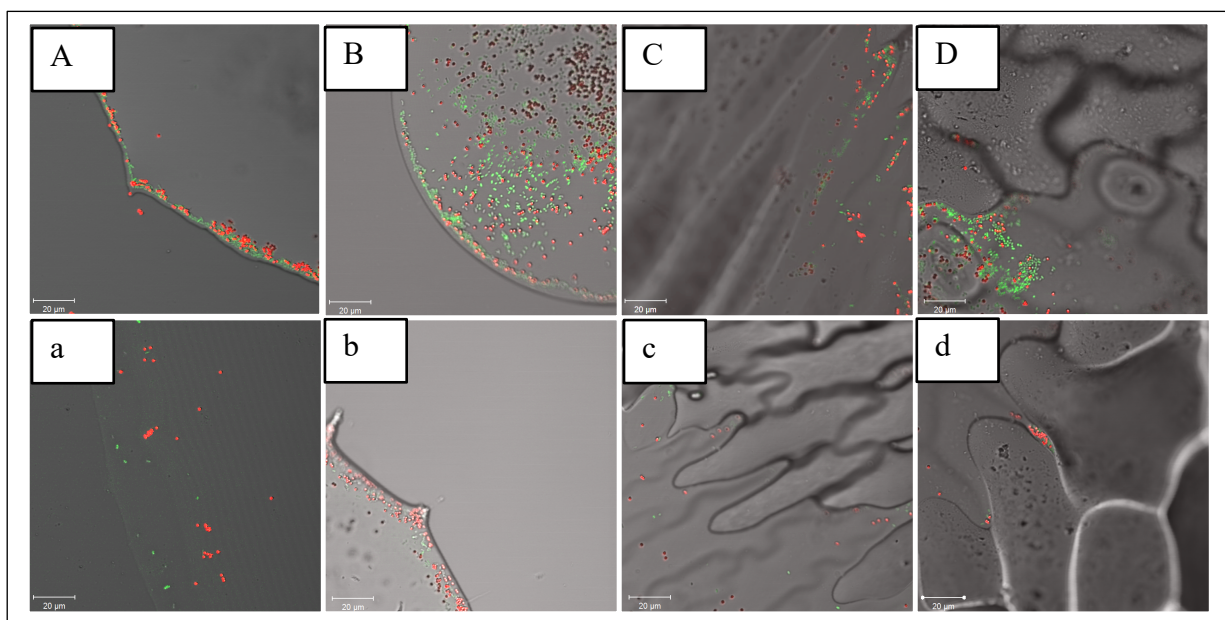


**Figure 2.11** Confocal microscopy images (780 LSM) of *Salmonella* (green) and colloids (red) at contact lines during evaporation for Water (uppercase letters) and 0.01% Tween (lowercase letters) droplets. A,a) Glass; B,b) PDMS Flat; C,c) PDMS Lettuce and D,d) PDMS Spinach. Scale bar is 20 μm. White arrows indicate pinned regions. Yellow arrows indicate direction of contact line movement from the air-water interface. Green arrows indicate direction of particle movement.

## 2.4 Summary

Here, the deposition patterns from evaporated Water or 0.01% Tween 80 droplets containing *Salmonella* and spherical colloids on Glass, PDMS Flat, PDMS Spinach, and PDMS Lettuce surfaces were qualitatively analyzed along with quantified surface properties, roughness and hydrophobicity, and evaporation dynamics, droplet evaporating time, droplet contact area, and contact line behavior.

Discussed in detail in **Chapter 4**, the results of the study conclude that i) Surface properties, roughness and hydrophobicity, changed the morphology of the deposition patterns of *Salmonella* and colloids. Droplets on the PDMS produce surfaces exhibited contact line pinning at surface features, which lead to particle deposition; ii) Lowering the surface tension of the solution with surfactant Tween 80 influenced the capillary forces and thickness of water films, which influenced particle mobilization and deposition. This led to an increase in the deposition area and a more uniform deposition of particles; iii) Although the deposition patterns between colloids and bacteria were similar, *Salmonella* appeared to better mobilize with the contact line compared to colloids in the water droplets, which may be due to the particle shape and size, among other factors. The findings suggest that colloids used as bacteria surrogates should be modeled after the size and shape characteristics of the study bacterium.

Transport, adhesion, and retention of microbes on plant surfaces is indeed complex and heavily dependent upon the properties of the system, which balances the contributions of bacteria characteristics and properties of the substratum and bulk fluid. Overall, this study highlights the important contributions of the many factors behind the mechanisms leading to contamination of microbes and particles on plant surfaces that should be factored into washing methods and other mitigation strategies.

## Chapter 3

### FACTORS INFLUENCING THE TRANSPORT DEPOSITION OF *SALMONELLA ENTERICA* AND COLLOIDS IN EVAPORATING SESSILE DROPLETS ON POLYDIMETHYLSILOXANE MICROPATTERNED SURFACES

#### 3.1 Introduction

Droplet evaporation is a natural and widely-studied phenomenon important to a variety of industries, including groundwater and wastewater management, inkjet printing, and biomedicine. The mechanisms behind particle transport to surfaces in evaporating droplets are complex and involve a combination of the properties of the interfaces between solids, liquids, and particulate matter. Droplets containing suspended particles will leave behind a pattern after evaporating. The “coffee ring” is the most ubiquitous of these deposition patterns: particles form a dense ring-like structure on the surface after evaporation (Deegan et al, 1997, 2000). The famous work by Deegan et al. (1997) detailed how this characteristic deposition pattern forms from hydrodynamic flows within the droplet from pinned droplet edges such that liquid flows from the interior of the droplet to the pinned edges to replace the liquid evaporating at the edges (Deegan et al., 1997). This capillary flow can carry particles with the liquid to the pinned edges where they deposit and form the ring-like structure. Utilizing droplet evaporations systems and analyzing the resulting deposition patterns can aid in the understanding of (bio)colloid transport and retention processes in unsaturated porous media.

This study begins to address the influence of surface topography, roughness, and hydrophobicity on the transport of colloids and *Salmonella enterica* sv. Enteritidis on simple micropatterned surfaces compared to ideal, smooth surfaces. In **Chapter 2**, polydimethylsiloxane (PDMS) replicas of real spinach and lettuce surfaces were

investigated. Natural leaf surface characteristics can be complex with a range of hierarchical surface structures and varying size and shape of epidermal cells. Using simplified PDMS patterns provides an opportunity to understand the influence of topography/roughness and hydrophobicity on the transport and deposition of particles on surfaces. This reductionist approach also enables the opportunity to model particle flow and transport in evaporating droplets. This Chapter includes the to-date work regarding this project and is the subject of ongoing work and collaboration, and detail discussion is provided in **Chapter 4**. Although the mechanisms are not fully elucidated in the text below, the following conclusions were made: 1) Surface topography/roughness strongly influenced the transport and deposition of colloids and bacteria, resulting in unique patterns based on surface properties. Patterned topography/roughness resulted in stick-slip evaporation behavior, where the contact line pinned at surface features, drove particles to the pinned regions and resulted in particle deposition. Roughness and hydrophobicity also influence film thickness, which changes the hydrodynamics behind particle flow within the droplet; 2) The addition of surfactant influenced the deposition pattern and evaporation dynamics due to a change in surface tension, which increased wetting of the suspension on the surface, decreased film thickness, altered the hydrodynamics, and reduced capillary forces.

## **3.2 Materials and Methods**

### **3.2.1 Micropattern Fabrication via Standard Lithography**

Micropatterns based on common geometric shapes were designed using Clewin5 software (Wieweb Software, The Netherlands) and fabricated onto resist-

coated silicon (Si) wafers (AZ<sup>®</sup> nLOF 2020, Microchemicals, Ulm, Germany) University Wafers Inc., Boston, MA, USA) using a laser writer (MLA, Heidelberg Instruments, Germany) in University of Delaware's Nanofabrication Facility (Newark, Delaware, USA). After patterning, the Si wafers were etched using F-ICP etcher (PlasmaTherm, St. Petersburg, FL, USA) and treated with hexamethyldisilazane (HMDS, Yes Engineering Systems, Inc., Livermore, CA, USA) in the procedure outlined below. The samples and processing steps were validated using metrology (Dektak profilometer, Bruker, Billerica, MA, USA) and microscopy (Axio Observer, Carl Zeiss, Germany). The final feature height/depression of the micropatterns varied from 1.5 - 2.0  $\mu\text{m}$ .

1. Spin-coat the polymeric resist (Nloft2020) onto 4" Silicon wafers at 4000 rpm for 60 s (achieves a polymer thickness of  $\sim 1.5 \mu\text{m}$ ).
2. Bake the wafer at 110°C for 60 s
3. Expose the wafer and write the pattern via laser writer
4. Bake the wafer (110°C for 60s) after exposure
5. Develop the wafer: 60 s in MIF300 developer (Microchemicals, Ulm, Germany) with gentle shaking followed by IPA/DI water rinse and dried with N<sub>2</sub> gas
6. Etch the wafer via F-ICP for 240 s (achieves an etch depth  $\approx 1.5\text{-}2.0 \mu\text{m}$ )
7. Expose the wafer to oxygen plasma for 10 min
8. Treat the wafer with HMDS (improves lift-off of PDMS by increasing surface hydrophobicity)

Etched micropatterns on silicon wafers were arranged in a 2 x 2 array of 3 cm x 3 cm. The wafer was cut into four, 3 cm x 3 cm pieces.

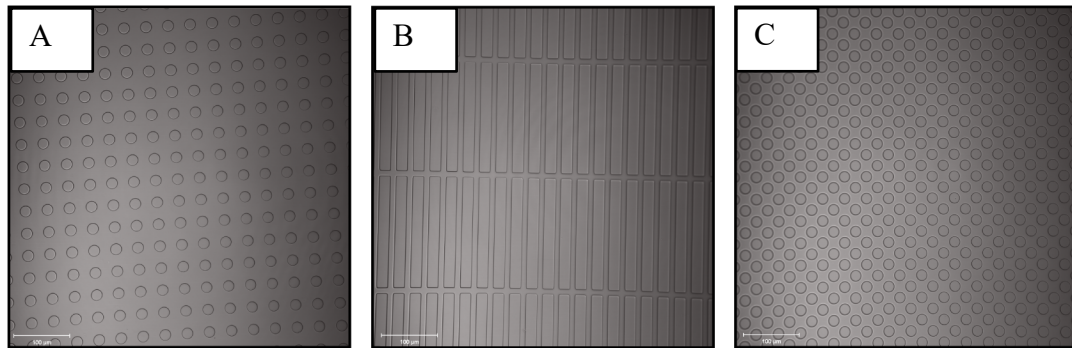


**Figure 3.1** Confocal images of the PDMS micropatterns. A) PDMS Pillars; B) PDMS Grooves; C) PDMS Depressions. Scale bar is 100  $\mu\text{m}$ .

**Figure 3.1** shows confocal images of the PDMS Micropatterns, and the pattern dimensions are summarized below:

- **PDMS Pillars:** arrayed raised dots with 20  $\mu\text{m}$  diameter spaced 20  $\mu\text{m}$  apart
- **PDMS Grooves:** arrayed raised rectangles with dimensions of 10  $\mu\text{m}$  width x 200  $\mu\text{m}$  length diameter spaced 20  $\mu\text{m}$  apart.
- **PDMS Depressions:** arrayed depressed dots with 20  $\mu\text{m}$  diameter spaced 10-20  $\mu\text{m}$  apart

### 3.2.2 Polydimethylsiloxane (PDMS) Soft Lithography

Polydimethylsiloxane (PDMS) is routinely used to replicate micro- and nano-patterns generated from lithography procedures. All procedures were performed in a chemical or biosafety hood where appropriate. Briefly, the PDMS elastomer base and curing agent (SLYGUARD184 Silicone Elastomer Kit, Dow Corning Corporation) at 10:1 mass ratio was vigorously mixed for 5 min and centrifuged at 2000 rpm (514  $\times g$ ) for 2 min followed by degassing under vacuum for 10 min. Then, the PDMS mixture

was cast onto a micropatterned silicon wafer piece (3 cm x 3 cm) in a sterile petri dish (~5-10 mL, depending upon application) covered, and incubated at 40°C for 12 h. Once cooled to room temperature, the PDMS was carefully separated from the silicon wafer. The PDMS micropatterns were rinsed with DI water, ethanol (70% in DI water), air dried with N<sub>2</sub> gas, and stored covered in a sterile petri dish until use. Note: the surface treatment of HMDS on Si wafers as a lift-off promotor for PDMS casting is a safe and highly effective method compared to silanization via vapor-deposition.

### 3.2.3 Surface Hydrophobicity

The equilibrium contact angle was used to determine surface hydrophobicity. A 5- $\mu$ L droplet of either DI water or 0.01% Tween 80 was applied onto each surface in triplicate and photographed with a high-resolution camera (Canon EOS T6i camera with Canon EF 100mm f/2.8 Macro Lens) immediately after deposition and every 5 min thereafter for a total of 25 min. Images were quantified with ImageJ DropSnake function (Schneider, Rasband, and Eliceiri, 2012), which calculates the contact angle via **Equation 1.1**. Surfaces are classified as hydrophobic if they have contact angles  $>90^\circ$  and hydrophilic if they have contact angles  $<90^\circ$ . Results were averaged and reported with  $\pm$  standard deviation values in **Table 3.1**.

### 3.2.4 Surface Roughness

Surface roughness was evaluated by the parameter  $S_a$ , the surface area analog of line roughness,  $R_a$ , and is given by **Equation 1.2**. Five (5) random locations per sample were imaged using a confocal microscope (Zeiss 780 LSM, Carl Zeiss, Inc., Jena, Germany) equipped with a 20x air lens objective (EC Epiplan Apochromat HDIC 20x, 0.6 NA). Z-stack images were also collected for each sample location. The

imaging parameters were: 1024 x 1024-pixel frame size; 12-bit; 1:1 zoom. Individual measurements (n=5) were performed on the same day for a given sample. Only the transmission channel off of a 488 nm laser line was analyzed in the software using the built-topography function in Zen2010d (Carl Zeiss, Inc., Jena, Germany). The images were fit to a plane to remove surface tilt and a high-pass Gaussian filter with a long-wavelength cutoff  $\gamma$  at 80  $\mu\text{m}$  (for consistency with the protocol in **Chapter 2 Section 2.2.3**, where a wavelength cutoff was applied to remove large-scale topography). Roughness was analyzed at the center of the image without any thresholding. Results were averaged and reported with +/- standard deviation values in **Table 3.1**.

### **3.2.5 Sessile Droplet Suspension**

A suspension of *Salmonella enterica* and fluorescent polystyrene latex colloids were prepared in either sterile ultra-pure DI water or 0.01% Tween 80 (100 ppm). The bacteria were prepared via standard procedures: a pure colony of pGFPuv-*Salmonella enterica* sv, Enteritidis (strain ME18, purchased from UGA Center for Food Safety, Griffin, GA) from a Tryptic Soy Agar (TSA; Becton Dickinson, Franklin Lakes, NJ) plate supplemented with 0.01% (w/v) ampicillin (Sigma-Aldrich, St. Louis, MO), maintained at 4°C) was transferred to a flask containing Tryptic Soy Broth (TSB, Becton Dickinson, Franklin Lakes, NJ) supplemented with 0.01% (w/v) ampicillin and incubated at 30°C with shaking (120 rpm) until stationary phase (~16 - 18 h, confirmed by OD 600 nm). The culture was centrifuged at 4°C / 5000 rpm (3412 xg) / 25 min, washed 1x with sterile 1x PBS, and re-suspended in sterile DI water or 0.01% Tween 80 to a concentration of  $\approx 10^6$  CFU/mL (via 1:1000 dilution; cell concentration was confirmed by a standard plate count method and OD 600 nm) in the colloid

suspension. For the colloid suspension, sulfate-modified polystyrene latex spheres (diameter = 2  $\mu\text{m}$ ; Molecular Probes/Invitrogen, Eugene, OR) were vortex-mixed for 2 min and suspended to a final concentration of 2 ppm (colloid concentration  $\approx 10^6$  particles/mL) in either water or 0.1% Tween 80. Suspensions were carefully mixed by tube inversion. The dimensions of the bacteria were  $2.1 \pm 0.4 \mu\text{m}$  length x  $1.1 \pm 0.1 \mu\text{m}$  width (**Table A.1, Appendix A**).

### **3.2.6 Droplet Evaporation via Confocal Microscopy**

#### **3.2.6.1 Deposition Patterns from Evaporated Droplets**

Deposition patterns of Water and 0.01% Tween 80 droplets containing *Salmonella* and colloids were imaged using an upright 780 Zeiss confocal laser scanning microscope with either a 10x (EC-Plan Neofluar) or 20x (EC-Epiplan Apochromat, HD DIC, 0.6 NA) objective lens. The GFP-bacteria were imaged using a 488nm laser line (green channel), and the colloids using a 561nm laser line (red channel). The surfaces were imaged using a transmission channel (gray channel).

Briefly, a 0.5  $\mu\text{L}$  aliquot of the bacteria-colloid suspension was added to a surface (Glass, PDMS Flat, PDMS Pillars, PDMS Depressions, PDMS Grooves) and imaged within 1 min of deposition using a time-lapse function (968.14 milli-seconds acquisition speed) and 10x objective lens (to accommodate for the entire margin of the droplet) with a frame size of 512 x 512 pixels. After the droplet evaporation event, the entire droplet, as well as close-up regions were imaged using the 10x or 20x lens with a frame size of 1024 x 1024 pixels. Z-stack images were collected with image sizes of 1024 x 1024 pixels. The experiments were carried out under ambient conditions (20-25°C and 48-55% relative humidity).

### 3.2.6.2 Droplet Evaporation Characteristics

The evaporation time, droplet contact area, and contact line evolution of colloid-only droplet suspensions (2 ppm) in DI water or 0.01% Tween 80 were obtained using a confocal microscope (LSM Zeiss 880, Carl Zeiss, Inc., Jena, Germany with a 10x (EC-Plan Neofluar) inverted objective lens, which images from the bottom. A 0.5- $\mu$ L droplet of the colloid-only suspension (either DI water or 0.01% Tween 80) was deposited on a given surface and imaged within 1 min of deposition using a time-lapse function ( $\sim$ 968.14 msec acquisition time) with a frame size of 1024 x 1024 pixels. A 561 nm laser line captured the fluorescence of the particles (red channel), and a transmission channel captures the surfaces (gray channel). After the droplet evaporation event, the videos were analyzed using built-in software (Zen2010d) to determine the droplet evaporation time and to measure the droplet transect length (described below) over the evaporation event. The total droplet evaporation time was quantified as the time between the start of the time-lapse imaging event (within 1 min of droplet deposition) and when the film breaks at the end of the evaporation event (n=3). The droplet contact area was determined by tracing the droplet perimeter from the evaporation videos (n=3) and quantifying the area in ImageJ using standard functions. The droplet contact line evolution was determined by measuring a transect from two points on the droplet edges throughout evaporation using Zen2010 software from a representative evaporation video, shown in **Figure 2.2**. The transect length was measured every 5 frames after the initial frame (frame 1, N<sub>time=0</sub>) for a normalized time, given by  $N_t/N_f$ , where  $N_t$  is the time,  $t$ , at a given frame and  $N_f$  is the time at the final frame,  $f$ . The experiments were carried out under ambient conditions (20-25°C and 48-55% relative humidity).

### 3.2.7 Image and Statistical Analyses

All microscopic data was analyzed using Zen2010D and ImageJ software (noted in text where appropriate). JMP statistical analysis program was used to determine the statistical significance at  $p < 0.05$  via One-way or Two-way ANOVA (with replication) and Tukey-Kramer post-hoc analysis.

## 3.3 Results and Discussion

### 3.3.1 Micropatterned Surface Properties

#### 3.3.1.1 Surface Roughness of Micropatterns

**Table 3.1.** shows the physicochemical characterizations of the micropatterned surfaces. Roughness values increased with adding micropatterned features to the PDMS surfaces compared to the PDMS Flat surface. Glass and PDMS Flat surfaces had practically identical roughness  $S_a$  values ( $p = 1.0000$ ) and are considered “smooth” control surfaces while the micropatterned surfaces are considered “rough” surfaces. There were significant differences for all micropatterned surfaces compared to the PDMS Flat and Glass ( $p < 0.0001$ , all comparisons). Among the micropatterned surfaces, there was a significant difference in the  $S_a$  values for PDMS Depressions compared to PDMS Pillars ( $p < 0.0001$ ) and PDMS Depressions compared to PDMS Grooves ( $p < 0.0001$ ). There was no significant difference between the PDMS Pillars and PDMS Grooves. Because  $S_a$  by **Equation 1.2** analyzes the mean absolute height deviations, the PDMS Pillars and PDMS Depressions would have identical roughness values if the patterns were inverse of each other (i.e., same array but one depressed and the other raised). The result of PDMS Depression differences with the PDMS Pillars is likely due to the spatial arrangement of the features: PDMS Depressions are

spaced closer together, which adds more patterns to the surface area. The effect is noticeable in the deposition pattern images in **Figure 3.2-3.5**.

**Table 3.1** Surface roughness (n=5) and hydrophobicity (n=3) of Glass, PDMS Flat, PDMS Pillars, PDMS Depressions, and PDMS Grooves in DI Water or 0.01% Tween 80 droplets

Surface	Roughness, $S_a$ $\mu\text{m}$ (n=5)	Equilibrium Contact Angle, $\theta_{water}$ , degrees (t=0min; n=3)	Final Equilibrium Contact Angle, $\theta_{water}$ , degrees (t=25 min; n=3)
Glass	$0.008 \pm 0.0004$	$34 \pm 5^\circ$ (hydrophilic)	$14 \pm 3^\circ$ (hydrophilic)
PDMS Flat	$0.008 \pm 0.0004$	$106 \pm 4^\circ$ (hydrophobic)	$93 \pm 5^\circ$ (hydrophobic)
PDMS Pillars	$0.365 \pm 0.01$	$111 \pm 4^\circ$ (hydrophobic)	$100 \pm 1^\circ$ (hydrophobic)
PDMS Depressions	$0.577 \pm 0.05$	$117 \pm 2^\circ$ (hydrophobic)	$102 \pm 3^\circ$ (hydrophobic)
PDMS Grooves	$0.396 \pm 0.01$	$123 \pm 7^\circ$ (hydrophobic)	$114 \pm 3^\circ$ (hydrophobic)

Averages reported with  $\pm$  standard deviation.

Ultra-pure deionized water,  $18.2 \text{ m}\Omega/\text{cm}^2$ ; ambient conditions.

### 3.3.1.2 Surface Hydrophobicity of Micropatterns

**Table 3.1** and **Figure 3.2** also show the equilibrium contact angle values for the different surfaces using  $5.0 \mu\text{L}$  water droplets. Based on these values, all PDMS surfaces are classified as hydrophobic (PDMS as a material is naturally hydrophobic) with contact angles  $\theta > 90^\circ$ , while Glass was classified as hydrophilic ( $\theta < 90^\circ$ ). The contact angles obtained for the Glass surfaces were significantly different compared to the PDMS surfaces via One-way ANOVA with Tukey-Kramer analysis ( $p < 0.0001$  for all comparisons). This is expected due to the hydrophilic nature of Glass, which had contact angle  $\theta = 34 \pm 5^\circ$ .

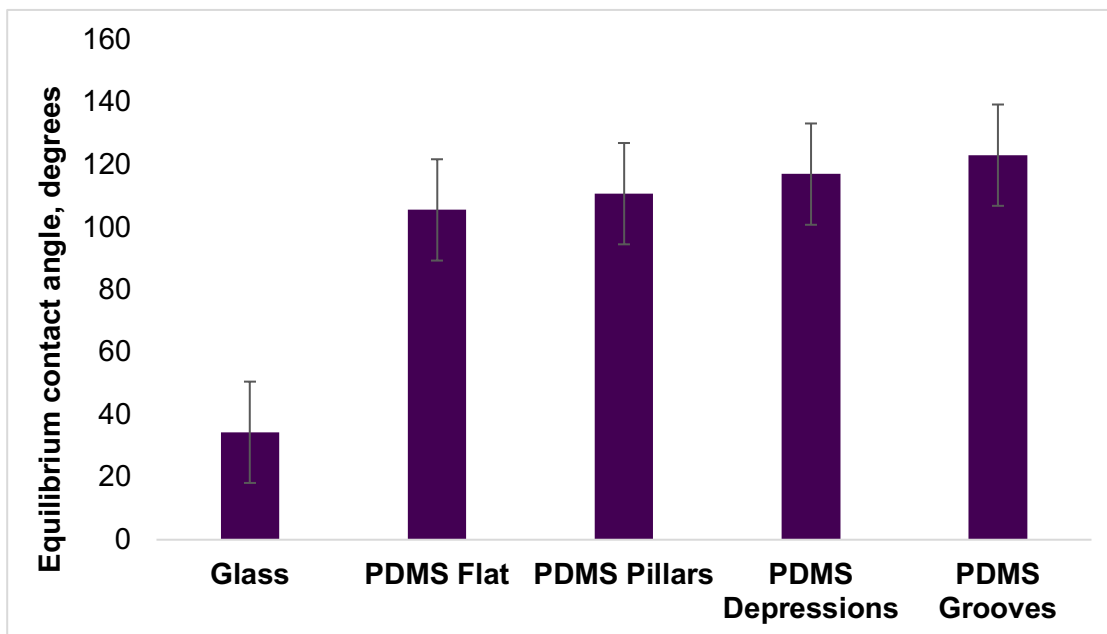


**Figure 3.2** Equilibrium contact angles 5.0  $\mu\text{L}$  DI water droplets on Glass, PDMS Flat, PDMS Pillars, PDMS Depressions, and PDMS Grooves.

The DI water contact angles for the PDMS micropatterns were higher compared to the PDMS Flat surface. Increasing surface roughness is known to increase contact angles for hydrophobic surfaces due to the way the liquid “sits” on top of the surface (Thormann, 2017). However, when comparing the PDMS surfaces via One-way ANOVA, only the mean contact angle obtained for PDMS Grooves was significantly different compared to the PDMS Flat surface ( $p = 0.0250$ ). From the resulting deposition patterns (**Figure 3.3**) and droplet transect length analysis (**Figure 3.8**) discussed later, it’s possible that this is due to the specific architecture of Grooves altering the wetting behavior. In microscopy videos, a transition in wetting states of the droplets on PDMS Grooves was observed: after initial deposition, air entrapped between the depression regions of the grooves. At later stages in the evaporation

process, the depressed regions were filled with the water droplet. This type of wetting transition is classified as Cassie-Baxter (with air entrapment between roughness features) to Wenzel wetting (wetting of fluid between roughness features) (Thormann, 2017).

### **3.3.2 Qualitative Analysis of Deposition Patterns**

**Figures 3.3-3.4**, and **Figures 3.5-3.6** show the deposition patterns of Water and 0.01% Tween 80 droplets, respectively, containing colloids and *Salmonella* on Glass, PDMS Flat, PDMS Pillars, PDMS Depressions, and PDMS Grooves.

#### **3.3.2.1 Deposition Patterns from Water Droplets**

**Figure 3.3** shows the deposition patterns of water droplets containing *Salmonella* and colloids on Glass, PDMS Flat, and the PDMS Micropatterned surfaces. The variation in the deposition patterns demonstrate the influence of surface properties, hydrophobicity and topography/roughness, in the resulting deposition patterns, discussed in detail below.

As Water droplets evaporated on Glass, colloids and bacteria were deposited along the contact line in aggregates as the contact line moved during evaporation or was pinned/immobilized. As a result, Glass deposition patterns were larger in area compared to the PDMS surfaces. Occasionally, the contact line would pin, demonstrated in **Figure 3.8** for the transect length changes. Pinning of the contact line is known to cause an outward flow of liquid to the edges of the droplet, known as capillary flow, which can transport particles towards the droplet edges resulting in deposition at the contact line (Deegan et al., 2000; Parsa et al., 2018). The effect is pronounced for hydrophilic surfaces. On Glass, particles arrived at the droplet edge

due to this flow and aggregated at the contact line, where they deposited in large aggregates ( $> 3$  particles), confirmed by the microscopy videos. The aggregation at the droplet edge may have caused a very thin film at the air-water-solid interface over the particles which could not mobilize the particles as the contact line receded (possible due to film straining).

Comparing the PDMS surfaces together allows for analyzing the influence of surface topography/roughness. On PDMS Flat, *Salmonella* and colloids followed the contact line and did not deposit until the last stages of evaporation when the film ruptured, leaving a small dot-like pattern that outlines the final droplet contact area. By comparison, micropattern architecture is clearly distinguishable from the deposition patterns in **Figure 3.3**. For the micropatterned surfaces, deposition occurred as the contact line receded and pinned at surface features. Surface features can pin the contact line, driving particle-surface interactions that can enhance pinning and lead to deposition.

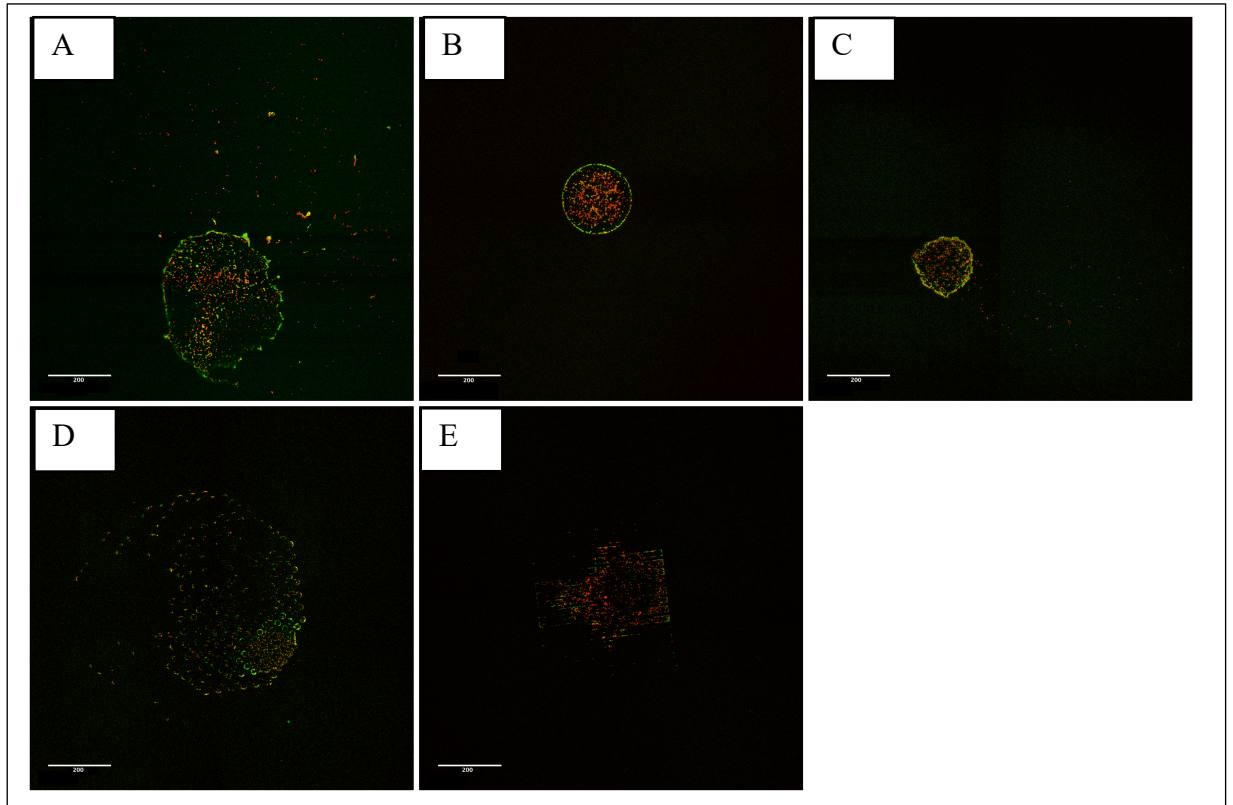


**Figure 3.3** Representative confocal images (780 LSM) of the deposition patterns of colloids (red) and *Salmonella* (green) in water droplets. A) Glass; B) PDMS flat; C) PDMS Pillars; D) PDMS Depressions; and E) PDMS Grooves. The transmission channel was removed to improve visibility. Scale bar is 200  $\mu\text{m}$ .

Deposition at the contact line as the contact line mobilized during evaporation occurred for PDMS Pillars and PDMS Depressions. For Grooves, the deposition did not occur in the latest stages of evaporation, due to an extended contact line pinning stage. Interestingly, droplets on PDMS Pillars exhibited capillary action-like movement at the final stages of evaporation evidenced in the microscopy videos. At the later stages of evaporation, the entire droplet mobilized across the patterned surface from one side of the droplet until the film finally ruptured and the particles

deposited. This action was not seen for other patterns. It's possible that the combination of pinning and particle flux at pinned sites mobilized the droplet while it simultaneously de-pinned from the opposite side of the droplet.

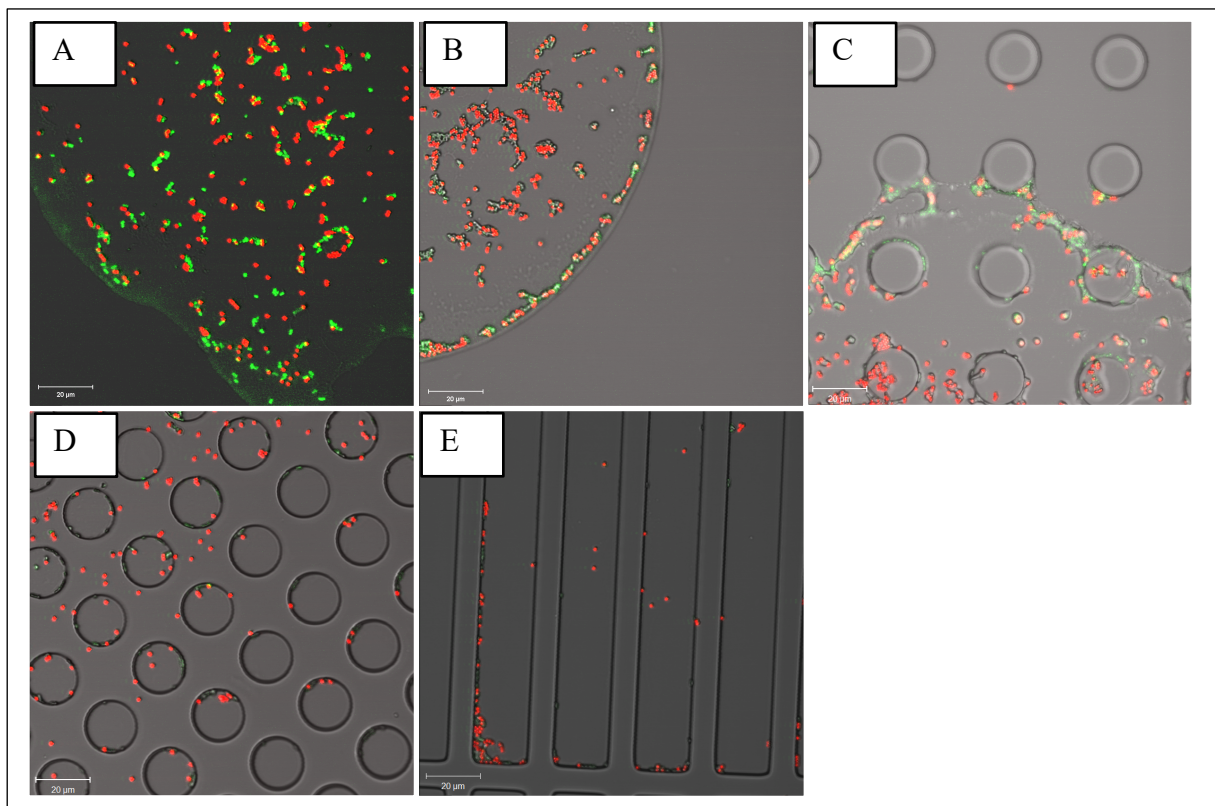


**Figure 3.4** Representative confocal images (780 LSM) of the deposition patterns of colloids (red) and *Salmonella* (green) in DI water droplets at close-up regions. A) Glass; B) PDMS flat; C) PDMS Pillars; D) PDMS Depressions; and E) PDMS Grooves. Arrows point to localization at surface features from pinning. Scale bar is 20 μm.

The deposition patterns of colloids and bacteria are similar, but bacteria appear localize at the edges of the droplet, particularly at the end stages of evaporation, seen

as a distinct ring of green in **Figure 3.3**. This indicates a potential ability of bacteria to transport with the contact line. It was observed that for Glass and PDMS Pillars, mostly colloids deposited along the mobile contact line as the droplet evaporated, while the bacteria seem to deposit at the final droplet contact region. By contrast, colloids and bacteria appear to deposit throughout the PDMS Depressions. This may be due to the difference in roughness that created more sites for pinning; PDMS Depressions had larger  $S_a$  values than PDMS Pillars, ( $0.577 \pm 0.05$  and  $0.365 \pm 0.01$ , respectively). Stick-slip mode of contact line behavior was indeed observed, resulting in the periodic deposition of particles at surface features where the contact pinned and de-pinned, discussed in more detail in **3.3.3**.

#### **3.3.2.2 Deposition Patterns from 0.01% Tween 80 Droplets**

The deposition patterns from evaporating 0.01% Tween 80 droplets on Glass, PDMS Flat, and the PDMS Micropatterned surfaces are presented in **Figure 3.5** with close-up images in **Figure 3.6**. Due to the variation in resulting deposition pattern area, the scale bars in **Figure 3.5** vary in length but are all set to 200  $\mu\text{m}$  for comparison

Compared to Water droplet patterns, Tween droplets resulted in patterns of a larger area. Similar to Water deposition patterns, the morphology of the deposition patterns of Tween droplets varies by surface, highlighting the influence of surface roughness/topography and hydrophobicity. In general, deposition patterns for Tween droplets are more uniform with respect to the localization of bacteria and colloids compared to Water deposition patterns.

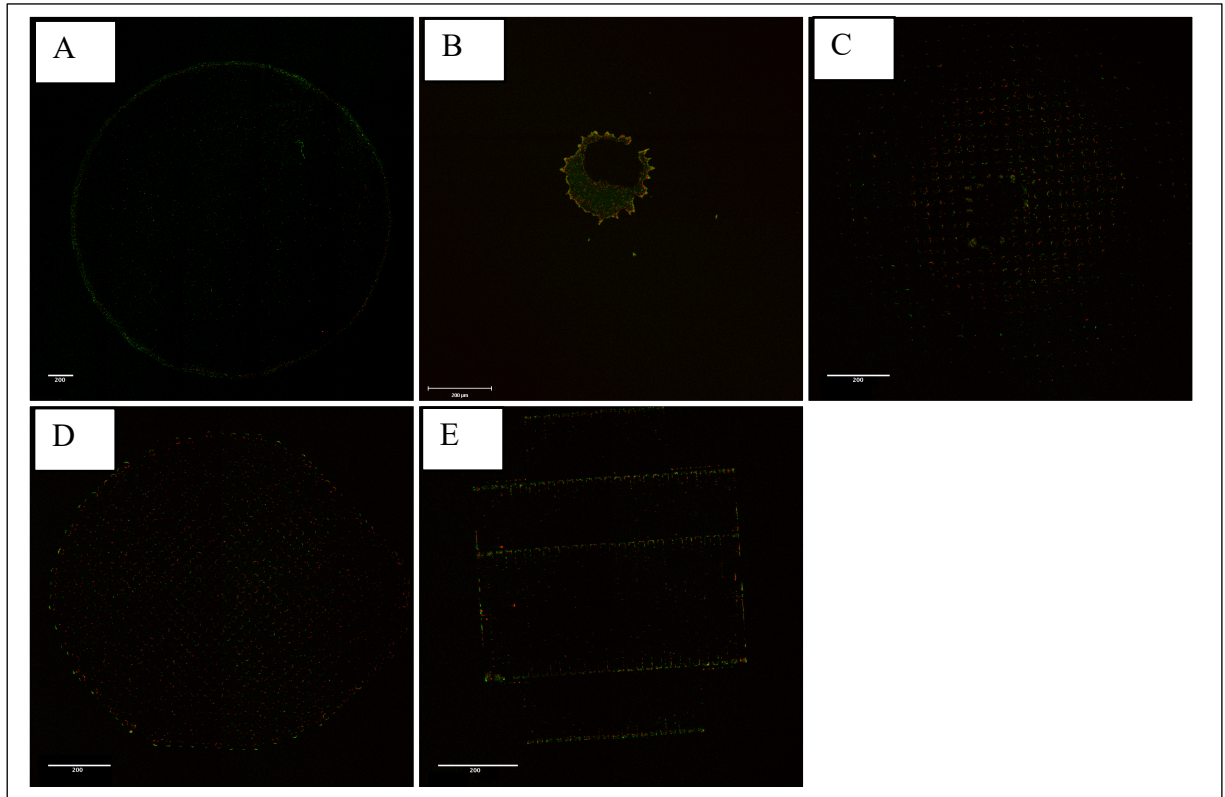


**Figure 3.5** Representative confocal images (780 LSM) of the deposition patterns of colloids (red) and *Salmonella* (green) in 0.01% Tween 80 droplets. A) Glass; B) PDMS flat; C) PDMS Pillars; D) PDMS Depressions; and E) PDMS Grooves. The transmission channel was removed to improve visibility. Scale bar is set to 200  $\mu\text{m}$  but varies by length due to the different scales in the images.

The deposition area for Tween droplets on Glass was the largest compared to the other patterns. This resulted from a combination of surface hydrophilicity and lower surface tension of the 0.01% Tween 80 solution ( $\sim 35$  mN/m), which increased the wetting area resulting in a thinner film compared to Water droplets. Two distinct coffee-ring like structures developed on Glass: one at the original contact line and a second at the final droplet contact area at the latest stages of evaporation. Between these two points, colloids and bacteria also deposited “in place,” as a result of the thin

film. The droplet on Glass remained pinned for most of the evaporation lifetime (**Figure 3.8-A**), causing a flux of particles to the edges to create the first ring structure. As the water evaporated from the Tween suspension, a surfactant residue was left behind as the contact line receded (**Figures 3.5-3.6**). These globules and micelles contained bacteria and colloids and were located within depressed or raised features for the micropatterned surfaces and are shown in **Figure 3.6**.

Marangoni-like fluxes were observed in the microscopy videos occurring at the pinned contact line edge for Glass, causing colloids to oscillate towards and away from the droplet edge. This was likely caused by the gradient in surface tension from the increased in surfactant as the droplet evaporated. The microscopy videos and images show that *Salmonella* were transported directly to the edge of the contact line and did not appear to oscillate around the contact line by Marangoni flows.

Tween droplets on the PDMS micropatterned surface demonstrated similar increased deposition area compared to Water droplets arising from increased wetting of the droplet. On PDMS Flat, particles did not deposit until the final stages of evaporation. By comparison, the PDMS micropatterned surfaces induced deposition from the original contact line and throughout evaporation at surface features, demonstrating the influence of patterned topography/roughness. Tween deposition patterns for PDMS Pillars and PDMS Depressed patterns are more comparable than their Water pattern counterparts. For PDMS Grooves, deposition of particles occurred at the edges of the patterned depressions due to a longer pinned phase (discussed further in **3.3.3**).

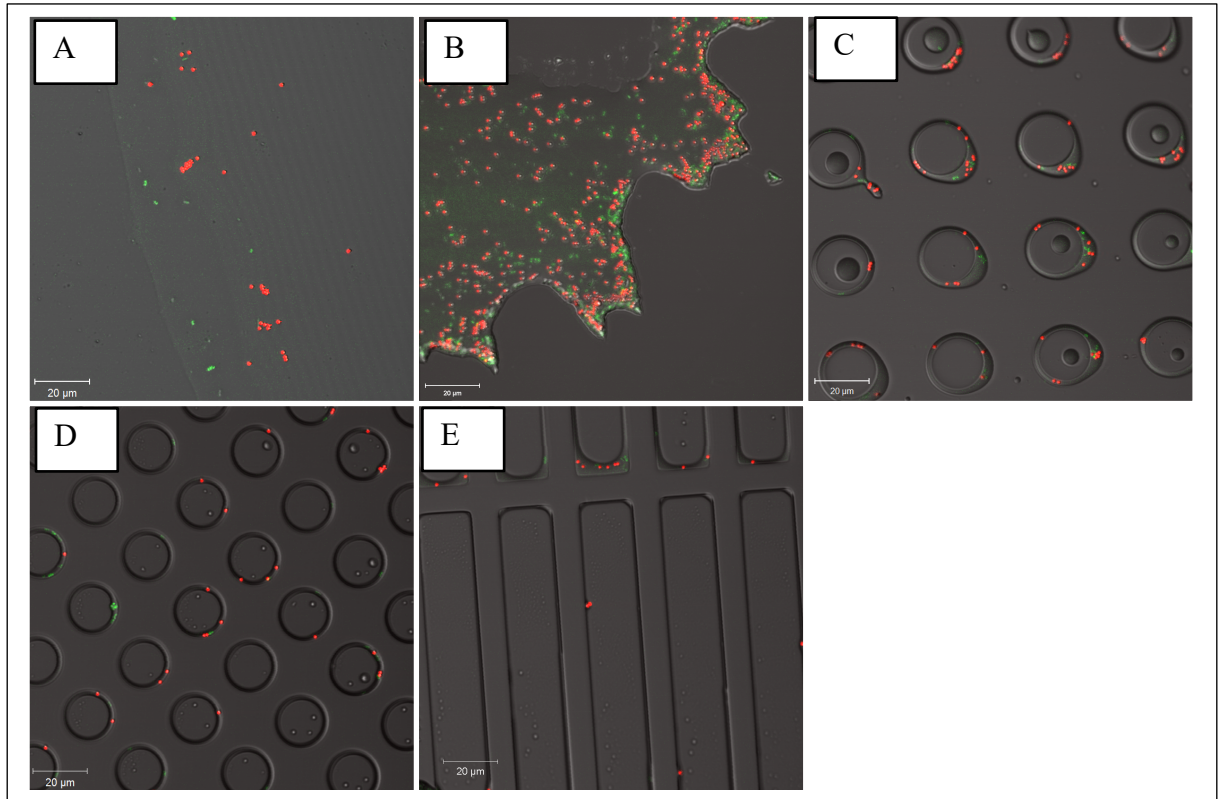


**Figure 3.6** Representative confocal images (780 LSM) of the deposition patterns of colloids (red) and *Salmonella* (green) in 0.01% Tween 80 droplets at close-up regions. A) Glass; B) PDMS flat; C) PDMS Pillars; D) PMS Depressions; and E) PDMS Grooves. Arrows point to regions with deposition in features or in surfactant micelles. Scale bar is 20  $\mu\text{m}$ .

### 3.3.3 Droplet Evaporation Dynamics

The droplet evaporation time and contact line behavior from time-lapse microscopy videos (LSM 880) are summarized in **Figures 3.7** and **3.8**, respectively.

#### 3.3.3.1 Droplet Evaporation Time

**Figure 3.7** shows the droplet evaporation time for the Water and 0.01% Tween 80 droplets on the different surfaces recorded by video microscopy (880 LSM).

Analysis via Two-Way ANOVA resulted in insignificance for the interaction term

between surface and suspension type (Water or Tween) ( $df=3$ ;  $F=0.9982$ ;  $p=0.4316$ ) but significance for the surface effect ( $p<0.0001$ ).

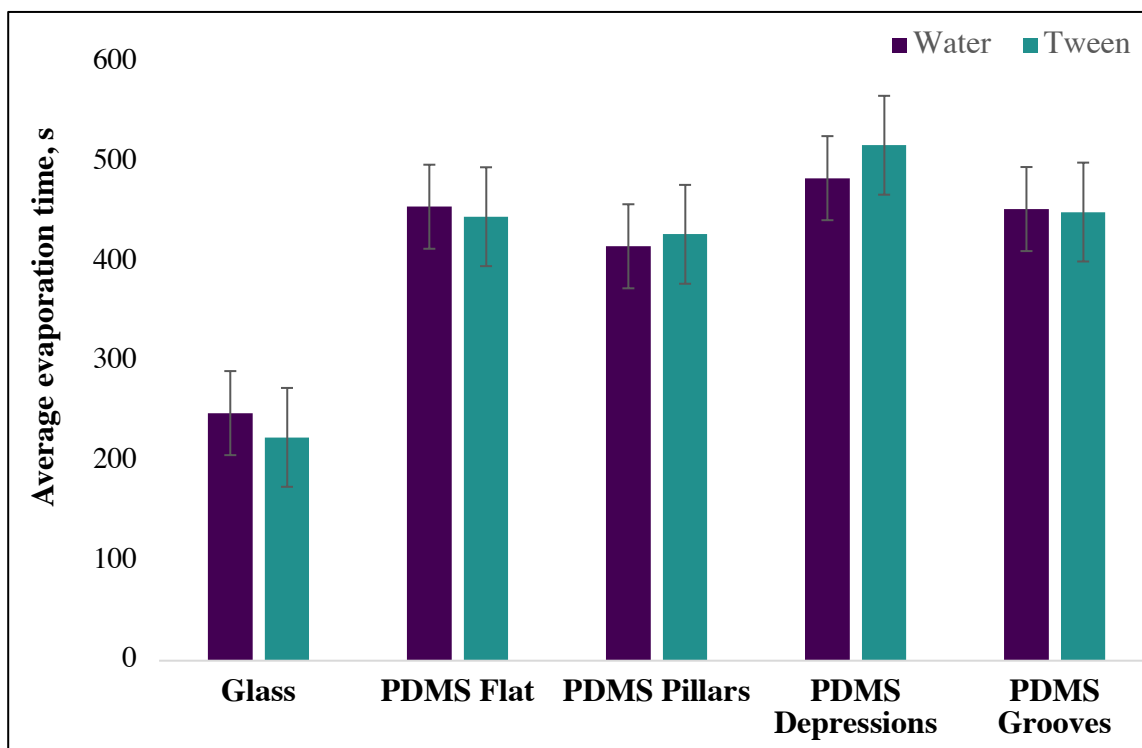


**Figure 3.7** Droplet evaporation for Water (purple) and 0.01% Tween 80 (teal) droplets on the different surfaces, with standard error bars.

Results of the One-way ANOVA show that for both Water and Tween droplets, evaporation time for Glass surfaces was significantly lower than the evaporation time for the PDMS surfaces. For water droplets on Glass, this resulted in the following p-values for the comparisons: Glass x PDMS Depressions,  $p < 0.0001$ ; Glass x PDMS Flat,  $p < 0.0001$ ; Glass x PDMS Grooves,  $p < 0.0001$ ; and Glass x PDMS Pillars,  $p = 0.0003$ .

For Tween 80 droplets on Glass, all comparisons to PDMS surface were significant, meaning that the evaporation time on Glass was faster compared to the evaporation times on PDMS surfaces. Glass x Depressions/Grooves/Flat/Pillars resulted in a p-value of  $< 0.0001$  (for each comparison). There were significant differences in the evaporation time for PDMS Depressions compared to the other PDMS Surface such that the evaporation rate for PDMS Depressions was significantly longer than the other PDMS surfaces (PDMS Depressions x PDMS Pillars,  $p=0.0084$ ; PDMS Depressions x PDMS Flat,  $p=0.0223$ ; and PDMS Depressions x PDMS Grooves,  $p=0.0464$ ). These results highlight the influence of surface properties, topography/roughness and hydrophobicity, on the evaporation rates. The hydrophilic Glass surface had the fastest evaporation rate, likely due to the thinner liquid films and pinning of the contact line. For PDMS Depressions, the increased roughness from the topography resulted in more frequent pin/de-pin phases, which lengthened evaporation time. The contact line behavior is summarized in more detail in **3.3.3.2**.

### **3.3.3.2 Droplet Contact Line Behavior**

The receding contact line behavior of evaporating droplets on the different surfaces is reported in **Figure 3.8**.

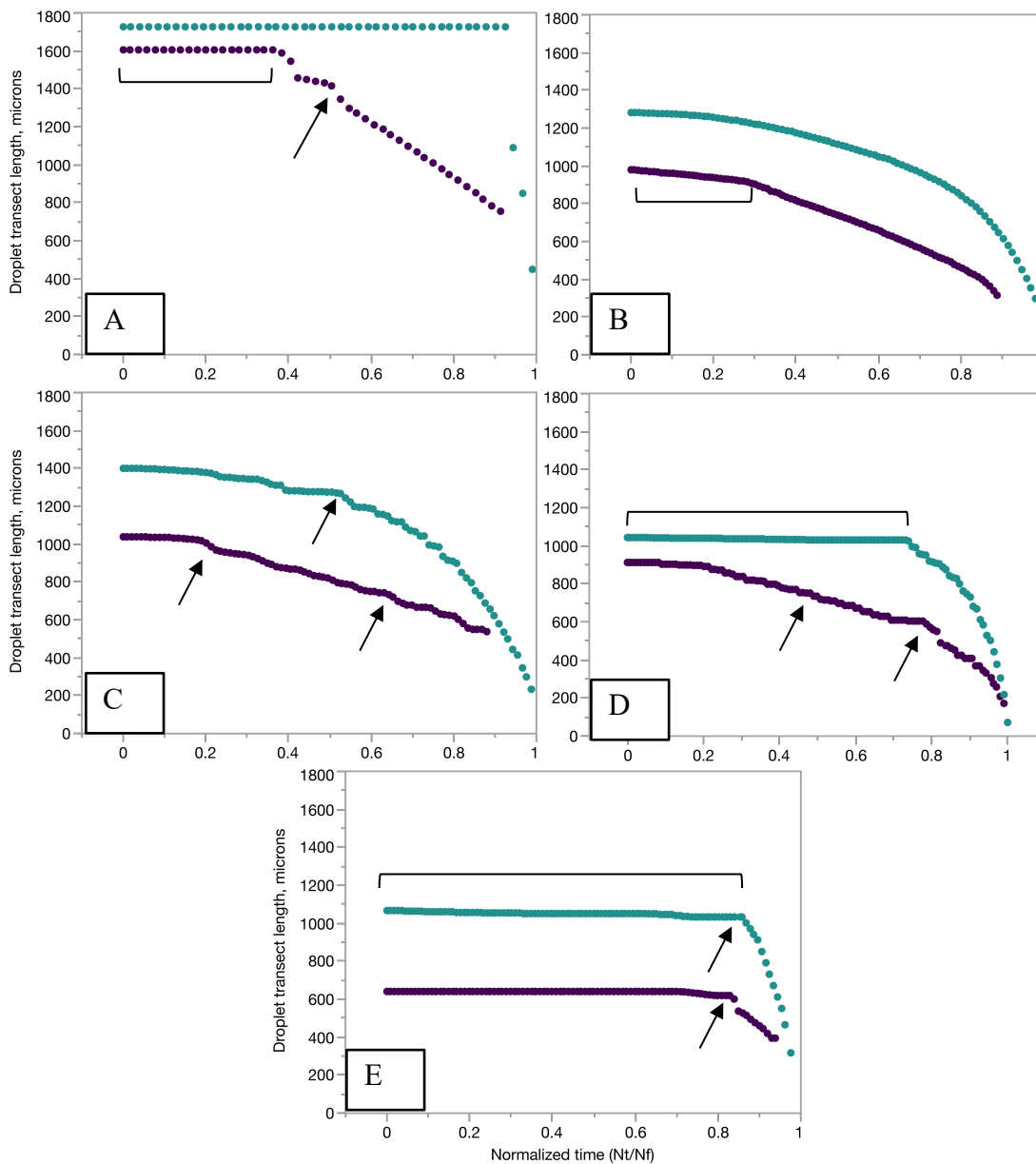


**Figure 3.8** Plot of the contact line evolution for representative Water (purple) or 0.01% Tween 80 (teal) droplets on A) Glass; B) PDMS Flat; C) PDMS Pillars, D) PDMS Depressions, and E) PDMS Grooves. The y-axis refers to a transect through two edge points over the droplet contact area, similar to a diameter. Due to the heterogeneity of the surface features, a true diameter is not apparent. Arrows point to example changes in contact line behavior, and brackets indicate example contact line pinning stages.

The experimental results for the characterization of droplet contact line behavior over time for Water droplets on the different surfaces is summarized in **Figure 3.8**. All droplets (**Figure 3.8 A-E**) exhibited mix modes of contact evaporation behavior, but with differences in the lengths of the first stage as a result of surface properties. For all surfaces, there was an initial pinning phase of the contact line. For the hydrophilic Glass substrate (**Figure 3.8-A**), there was virtually no change in the droplet transect length due to contact line pinning for ~40% of the droplet evaporation lifetime, which is evidenced in **Figure 3.8** as a flat trend/plateau and can be characterized by the constant contact line (CCL) modal. Additionally, the contact line temporarily pinned and de-pinned until it eventually a linear-like decrease in the droplet transect length overtime in the second phase occurred for the remainder of the droplet lifetime.

For the PDMS surfaces (**Figure 3.8 B-E**), the droplet transect length changed more gradually with time compared to the Glass surface (**Figure 3.8-A**) due to a combination of surface topography/roughness and hydrophobicity. The initial stage evolved similar to a constant contact diameter mode. As the evaporation progresses, the droplet contact line lengths changed at varying rates depending upon the surface, transitioning from a relatively constant length in the first stage of evaporation to a stick-slip or mix mode of evaporation. These modes reflect how a droplet contact angle and line length change dynamically at pinned sites. Compared to the other PDMS surfaces, PDMS Flat proceeded with a steady and gradual decrease in droplet diameter as it transitioned likely to a constant contact angle (CCA) mode. Transitions in the evaporation dynamics are obvious when comparing PDMS Flat to PDMS Micropatterns (Pillars, Depressions, and Grooves). For the PDMS micropatterns,

stick-slip evaporation modes are apparent with the step-wise changes in droplet diameter over time and occur at different points during the evaporation process depending on the surface. PDMS Grooves demonstrated the most extended of its original contact line length relative to the droplet's lifetime compared to the other surfaces. The PDMS Grooves had the highest equilibrium contact angle compared to the other surfaces, which likely caused evaporation from the apex of the droplet rather than the edges. As mentioned previously, it's possible this was due to the architecture of the surface causing entrapped air and a higher contact angle until the wetting transitioned to fill the surface depressions with fluid and subsequently cause pinning and deposition.

The experimental results for the Tween droplet contact diameter evolution versus time showed an extended pinning phase that maintained for longer periods in the evaporation process relative to the droplet's lifetime compared to water droplets. Transitions to mix-mode evaporation did not occur until after > 50 % droplet lifetime, although this is not the case for PDMS Pillars and PDMS Flat. PDMS Flat proceeded with a gradual decrease in contact line length, likely due to both a change in the contact angle and droplet diameter characterized by mix-mode of evaporation. For PDMS Pillars, the onset of stick-slip transition occurred after ~20% of the evaporation time. Tween droplets on PDMS Grooves had the longest initial pinning phase for ~85% of the droplet lifetime, again reflecting the higher contact angle and thus different hydrodynamics and evaporative fluxes resulting in the droplet. Similar to water, the PDMS micropatterns have stick-slip behavior demonstrated as step-wise changed in droplet transect length depicted in **Figure 3.8** and highlighted with arrows. The stick-

slip behavior and the corresponding deposition at these pin/de-pinning sites was also confirmed in the microscopy videos.

### 3.4 Summary

In this study, the droplet contact line behavior and deposition patterns of sessile droplets containing GFP-*Salmonella enterica* sv. Enteritidis and fluorescent colloids was characterized on smooth and micropatterned surfaces. Here, it was demonstrated that surface hydrophobicity influenced the contact line behavior by comparing deposition patterns of Glass to PDMS Flat surfaces, which have similar roughness values but very different hydrophobicity. The influence of patterned roughness and topography on contact line behavior was also demonstrated by comparing PDMS micropatterns to the PDMS Flat surface. Finally, the addition of surfactant Tween 80 had several effects caused by the reduced surface tension compared to Water droplets: 1) increased wetting and deposition area and decreased film thickness 2) altered fluid flow within the droplets preventing particle transport to the edges and 3) decreased capillary forces leading to more uniform deposition patterns over a larger area. As the Tween 80 droplets evaporated, the concentration of surfactant increased with time and caused a surface tension gradient. Gradients in surface tension can lead to Marangoni flows, which prevent particles from transporting to the contact line. This generally leads to more uniform deposition of particles on surfaces, which was also observed in this study. Surface roughness also plays a role by introducing pinning sites that can alter the flow of particles at these regions. This pinning by surface features may also drive surfactant molecules to the edges, entrapping particles. Large globules and smaller micelles that formed at the edges of either the final deposition pattern or at pinned regions were observed.

Importantly, the lower surface tension also creates a thin film, in addition to weaker capillary forces. This effect decreases the mobilization of particles with the contact line. In combination with the flow and surface feature pinning effects, the total effect limited particle transport and lead to deposition. A more detailed discussion is provided in **Chapter 4**.

## Chapter 4

### DISCUSSION, CONCLUSIONS, AND FUTURE WORK

#### 4.1 Discussion

##### 4.1.1 Mechanisms Leading to *Salmonella* and Colloid Transport and Deposition in Evaporating Sessile Droplets

Droplet evaporation and particle deposition at contact lines is a dynamic process that is characterized by the spatiotemporal changes in contact line behavior. This dynamic behavior is influenced by surface, solution, and particle properties (e.g., Lazouskaya et al., 2013; Parsa et al., 2018) and are further discussed below in relation to the observed data reported in section **Results 2.3** and **3.3**.

##### 4.1.1.1 Surface Roughness

Surface roughness features can act as pinning sites that can temporarily immobilize the contact line and lead to deposition of particles (Parsa, Harmand, and Sefiane, 2018; e.g., Nguyen et al., 2012). In this study, it was demonstrated that surface topography and roughness resulted in differences in the deposition patterns of *Salmonella* and colloids on the Glass, PDMS Flat, PDMS produce surfaces, and PDMS Micropatterned surfaces. To compare the effect of surface roughness, the discussion is focused on the deposition patterns of water droplets for the PDMS Flat and the PDMS rough surfaces, which have the same chemical composition but differ by surface topography/roughness and hydrophobicity.

Without roughness features, the deposition pattern of colloids and *Salmonella* on PDMS Flat assumes a small area of residue in a spherical shape (**Figure 2.4-B** and **Figure 3.3-B**). By contrast, the shape of plant cells on PDMS Lettuce and PDMS Spinach replicas is distinctly outlined (**Figure 2.4-2.7**) as well as the topography of the

micropatterned surfaces (**Figures 3.3-3.6**). PDMS Spinach and PDMS Lettuce had large roughness scales with  $S_a > 3 \text{ um}$  (Lazouskaya et al., 2016) compared to the smooth Glass and PDMS Flat surfaces ( $S_a \ll 3 \text{ um}$ ). PDMS Micropatterned surfaces were also statistically different in  $S_a$  values compared to those of Glass and PDMS Flat ( $S_a \sim 0.35-0.58$ ). The microscopy videos showed how roughness caused pinning of the contact line during evaporation, quantified as transect line length and shown in **Figure 2.11 and Figure 3.8**. The transect lengths for PDMS Spinach and PDMS Lettuce surfaces changed in a step-wise fashion after an initial pinning phase. This was also evidenced for the PDMS micropatterns, which was more periodic due to the regularity in surface patterns. By contrast, the transect length for PDMS Flat changed more gradually with time after an initial semi-pinning phase. As mentioned in the results (**Results 2.3, 3.3**) for the rough surfaces, some regions of the droplet pinned while other regions de-pinned (e.g., in the y-direction or in the x-direction). This pinning and de-pinning action continued for the remainder of the evaporation event. This effect is attributed to the surface heterogeneities caused by roughness features and was pronounced for the PDMS Spinach and PDMS Lettuce surfaces compared to the PDMS Micropatterned surfaces due to the spatial variation in topography/roughness (PDMS micropatterns have periodic spacing between features of the defined distances).

It is well known in the droplet literature that pinning can cause changes in evaporative fluxes within a droplet (reviewed by Parsa et al., 2018). Most often, pinning contributes to a fluid flux, known as capillary flow, towards the pinned contact line, which can carry particles to this region (Deegan et al., 2000). Rough surfaces that pin contact lines (e.g., Nguyen et al., 2012) can direct fluid fluxes at

these sites, driving particle transport to the surface features. The PDMS Flat surface did not pin the contact line during the evaporation event, therefore deposition of particles caused by pinning was not observed. However, on PDMS Spinach, PDMS Lettuce, and the PDMS Micropatterned surfaces, the contact line temporarily immobilized at surface features. *Salmonella* and colloids transported to this pinned contact line at surface features, and occasionally were left behind (i.e., deposited) as the contact line de-pinned and moved (e.g., **Figure 2.10** and **Figure 3.8**). For the PDMS Spinach and PDMS Lettuce surfaces, the majority of *Salmonella* and colloids, however, did not deposit until the last stages of evaporation, likely due to the combination of the hydrophobicity of the surface influencing the droplet height and the thickness of water films at roughness features, discussed further in **4.1.1.2** and **4.1.1.3**.

#### **4.1.1.2 Surface Hydrophobicity**

In addition to surface roughness, surface hydrophobicity influences contact line behavior and thus particle deposition (e.g., Orejon et al., 2011) by altering the droplet height and thickness of water films. The surface hydrophobicity via the equilibrium contact angle method determined that Glass was the only hydrophilic surface ( $\theta = 34 \pm 5^\circ$ ) and PDMS Surfaces as hydrophobic ( $\theta > 95^\circ$ ). Here, Water droplets on Glass and PDMS Flat surfaces are considered. Due to the wettability of Glass, the water droplet spreads across a larger area compared to the PDMS Flat surface (i.e., a larger droplet contact area, shown in **Figure 2.9**) and is thinner at the edges. From the microscopy videos, there was noticeable pinning on Glass that lead to particle transport to the edges and subsequently deposition from the contact line as it receded during evaporation. For Glass, the contact line remained pinned for  $\sim 40\%$  of

the droplet lifetime in the initial stages and pinned again during evaporation. This pinning modal is supported by the transect length changes in **Figure 2.10-A**/**Figure 3.8-A** and the deposition pattern in **Figure 2.4-A**/**Figure 3.3-A**, and was also observed in the microscopy videos. Hydrophilic surfaces are known to induce pinning of contact lines leading to capillary flow that drives particles to the edges where they may accumulate (Deegan et al., 2000; Deegan, 2000). In the microscopy videos, *Salmonella* and colloids were observed transporting to the pinned contact line, demonstrated in **Figure 2.10-A**, which continued as the contact line receded. At this region, particles aggregated and deposited on the surface, e.g., **Figure 2.10-A**, in large aggregates (>3 particles, see **Figure 2.4**). This particle deposition via contact line pinning due to particles did not always induce a static transect length.

The hydrophobic PDMS surfaces exhibited different contact line behavior and thus evaporation fluxes (e.g., Nguyen et al., 2012). Clear differences in the deposition pattern of Water droplets on PDMS Flat compared to Glass surfaces were observed to support this effect. As mentioned in the previous subsection about roughness, no pinning occurred on the PDMS Flat surfaces after the initial stages of evaporation. The droplet assumed a small, spherical contact area that decreased gradually throughout evaporation, and the deposition of particles during contact line movement was not observed, which suggests a greater droplet height from larger contact angles. If the edges of droplets on smooth, hydrophobic surfaces do not pin, there is minimal flux to this region of the droplet. Due to the lack of pinning, particles are not transported to the edges as in the case of hydrophilic surfaces (e.g., Hu and Larson, 2006) and likely a greater evaporative rate at the apex of the droplet. In this case, particles may aggregate within the droplet due to the increase in particle-particle interactions and

may experience recirculatory flow from Marangoni fluxes or simple diffuse (Michen et al., 2014; Yu, Wang, and Huang, 2017). Aggregates were observed during the later stages of evaporation in the microscopy videos, also shown in **Figure 2.11-B**. Only at the last stage of evaporation was the film was thin enough to cause pinning and a fluid flux via capillary flow to the edges, and the overall result was a dot-like pattern (e.g., Parsa et al., 2018) seen in **Figure 2.4-B/Figure 3.3-B**.

#### **4.1.1.3 Hydrodynamics, Capillary Forces, and Film Thickness**

As mentioned, the fluid flux within droplets influences the transport of particles during evaporation. Outward flow in a drying drop is produced when the contact line is pinned from the edge, causing an increase in the evaporation rate and driving liquid from the bulk to the edges to replenish the loss of fluid (Deegan et al., 2000). It was observed that the hydrophilic surface, Glass, resulted in particle transport to and deposition from the pinned contact line as a result of this flow. For hydrophobic surfaces, a lack of capillary flow prevented particle transport to the edges, which subsequently prevented deposition during evaporation, demonstrated with the PDMS Flat surface. It was also demonstrated in this study that the surface features of PDMS Spinach, PDMS Lettuce, and the PDMS Micropatterns can provide a foothold onto which the contact line could stick and drive some outward flow of bacteria and colloids to the edges, although this did not always lead to their deposition at these regions, which may be attributed to larger contact angles and thicker films. It was found that the addition of surfactant in the droplets lead to changes in the deposition pattern morphology, an increase in the deposition area, and longer pinning of the contact line compared to water droplets. This observation was attributed to the reduction in capillary forces and the thickness of the droplet films that, combined with

surface features, inhibited particle mobilization and altered the capillary flux within the droplet, leading to deposition over a larger area. These concepts are explored in more detail below.

Air-water interfaces interact with colloidal particles mainly by capillary forces (Lazouskaya et al., 2013; Aramrak et al., 2013). The surface tension of 0.01% Tween 80 suspension is ~35 mN/m, compared to ~72 mN/m for Water, which would cause a decrease in the capillary forces by **Equation 1.3**, shown again below:

$$F_{\sigma} = 2\pi r\sigma\sin\phi\sin(\theta - \phi) \quad (1.3)$$

where  $\sigma$  is the liquid surface tension,  $\theta$  is the dynamic contact angle on the colloid surface, and  $\phi$  is the angle determining the AWI position on the colloid surface. Calculating the exact surface tension force by this equation requires measurement/knowledge of the particle radius, liquid surface tension, and particle and substrate dynamic contact angles. Because the particle contact angle was not experimentally determined, it was not possible to calculate the maximum surface tension forces for the particles in these experiments. Also, the contributions from surface roughness make interpretations for this calculation not as straightforward. Determining these theoretical parameters is intended for future work. It is possible to theorize the influence of capillary forces on particle mobilization provided from the work by Lazouskaya et al. (2013) and the experimental results in this study.

A reduction in surface tension forces resulting in particle immobilization with the contact line is supported by the observed differences between Tween and Water droplet pattern morphology and size of deposition area. As mentioned in the results, Tween deposition patterns were more uniform in their distribution of *Salmonella* and colloids compared to Water patterns. The equilibrium contact angles in **Table 2.1** and

**Table 3.1** and droplet contact area in **Figure 2.9** demonstrate that an increase in wetting results in a subsequently increase in droplet contact area, respectively, for all surfaces. A significant difference in the contact line behavior in Tween droplets compared to Water droplets was also observed. Tween droplets maintained a pinned or quasi-pinned contact line phase for longer than Water droplets on the same surface (e.g., **Figure 2.10** and **Figure 3.8**). Although some particles approached the contact line, this pinning did not cause a large flux of particles to the edges as demonstrated in Water; decreased surface tension of the suspension likely decreased capillary flux to particle edges. It possible that Marangoni flows were present which would redirect particles back towards the center of the droplet. Marangoni flow occurs with surface tension gradients and can suppress capillary flows (Mampallil and Eral, 2018; Hu and Larson, 2006). In this study, water in Tween droplets would continually evaporate, which would lead to an increase in the relative concentration of surfactant in the droplet. This change in surfactant concentration with time would cause a gradient in surface tension, thereby theoretically suppressing capillary flow to the edges and inducing Marangoni flow, which redirects particles from the droplet edges to the center. From the microscopy videos for Glass, this backward flux near the contact line was observed for colloids but not with bacteria; although not clear, bacteria were observed closer to the contact line than the colloids which may have impacted their flux with the hydrodynamics at this region. Additionally, the surface tension gradients would decrease particle transport to the edges. Also evident in the microscopy videos for Glass was the immobilization of particles with the droplet contact line as water from the Tween solution evaporates. It was observed that a surfactant residue was left at the edges of the original contact line following evaporation. For PDMS surfaces,

aggregates of bacteria and colloids pin the contact line and lead to the deposition of large globules and surfactant micelles at the later stages of evaporation at surface features (e.g. **Figure 2.7** and **Figure 3.6**). Notably, deposition on PDMS rough surfaces demonstrated how a decrease in film thickness and contact angle lead to a pinned contact line at features for longer droplet lifetime (e.g., **Figure 2.10** and **Figure 3.8**) and lead to deposition over a larger area.

Droplets on surfaces assume a certain droplet height and shape based on the surface roughness and hydrophobicity and the properties of the solution. As droplets evaporate, the contact lines at the edges mobilize and can be come pinned on the surfaces, which was observed in this study. The thickness of the water films formed by the droplet on the surface as the contact line moves is influenced by the surface properties and solution properties. Film thickness,  $h$ , can be described for plate of smooth surface by the LLD law given by **Equation 4.1**:

$$h = 0.94aCa^{2/3} \quad (4.1)$$

where  $a = (\sigma/\rho g)^{1/2}$  is the capillary length,  $Ca = \eta U/\sigma$  is capillary number,  $g$  is gravitational acceleration,  $\sigma$ ,  $\rho$ , and  $\eta$  are surface tension, density, and viscosity of the liquid phase, respectively (Lazouskaya et al., 2016). Lazouskaya et al (2016) characterized the effect of surface properties on colloid retention on and removal from fresh produce surfaces. Their estimated capillary number and film thickness values were  $1.2 \times 10^{-3}$  and  $29.3 \mu\text{m}$ , respectively. The LLD law expression is valid for Capillary numbers  $Ca < 10^{-2}$  and ideal, smooth surfaces (Lazouskaya et al., 2013). The authors noted how their predicted film thickness was too thick compared to the size of their colloids ( $1 \mu\text{m}$  in diameter) to affect colloid mobilization as they removed their submerged samples from different washing solutions at two different velocities. When

surface heterogeneities are present, as is the case for fresh produce surfaces, the film thickness equation (**Equation 4.1**) is not valid. Surface asperities (e.g. roughness), as well as solution characteristics (e.g., surface tension), can change the thickness of water films at local regions in addition to a change in capillary forces. For example, lowering the surface tension with a surfactant, as done here with 0.01% Tween 80, would decrease the thickness of the water films, confirmed by an increase in droplet contact area and lower substrate contact angles. Also, liquid can entrap within pitted features of the surface and cause thicker water films compared to liquid on a smooth surface. Surface hydrophobicity also impacts the thickness of water films. Hydrophobic surfaces have thicker, less stable water films that de-wet the surface while hydrophilic surfaces, which have increased wetting behavior and thus thinner films (Lazouskaya et al., 2016). During droplet evaporation, the contact line recession and thickness of this interface depends on this combination of surface and solution properties. Lazouskaya et al. (2013, 2016) also noted how the presence of thin films affect contact line behavior for rougher surfaces. As the droplet contact line recedes, a film of varying thickness exists and can be modified by surface roughness, hydrophobicity, and surface tension of the solution. Given the lower surface tension and increased wetting, 0.01% Tween 80 films would have thinner water films than Water droplets and lower capillary forces via **Equation 1.3**. Importantly, roughness features can also modify contact line mobilization and result in discontinuous water films, thereby driving evaporation in-place at these local sites, supported by the microscopy videos. As the droplet evaporates, the film ruptures and residue deposited between the wetted surface features on surfaces is critical for colloid mobilization by altering the surface tension forces experienced by particles at the air-water-interface.

#### 4.1.1.4 Particle Characteristics

As a final observation, there were qualitative differences in *Salmonella* and colloid localization demonstrated in the deposition pattern results (**Sections 2.3 and 3.3**). Interestingly, bacteria appear to better mobilize with the contact line and densely accumulate at the edges of final droplets contact areas, resembling a coffee ring pattern. This localization occurs when contact lines are pinned at the final stages of evaporation. From the microscopy videos, it was observed that bacteria at the contact line are oriented parallel to the interface. Additionally, when the contact line pinned, bacteria rapidly transported to the edges where they localized after evaporation. This effect is pronounced for the Water droplet deposition patterns.

It's possible their shape lends to improved transport with the capillary flux that occurs within evaporating droplets (Yang, Blair, and Salama, 2016). Work by Aramrak et al., (2013) noted how colloid detachment is dependent upon particle shape, in addition to the contact angle of the air-water interface. Rod-shaped particles that had a minor axis smaller than the diameter of a spherical particle required less predicted detachment forces to mobilize with contact lines. Liu et al. (2010) observed the influence of particle shape in transport behavior. They noted that the minor axis of rod-shaped particles influenced the retention and the bulk transport process of rods in porous media. They also indicate that the rod-shaped particles may be oriented with the flow direction during transport, and such orientation of bacteria to flow fields had been observed in microfluidic systems (e.g., Rusconi, Guasto, and Stocker, 2014; Yawata et al., 2016).

Particle characteristics like shape and size appear to dominate the transport mechanisms of bacteria as opposed to active bacterial mechanisms, which would vary based on the system. Currently, active bacterial transport in evaporating droplets is not

fully understood. Thokchom, Swaminathan, and Singh (2014) determined the flow fields in evaporating droplets containing live and dead *E. coli* with and without a chemoattract to determine the effect of motility on deposition patterns. They found that bacteria show a strong chemotactic response that results in a different deposition pattern compared to the dead bacteria. However, without a chemoattractant, the deposition patterns of live and dead bacteria were very similar with similar flow fields, suggesting that in the absence of chemical cues, bacteria are influenced by the flow fields rather than active motility effects. In this study, there is no chemoattractant to drive bacterial response, but the differences between the transport and deposition of spherical colloids and rod-shaped bacteria indicate the role of particle size and shape. Although more experimental and theoretical analyses would be performed to understand better the contributions of the many dynamics involved in our system, the dynamics in the evaporating droplets, which is strongly influenced by the surface and particle properties are suspected to be the dominant mechanisms for mobilization, transport, and deposition of particles.

## **4.2 Conclusions**

Colloidal particles and bacteria in evaporating droplets can occur on soil, plant, and a variety of other interfaces that lead to their desired or undesired deposition on surfaces. The mechanisms behind particle transport can be aided by analyzing droplet evaporation events and resulting deposition patterns on surfaces. In this study, the influence of the properties of the surface, solution, and particle on particle transport were considered. Particle size, shape, and aggregation will likely influence the transport and deposition behavior in addition to the hydrodynamics in the droplet

resulting from surface tension gradients and surface properties, notably roughness and hydrophobicity.

Previous work addressing fresh produce safety with human bacterial pathogens has looked into the application of decontamination methods to limited success. What is typically ignored in these applications are the local-scale dynamics that influence particle mobilization, transport, deposition, and retention as a function of the solution, surface, and particle properties. The few reports that detail these mechanisms in the context of plant surfaces provide valuable insights: Lazouskaya et al. (2016) determined that colloid retention on fresh produce surfaces is controlled by water distribution, which is in turn controlled by the solution and surface properties. Sun et al. (*in review*) determined that the withdrawal velocity of a produce sample from a washing solution influences the mobilization due to the alteration of the thickness of water films for surfactant and water systems. Others note the significance of surface features on the attachment and retention of bacterial pathogens on produce surfaces (Wang et al., 2009, 2012; Zhang et al., 2014).

In the context of food safety, surfactants at high concentrations are unlikely to remove strongly-attached particles from rough surfaces due to thin liquid films and lower capillary forces, limiting particle mobilization. Washing solutions should incorporate air-water interfaces that can generate strong capillary forces to mobilize particles and remove them from fresh produce surfaces. Bacteria deposition within grooves features also requires stronger capillary forces, due to the necessity to mobilize these particles across large height deviations caused by surface features. Additionally, it may be more advantageous to decrease plant wettability to limit water interactions on plant surfaces that could lead to bacteria attachment and deposition, for

example by promoting/altering cuticular wax gene expression to increase plant surface hydrophobicity.

Overall, the work in this study improved the understanding of the contributions of factors that lead to the transport and deposition of (bio)colloids, here with a focus on human pathogen, *Salmonella enterica* on biomimics of produce surfaces. This insight can be used to inform the industry toward better efforts in methods in reducing contamination with science-based strategies, as well provide valuable insight into the dynamics behind microbial transport in a variety of systems.

### **4.3 Future Work**

As demonstrated in this work, there are multiple factors behind (bio)colloid transport and deposition to biointerfaces. Future work will systematically evaluate the further the contributions from solution, surface, and particle properties in the mechanisms behind particle transport processes.

## REFERENCES

- Aramrak, S.; Flury, M.; Harsh, J. B.; Zollars, R. L.; Davis, H. P. Does colloid shape affect detachment of colloids by a moving air-water interface? *Langmuir* **2013**, *29* (19), 5770–5780.
- Beattie, G. a; Lindow, S. E. Bacterial colonization of leaves: a spectrum of strategies. *Phytopathology* **1999**, *89* (5), 353–359.
- Berger, C. N.; Sodha, S. V.; Shaw, R. K.; Griffin, P. M.; Pink, D.; Hand, P.; Frankel, G. Fresh fruit and vegetables as vehicles for the transmission of human pathogens. *Environmental Microbiology*. **2010**.
- Beuchat, L. R. Ecological factors influencing survival and growth of human pathogens on raw fruits and vegetables. *Microbes Infect.* 2002, *4* (4), 413–423.
- Boyer, R. R.; Sumner, S. S.; Williams, R. C.; Pierson, M. D.; Popham, D. L.; Kniel, K. E. Influence of curli expression by *Escherichia coli* O157:H7 on the cell's overall hydrophobicity, charge, and ability to attach to lettuce. *J. Food Prot.* **2007**, *70* (6), 1339–1345.
- Bradford, S.A. and Torkzaban, S. Colloid transport and retention in unsaturated porous media: a review of interface-, collector-, and pore-scale processes and models. *Vadose Zone J* **2008**, *7*: 667-681.
- Brandl, M. T. Fitness of human enteric pathogens on plants and implications for food safety. *Annu Rev Phytopathol* **2006**, *44*, 367–392.
- Brandl, M. T. Plant lesions promote the rapid multiplication of *Escherichia coli* O157:H7 on postharvest lettuce. *Appl. Environ. Microbiol.* **2008**, *74* (17), 5285–5289.
- Brandl, M. T., and Huynh, S. Effect of the surfactant Tween 80 on the detachment and dispersal of *Salmonella enterica* serovar Thompson single cells and aggregates from cilantro leaves as revealed by image analysis. *Appl. Environ. Microbiol.* **2014**, *80*:5037-5042.
- Brandl, M. T.; Amundson, R. Leaf age as a risk factor in contamination of lettuce with *Escherichia coli* O157:H7 and *Salmonella enterica*. *Appl. Environ. Microbiol.* **2008**, *74* (8), 2298–2306.
- Callejón, R. M.; Rodríguez-Naranjo, M. I.; Ubeda, C.; Hornedo-Ortega, R.; Garcia-Parrilla, M. C.; Troncoso, A. M. Reported foodborne outbreaks due to fresh produce in the United States and European Union: trends and causes. *Foodborne Pathog. Dis.* **2015**, *12* (1), 32–38.

- Center for Food Safety and Applied Nutrition. (n.d.). Current Good Manufacturing Practices (CGMPs) - Good Manufacturing Practices (GMPs) for the 21st Century - Food Processing. Retrieved from <https://www.fda.gov/Food/GuidanceRegulation/CGMP/ucm110877.htm>
- Crawford, R. J.; Webb, H. K.; Truong, V. K.; Hasan, J.; Ivanova, E. P. Surface topographical factors influencing bacterial attachment. *Adv. Colloid Interface Sci.* 2012, 179–182, 142–149.
- Critzer, F. J.; Doyle, M. P. Microbial ecology of foodborne pathogens associated with produce. *Curr. Opin. Biotechnol.* **2010**, 21 (2), 125–130.
- Deegan, R. D. Pattern formation in drying drops Robert. *Phys. Rev. E - Stat. Physics, Plasmas, Fluids, Relat. Interdiscip. Top.* **2000**, 61 (1), 475–485.
- Deegan, R. D.; Bakajin, O.; Dupont, T. F.; Huber, G.; Nagel, S. R.; Witten, T. A. Contact line deposits in an evaporating drop. *Phys. Rev. E - Stat. Physics, Plasmas, Fluids, Relat. Interdiscip. Top.* **2000**, 62 (1 B), 756–765.
- Doan, H. K.; Leveau, J. H. J. Artificial Surfaces in Phyllosphere Microbiology. *Phytopathology* **2015**, 105 (8), 1036–1042.
- Doyle, M. P.; Erickson, M. C. Summer meeting 2007 - The problems with fresh produce: An overview. *J. Appl. Microbiol.* **2008**, 105 (2), 317–330.
- Engström, E.; Thunvik, R.; Kulabako, R.; Balfors, B. Water transport, retention, and survival of *Escherichia coli* in unsaturated porous media: A comprehensive review of processes, models, and factors. *Crit. Rev. Environ. Sci. Technol.* **2015**, 45 (1), 1–100.
- Fao/Who. Microbiological hazards in fresh fruits and vegetables. *World Health* **2008**, 1–38.
- FDA/CFSAN, 2001a. Center for Food Safety and Applied Nutrition. “Current Good Manufacturing Practices (CGMPs) - GMPs Section Two: Literature Review of Common Food Safety Problems and Applicable Controls.” *US Food and Drug Administration Home Page*, Center for Drug Evaluation and Research, [www.fda.gov/food/guidanceregulation/cgmp/ucm110911.htm](http://www.fda.gov/food/guidanceregulation/cgmp/ucm110911.htm).
- Fernandes, P. É.; São José, J. F. B.; Zerdas, E. R. M. A.; Andrade, N. J.; Fernandes, C. M.; Silva, L. D. Influence of the hydrophobicity and surface roughness of mangoes and tomatoes on the adhesion of *Salmonella enterica* serovar Typhimurium and evaluation of cleaning procedures using surfactin. *Food Control* **2014**, 41 (1), 21–26.

- Flemming, H.-C.; Wingender, J.; Szewzyk, U.; Steinberg, P.; Rice, S. A.; Kjelleberg, S. Biofilms: an emergent form of bacterial life. *Nat. Rev. Microbiol.* **2016**, *14* (9), 563–575.
- Food and Agriculture Organization/World Health Organization, 2008
- Gibson, H., Taylor, J. H., Hall, K. E., & Holah, J. T. (1999). Effectiveness of cleaning techniques used in the food industry in terms of the removal of bacterial biofilms. *Journal of Applied Microbiology*, *87*(1), 41e48.
- Goulter, R.M., Gentle, I.R. and Dykes, G.A. Issues in determining factors influencing bacterial attachment: a review using the attachment of *Escherichia coli* to abiotic surfaces as an example. *Letters in Appl. Microbiol.* **2009**, *49*: 1–7.
- Guentzel, J. L.; Liang, K.; Callan, M. A.; Emmons, S. A.; Dunham, V. L.; Liang Lam, K.; Callan, M. A.; Emmons, S. A.; Dunham, V. L.; Liang, K. Reduction of bacteria on spinach, lettuce, and surfaces in food service areas using neutral electrolyzed oxidizing water. *Food Microbiol.* **2008**, *25* (1), 36–41.
- Gündüz, G. T., Gönül, Ş. A., & Karapınar, M. Efficacy of oregano oil in the inactivation of *Salmonella typhimurium* on lettuce. *Food Control*, 2010, *21*(4), 513–517.
- Hassan, A. N.; Frank, J. F. Attachment of *Escherichia coli* O157:H7 grown in tryptic soy broth and nutrient broth to apple and lettuce surfaces as related to cell hydrophobicity, surface charge, and capsule production. *Int. J. Food Microbiol.* **2004**, *96* (1), 103–109.
- Haznedaroglu, B. Z.; Kim, H. N. Relative Transport Behavior of Pullorum in Packed Bed Column Systems : Influence of Solution Chemistry and Cell Concentration. **2009**, *43* (6), 1838–1844.
- He, M.; Liao, D.; Qiu, H. Multicomponent Droplet Evaporation on Chemical Micro-Patterned Surfaces. *Sci. Rep.* **2017**, *7* (December 2016), 1–12.
- Heaton, J. C.; Jones, K. Microbial contamination of fruit and vegetables and the behaviour of enteropathogens in the phyllosphere: A review. *J. Appl. Microbiol.* **2008**, *104* (3), 613–626.
- Hennes, M.; Tailleur, J.; Charron, G.; Daerr, A. Active depinning of bacterial droplets: The collective surfing of *Bacillus subtilis*. *Proc. Natl. Acad. Sci.* **2017**, *114* (23), 5958–5963.
- Hou, S.; Gu, H.; Smith, C.; Ren, D. Microtopographic patterns affect *Escherichia coli* biofilm formation on poly(dimethylsiloxane) surfaces. *Langmuir* **2011**, *27* (6), 2686–2691.

- Hsu, L. C.; Fang, J.; Borca-Tasciuc, D. A.; Worobo, R. W.; Moraru, C. I. Effect of micro- and nanoscale topography on the adhesion of bacterial cells to solid surfaces. *Appl. Environ. Microbiol.* **2013**, *79* (8), 2703–2712.
- Hu, H.; Larson, R. G. Marangoni effect reverses coffee-ring depositions. *J. Phys. Chem. B* **2006**, *110* (14), 7090–7094.
- Huang, K.; Wrenn, S.; Tikekar, R.; Nitin, N. Efficacy of decontamination and a reduced risk of cross-contamination during ultrasound-assisted washing of fresh produce. *J. Food Eng.* **2018**, *224*, 95–104.
- Hwang, I. G.; Kim, J. Y.; Weon, B. M. Droplet evaporation with complexity of evaporation modes. *Appl. Phys. Lett.* **2017**, *110* (3).
- James, J. (2006). *Microbial hazard identification in fresh fruit and vegetables*. Hoboken (NJ): Wiley-Interscience.
- Jung, Y.; Jang, H.; Matthews, K. R. Minireview Effect of the food production chain from farm practices to vegetable processing on outbreak incidence. **2014**.
- Katsikogianni, M.; Missirlis, Y. F. Concise review of mechanisms of bacterial adhesion to biomaterials and of techniques used in estimating bacteria-material interactions. *Eur. Cells Mater.* **2004**, *8*, 37–57.
- Koch, K.; Bhushan, B.; Barthlott, W. Diversity of structure, morphology and wetting of plant surfaces. *Soft Matter* **2008**, *4* (10), 1943.
- Kumar, G. D., Crosby, K., Leskovar, D., Bang, H., Jayaprakasha, G. K., Patil, B., & Ravishankar, S. A Surveillance of cantaloupe genotypes for the prevalence of *Listeria* and *Salmonella*. *Agriculture Food and Analytical Bacteriology*, **2015**, *5*, 73-84.
- Kumar, G. D., Macarisin, D., Micallef, S. Filamentation in *Salmonella*: Evidence of a short-term high output response to stress. *Appl. Environ. Microbiol.* **2018**, *accepted*.
- Kumar, G. D. & Micallef, S. A. Susceptibility of *Salmonella enterica* Isolates from Tomato Farm Environments to Fatty Acids Naturally Found on Tomato Fruit. *Foodbrn. Path. and Dis.* **2017**, *14*(5), 293-301.
- Kumar, G. D. & Micallef, S. A. Biofilms: A Community-Based Strategy for Bacterial Persistence and Relevance to Food Safety. *Trends in Food Safety and Protect.*, **2017**, CRC Press/Taylor & Francis, FL.

- Kumar, G. D., Micallef, S. A., Ravi, S., Brown, E.W., Macarisin, D. Aeolian Contamination of Fruits by Enteric Pathogens: An Unexplored Paradigm. *Current Opinion in Food Science*, **2017**, 19:138-144.
- Kumar, G. D. and Ravishankar, S. Ozonized Water with Plant Antimicrobials: An Effective Method to Inactivate *Salmonella enterica* on Iceberg Lettuce in the Produce Wash Water. *Enviro. Research*. **2018**, in Review.
- Kumar, G. D., Ravishankar, S., & Juneja, V. K. Interventions for Fresh Produce. In *Micro. Cont. and Food Preserv*. **2017**, (pp. 199-223), Springer, New York, NY.
- Kumar, G. D., Williams, R. C., Al Qublan, H. M., Sriranganathan, N., Boyer, R. R., & Eifert, J. D. Airborne soil particulates as vehicles for *Salmonella* contamination of tomatoes. *Internat. J. of Food Microbiol.*, **2017**, 243, 90-95.
- Kumar, G. D., Williams, R. C., Sriranganathan, N., Boyer, R. R., & Eifert, J. D. Survival of Tomato Outbreaks Associated *Salmonella* Serotypes and the Role of Biofilms in Abiotic Surface Attachment. *Foodborne Path. and Dis.*, **2018**.
- Kumar, G. D., Williams, R. C., Sumner, S. S., & Eifert, J. D. (2015). Effect of Ozone and Ultraviolet Light on *Listeria monocytogenes* Populations in Fresh and Spent Chill Brines. *Food Cont.* **2015**, 59, 172-177.
- Lazouskaya, V.; Jin, Y. Colloid retention at air-water interface in a capillary channel. *Colloids Surfaces A Physicochem. Eng. Asp.* **2008**, 325 (3), 141–151.
- Lazouskaya, V.; Jin, Y.; Or, D. Interfacial interactions and colloid retention under steady flows in a capillary channel. *J. Colloid Interface Sci.* **2006**, 303 (1), 171–184.
- Lazouskaya, V.; Sun, T.; Liu, L.; Wang, G.; Jin, Y. Effect of Surface Properties on Colloid Retention on Natural and Surrogate Produce Surfaces. *J Food Sci* **2016**, 00 (0).
- Lazouskaya, V.; Wang, L. P.; Or, D.; Wang, G.; Caplan, J. L.; Jin, Y. Colloid mobilization by fluid displacement fronts in channels. *J. Colloid Interface Sci.* **2013**, 406, 44–50.
- Lima, P. M.; São, J. F. B.; Andrade, N. J.; Clarissa, A.; Pires, S.; Ferreira, S. O. Interaction between natural microbiota and physicochemical characteristics of lettuce surfaces can influence the attachment of *Salmonella* Enteritidis. *Food Control* **2013**, 30 (1), 157–161.
- Lindow, S. E. (2004). *Phyllosphere microbiology*. St. Paul: American Phytopathological Society.

- Liu, Q.; Lazouskaya, V.; He, Q.; Jin, Y. Effect of Particle Shape on Colloid Retention and Release in Saturated Porous Media. *Journal of Environment Quality*, 2010, 39, 500.
- Lu, N.; Zhang, W.; Weng, Y.; Chen, X.; Cheng, Y.; Zhou, P. Fabrication of PDMS surfaces with micro patterns and the effect of pattern sizes on bacteria adhesion. *Food Control* **2016**, 68, 344–351.
- Nguyen, T. A. H.; Nguyen, A. V.; Hampton, M. A.; Xu, Z. P.; Huang, L.; Rudolph, V. Theoretical and experimental analysis of droplet evaporation on solid surfaces. *Chem. Eng. Sci.* **2012**, 69 (1), 522–529.
- Mampallil, D.; Eral, H. B. A review on suppression and utilization of the coffee-ring effect. *Adv. Colloid Interface Sci.* **2018**, 252, 38–54.
- Meireles, A.; Giaouris, E.; Simões, M. Alternative disinfection methods to chlorine for use in the fresh-cut industry. *Food Res. Int.* **2016**, 82, 71–85.
- Michen, B.; Balog, S.; Rothen-Rutishauser, B.; Petri-Fink, A.; Vanhecke, D. TEM Sample Preparation of Nanoparticles in Suspensions. *G.I.T. Imaging Microsc.* **2014**, 3, 39–41.
- Oregon, D.; Sefiane, K.; Shanahan, M. E. R. Stick-slip of evaporating droplets: Substrate hydrophobicity and nanoparticle concentration. *Langmuir* **2011**, 27 (21), 12834–12843.
- Painter, J. A., Hoekstra, R. M., Ayers, T., Tauxe, R. V., Braden, C. R., Angulo, F. J., Griffin, P. M. (2013). Attribution of Foodborne Illnesses, Hospitalizations, and Deaths to Food Commodities by using Outbreak Data, United States, 1998–2008. *Emerging Infectious Diseases*, 19(3), 407–415. <https://dx.doi.org/10.3201/eid1903.111866>.
- Parsa, M.; Harmand, S.; Se, K. Mechanisms of pattern formation from dried sessile drops. **2018**, 254, 22–47.
- Paxson, A. T.; Varanasi, K. K. Self-similarity of contact line depinning from textured surfaces. *Nat. Commun.* **2013**, 4, 1492–1498.
- Perni, S.; Prokopovich, P. Micropatterning with conical features can control bacterial adhesion on silicone. *Soft Matter* **2013**, 9, 1844–1851.
- Rijnaarts, H. H.; Norde, W.; Bouwer, E. J.; Lyklema, J.; Zehnder, A. J. Bacterial Adhesion under Static and Dynamic Conditions. *Appl. Environ. Microbiol.* **1993**, 59 (10), 3255–3265.

- Rusconi, R.; Guasto, J. S.; Stocker, R. Bacterial transport suppressed by fluid shear. *Nat. Phys.* **2014**, *10* (3), 212–217.
- Sagong, H. G.; Cheon, H. L.; Kim, S. O.; Lee, S. Y.; Park, K. H.; Chung, M. S.; Choi, Y. J.; Kang, D. H. Combined effects of ultrasound and surfactants to reduce *Bacillus cereus* spores on lettuce and carrots. *Int. J. Food Microbiol.* **2013**, *160* (3), 367–372.
- Sapers, G. M., Matthews, K. R., & Gerba, C. P. (2014). *The produce contamination problem: Causes and solutions*. Amsterdam: Elsevier.
- Schneider, C. A.; Rasband, W. S. & Eliceiri, K. W. (2012), "[NIH Image to ImageJ: 25 years of image analysis](#)", *Nature methods* **9**(7): 671-675, PMID 22930834 ([on Google Scholar](#)).
- Sefiane, K. On the formation of regular patterns from drying droplets and their potential use for bio-medical applications. *J. Bionic Eng.* **2010**, *7* (SUPPL.), S82–S93.
- Sempels, W.; De Dier, R.; Mizuno, H.; Hofkens, J.; Vermant, J. Auto-production of biosurfactants reverses the coffee ring effect in a bacterial system. *Nat. Commun.* **2013**, *4*, 1757–1758.
- Shen, C.; Lazouskaya, V.; Zhang, H.; Li, B.; Jin, Y.; Huang, Y. Influence of surface chemical heterogeneity on attachment and detachment of microparticles. *Colloids Surfaces A Physicochem. Eng. Asp.* **2013**, *433*, 14–29.
- Shen, C.; Lazouskaya, V.; Zhang, H.; Wang, F.; Li, B.; Jin, Y.; Huang, Y. Theoretical and experimental investigation of detachment of colloids from rough collector surfaces. *Colloids Surfaces A Physicochem. Eng. Asp.* **2012**, *410*, 98–110.
- Shi, X.; Zhu, X. Biofilm formation and food safety in food industries. *Trends Food Sci. Technol.* **2009**, *20* (9), 407–413.
- Solomon, E. B.; Matthews, K. R. Interaction of live and dead *Escherichia coli* O157:H7 and fluorescent microspheres with lettuce tissue suggests bacterial processes do not mediate adherence. *Lett. Appl. Microbiol.* **2006**, *42* (2), 88–93.
- Soni, K. A.; Balasubramanian, A. K.; Beskok, A.; Pillai, S. D. Zeta potential of selected bacteria in drinking water when dead, starved, or exposed to minimal and rich culture media. *Curr. Microbiol.* **2008**, *56* (1), 93–97.
- Srey, S.; Jahid, I. K.; Ha, S. Do. Biofilm formation in food industries: A food safety concern. *Food Control* **2013**, *31* (2), 572–585.

- Still, T.; Yunker, P. J.; Yodh, A. G. Surfactant-Induced Marangoni Eddies Alter the Coffee-Rings of Evaporating Colloidal Drops. *Langmuir* **2012**, *28*, 4984–4988.
- Thiele, U. Patterned deposition at moving contact lines. *Adv. Colloid Interface Sci.* **2014**, *206*, 399–413.
- Thokchom, A. K.; Swaminathan, R.; Singh, A. Fluid flow and particle dynamics inside an evaporating droplet containing live bacteria displaying chemotaxis. *Langmuir* **2014**, *30* (41), 12144–12153.
- Thormann, E. Surface forces between rough and topographically structured interfaces. *Curr. Opin. Colloid Interface Sci.* **2017**, *27*, 18–24.
- Verwey, E.J.W. and Overbeek J.T.G. Theory of the Stability of Lyophobic Colloids. **1948**. Elsevier, New York.
- Wang, G.; Or, D. Aqueous films limit bacterial cell motility and colony expansion on partially saturated rough surfaces. *Environ. Microbiol.* **2010**, *12* (5), 1363–1373.
- Wang, H.; Feng, H.; Liang, W.; Luo, Y.; Malyarchuk, V. Effect of surface roughness on retention and removal of Escherichia coli O157:H7 on surfaces of selected fruits. *J. Food Sci.* **2009**, *74* (1), E8–E15.
- Wang, H.; Zhou, B.; Feng, H. Surface Characteristics of Fresh Produce and their Impact on Attachment and Removal of Human Pathogens on Produce Surfaces. *Decontam. Fresh Minim. Process. Prod.* **2012**, No. December, 43–57.
- Whitehead, K. A., Verran, J. The effect of surface topography on the retention of microorganisms. *Food Bioprod. Process.* **2006**, *84* (C4), 253–259.
- WHO/FAO. Promoting fruit and vegetable consumption around the world. (2015, March 09). Retrieved from <http://www.who.int/dietphysicalactivity/fruit/en/>
- Xu, S.; Qi, J.; Chen, X.; Lazouskaya, V.; Zhuang, J.; Jin, Y. Coupled effect of extended DLVO and capillary interactions on the retention and transport of colloids through unsaturated porous media. *Sci. Total Environ.* **2016**, *573*, 564–572.
- Yang, D. C.; Blair, K. M.; Salama, N. R. Staying in Shape: the Impact of Cell Shape on Bacterial Survival in Diverse Environments. *Microbiol. Mol. Biol. Rev.* **2016**, *80* (1), 187–203.
- Yaron, S.; Römling, U. Minireview Biofilm formation by enteric pathogens and its role in plant colonization and persistence. 2014.

- Yawata, Y.; Nguyen, J.; Stocker, R.; Rusconi, R. Microfluidic studies of biofilm formation in dynamic environments. *J. Bacteriol.* **2016**, *198* (19), 2589–2595.
- Yildirim Erbil, H. Control of stain geometry by drop evaporation of surfactant containing dispersions. *Adv. Colloid Interface Sci.* **2015**, *222*, 275–290.
- Yu, Y. S.; Wang, M. C.; Huang, X. Evaporative deposition of polystyrene microparticles on PDMS surface. *Sci. Rep.* **2017**, *7* (1), 1–9.
- Yunker, P. J.; Still, T.; Lohr, M. A.; Yodh, A. G. Suppression of the coffee-ring effect by shape-dependent capillary interactions. *Nature* **2011**, *476*, 308.
- Zhang, B.; Luo, Y.; Pearlstein, A. J.; Aplin, J.; Liu, Y.; Bauchan, G. R.; Payne, G. F.; Wang, Q.; Nou, X.; Millner, P. D. Fabrication of Biomimetically Patterned Surfaces and Their Application to Probing Plant–Bacteria Interactions. *Appl. Mater. Interfaces* **2014**.
- Zhang, X.; Wang, L.; Levänen, E. Superhydrophobic surfaces for reduction of bacterial adhesion. *RCS Adv.* **2013**, 1–53.
- Zhao, M.; Yong, X. Modeling Evaporation and Particle Assembly in Colloidal Droplets. *Langmuir* **2017**, *33* (23), 5734–5744.
- Zheng, W.; Wang, L. P.; Or, D.; Lazouskaya, V.; Jin, Y. Role of Mixed Boundaries on Flow in Open Capillary Channels with Curved Air–Water Interfaces. *Langmuir* **2012**, *28* (35), 12753–12761.

## Appendix A

### PARTICLE CHARACTERISTICS

A Zeiss 880 confocal microscope (Zeiss 880 LSM, Carl Zeiss, Inc., Jena, Germany) with a 40x/W lens along with ImageJ software was used to determine the dimensions of pGFPuv-*Salmonella enterica* sv, Enteritidis (n=100) from culture preparation (pure colony in Tryptic Soy Broth with 0.01% (w/v) ampicillin incubated at 30°C with shaking (120 rpm) until stationary phase (~16 - 18 h), followed by centrifugation at 4°C / 5000 rpm (3412 xg) / 25 min, washed 1x with sterile 1x PBS, and re-suspended in sterile DI water to a concentration of  $\approx 10^6$  CFU/mL (via 1:1000 dilution). Colloid properties were provided by manufacturer. Values are reported in **Table A.1**.

**Table A.1** Particle Characteristics

Particle	Shape	Dimensions ( $\mu\text{m}$ )	Hydrophobicity	Zeta potential (mV)
<i>Salmonella enterica</i> sv. Enteritidis	rod	$(2.1 \pm 0.4)l$ $\times (1.1 \pm 0.1)w$	Hydrophobic <sup>a</sup>	$-16 \pm 1.4 \text{ mV}^b$
Sulfate-modified Colloids	sphere	$(2.0)d$	Hydrophobic <sup>c</sup>	$-66 \pm 3.3 \text{ mV}^d$

*l* refers to length; *w* refers to width; and *d* refers to diameter

<sup>a</sup>Haznedaroglu et al., 2009

<sup>b</sup>Soni et al., 2008. Overnight growth in Tryptic Soy and prepared in sterile drinking water; cell length:  $2.2 \pm 0.3$ .

<sup>c</sup>Provided by manufacturer

<sup>d</sup>Lazouskaya et al., 2008 (measured in DI water with ionic strength of  $1.5 \times 10^{-6}$  M for a resistance value of 18.3 m $\Omega$ cm)